Ttc7 is a *Trans*-Acting Regulator of Cell Proliferation

Dissertation

zur

Erlangung der naturwissenschaftlichen Doktorwürde
(Dr. sc. nat.)

vorgelegt der

Mathematisch-naturwissenschaftlichen Fakultät

der

Universität Zürich

von

Ursina Nüesch

von

Balgach SG

Promotionskommission

Prof. Dr. Christian Münz (Vorsitz der Dissertation)

Prof. Dr. Jana Pachlopnik Schmid (Leitung der Dissertation)

Prof. Dr. Burkhard Becher

Zürich, 2017

TABLE OF CONTENTS

I. SUMMARY

Mutations in tetratricopeptide repeat domain 7A (*TTC7A*) and its mouse orthologue *Ttc7* — a ubiquitously expressed protein — result in a life-threatening multisystemic disease, severely affecting epithelial body barriers and the immune system. Patients mainly suffer from intestinal atresias and immunodeficiency. Furthermore, surgical treatment of the atresias is associated with poor outcomes, and the potentially fatal condition progresses despite successful allogeneic hematopoietic stem cell transplantation. There is an ongoing debate of whether *TTC7A* mutations uniquely dysregulate epithelial cells, or whether a defect in lymphocytes contributes to the pathogenesis of the disease. Therefore, a deeper understanding of mechanisms underlying the multisystemic nature of *TTC7A* deficiency is needed.

The flaky skin mutant mouse (*Ttc7*$^{fsn/fsn}$) has been regarded as a model for human psoriasis because of its hyperplastic skin disease. *Ttc7*$^{fsn/fsn}$ mice present with a severe hyperplastic dermatitis as the main feature of a complex phenotype including a hyperproliferative immune disorder (splenomegaly and peripheral lymphadenopathy), gastric forestomach papillomas, and anemia. The mechanisms leading to the flaky skin phenotype remain largely unknown. In particular, it is unclear whether the hyperplastic skin disease is uniquely due to an intrinsic epithelial dysfunction or if altered immune activation leads to reactive epidermal hyperplasia. To investigate this, we generated double homozygous mutant *Rag2*$^{-/-}$*Ttc7*$^{fsn/fsn}$ mice — lacking adaptive lymphocytes — and triple homozygous mutant mice *Rag2*$^{-/-}$*IL2rg*$^{-/-}$*Ttc7*$^{fsn/fsn}$ mice — completely lacking the innate and adaptive lymphocytic compartment. Both immunodeficient mouse strains were not protected from epithelial hyperproliferation and even developed peripheral lymphadenopathy but less severe than observed in the *Ttc7*$^{fsn/fsn}$ mouse model. Furthermore, the transfer of Ttc7-mutated hematopoietic stem cells did not induce epithelial hyperproliferation or peripheral lymphadenopathy in wild-type animals. Thus, lymphocytes are able to aggravate the severity of epithelial hyperproliferation and inflammation in *Ttc7*$^{fsn/fsn}$ stroma but cannot elicit the flaky skin phenotype. Serum cytokine profiles revealed high levels of IL-22 in single, double and triple homozygous mutant mice. We herewith identified non-lymphoid *Ttc7*$^{fsn/fsn}$ cells as the major source of

IL-22. In a xenograft model, Ttc7-mutated mouse fibroblasts markedly increased epithelial proliferation of human keratinocytes. The analyses of transcriptomic data from Ttc7-mutated fibroblasts displayed an mRNA expression pattern that suggested alterations in phosphoinositide-dependent signaling pathways. These pathways play an important role in cytoskeleton regulation and in cell-cell-interactions. In addition, we found an increased expression of IGF-1. Consequently, Ttc7-mutated fibroblasts were identified to critically induce the hyperproliferative behavior of keratinocytes in the presence of the proliferation-inducing factors IL-22 and IGF-1.

Our work shows that fibroblasts harmfully alter the dynamic and behavior of epidermal cell maturation, while Ttc7-mutated lymphocytes contribute to epidermal homeostasis. The dysfunctional crosstalk between stromal cells adds an unsuspected new dimension to the pathogenesis of the multisystemic disease associated with *TTC7A* deficiency. This suggested mechanism reveals why previous HSCT treatments together with intestinal surgery may only partially relieve the multisystemic disease seen *TTC7A*-deficient patients. Thus, a new targeted therapeutic approach is needed to achieve treatment strategies that intervene in the disturbed interaction between stromal cells.

II. ZUSAMMENFASSUNG

Tetratricopeptid-Repeat-Domäne 7A (*TTC7A*) ist ein Protein, welches in allen Körperzellen exprimiert wird, über dessen Funktion jedoch wenig bekannt ist. Mutationen im TTC7A-Gen und dessen Maus-Ortholog *Ttc7* verursachen eine lebensbedrohliche multisystemische Erkrankung bei der die Epithelbarrieren des Körpers und das Immunsystem stark beeinträchtigt sind. Die Patienten leiden hauptsächlich an intestinalen Atresien und einer Immunschwäche. Trotz Darmoperationen und erfolgreicher hämatopoietischer Stammzelltransplantation kann die intestinale Manifestation weiter fortschreiten. Unklar ist, ob die Mutationen in *TTC7A* ausschliesslich eine Funktionsstörung von Epithelzellen hervorrufen, oder zugleich eine zell-intrinsische Dysfunktion in Lymphozyten verursachen.

Die „flaky skin" Maus (mit homozygoter *Ttc7*$^{fsn/fsn}$ Mutation) wurde ursprünglich, aufgrund ihrer Hauterkrankung, als Modell für Psoriasis verwendet. Das Hauptmerkmal der *Ttc7*$^{fsn/fsn}$-Maus ist eine schwerwiegende hyperplastische Dermatitis, die begleitet ist von einer hyperproliferativen Immunerkrankung (Splenomegalie und periphere Lymphadenopathie), der spontanen Bildung von Magenpapillomen und einer schweren Anämie. Anhand des „flaky skin" Mausmodells sind wir der Frage nachgegangen, ob die homozygote *Ttc7*$^{fsn/fsn}$ Mutation ausschliesslich Epithelzellen beeinträchtigt, oder ob auch andere Zellarten betroffen sind. Dazu wurden immundefiziente Mausmutanten, denen adaptive Lymphozyten fehlen — zweifach homozygot mutierte *Rag2*$^{-/-}$*Ttc7*$^{fsn/fsn}$ Mäuse — und Mausmutanten, denen sowohl Lymphozyten des adaptiven, als auch diejenigen des angeborenen Immunsystem fehlen — dreifach homozygot mutierte *Rag2*$^{-/-}$*IL2rg*$^{-/-}$*Ttc7*$^{fsn/fsn}$ Mäuse — gezüchtet und untersucht. Beide Mausmutanten haben eine entzündliche Hyperplasie der Haut und periphere Lymphadenopathie entwickelt. Der Schweregrad dieser Veränderungen war jedoch geringer in den zweifach- und dreifach mutierten Mäusen im Vergleich zur „flaky skin" Maus mit nur einer Mutation. Zudem zeigten Wildtyp-Mäuse nach Transfer von Ttc7-mutierten hämatopoetischen Stammzellen unauffällige Hautverhältnisse und normale Lymphknoten. Es ist also davon auszugehen, dass Lymphozyten die Hyperproliferation des Epithels und die Entzündung des Stromas verschlimmern können, jedoch nicht den Phänotyp auslösen. Im Blutserum von allen

mutierten Mäusen haben wir einen erhöhten Wert des proliferations-induzierenden Zytokins IL-22 gemessen. Da auch bei zweifach- und dreifach mutierten Mäusen stark erhöhte IL-22 Werte vorlagen, waren nicht-lymphozytäre *Ttc7*$^{fsn/fsn}$-Zellen die Hauptquelle der IL-22-Produktion. In einem Xenotransplantat-Modell haben wir festgestellt, dass isolierte Ttc7-mutierte Mausfibroblasten im Stande waren eine Hyperproliferation menschlicher Keratinozyten zu induzieren. Die Transkriptom-Analyse von Ttc7-mutierten Fibroblasten zeigte ein mRNA Expressionsmuster, welches auf Veränderungen in Phosphoinositid-abhängigen Signalwegen schliessen. Diese Signalwege spielen eine wichtige Rolle in der Zytoskelett-Regulierung und in Zell-Zell-Interaktionen. Zusätzlich fanden wir eine erhöhte Expression von Wachstumshormon IGF-1 in den Ttc7-mutierten Fibroblasten. Zusammenfassend lässt sich sagen, dass *Ttc7*$^{fsn/fsn}$-mutierte Fibroblasten eine vermehrte Keratinozytenproliferation auslösen, und dass dies in Anwesenheit der proliferations- und wachstums-induzierenden Faktoren IL-22 und IGF-1 geschieht.

Unsere Arbeit zeigt, dass Ttc7 in Fibroblasten die Dynamik und das Verhalten epidermaler Zellen beeinflussen kann, und dass Ttc7 in Lymphozyten bei der Kontrolle der Hauthomöostase mitwirkt. Wir postulieren deshalb, dass Mutationen in Ttc7 eine Störung in der Wechselwirkung zwischen Stromazellen verursachen und damit zur Pathogenese der multisystemischen Erkrankung beitragen während Lymphozyten eine untergeordnete Rolle spielen. Dies würde erklären, weshalb eine TTC7A-Defizienz nicht mittels Darmoperationen und hämatopoietischer Stammzelltransplantation geheilt werden kann. Ein neuer Therapieansatz wird benötigt, der gezielt in die gestörte Wechselwirkung zwischen Stromazellen einzugreifen vermag.

III. INTRODUCTION

We are continually exposed to pathogens and irritants that are inhaled, swallowed, sitting on our skin or mucous membranes. The essential function of our immune system is best illustrated when something goes wrong resulting in inflammation, infections, allergies, immunodeficiencies, or autoimmune diseases. Mutations in the tetratricopeptide repeat domain 7A (*TTC7A)* result in a life-threating multi-systemic disease affecting epithelial barriers and the immune system. This thesis focuses on the mouse orthologue *Ttc7* in the flaky skin mutant model presenting with anemia, a hyperproliferative immune disorder and a hyperplastic skin disease. Our intention was to gain a deeper understanding of the mediator(s) causing the multi-systemic disease in this mouse model with the aim to better understand the mechanisms that underlie the pathology in mice and men.

1. The Hematopoietic System – Hematopoiesis

Hematopoiesis comprises the formation and development of all blood cell lineages, that are, the red blood cells, the lymphocytes and the myeloid cells (incl. thrombocytes) (**Figure 1**). Hematopoiesis starts in the yolk sac during embryogenesis and, as development progresses, occurs in the spleen, liver, and lymph nodes. Eventually, the bone marrow assumes this task and forms most of the blood cells. Extramedullary hematopoiesis stops in humans after birth, whereas it remains a normal finding in the spleen of some species such as the mouse [1]. Hematopoietic stem cells (HSC) are self-renewing and pluripotent, meaning that a single HSC can generate all different types of blood cells, respectively, white and red blood cells [2]. The HSC can be divided into short-term reconstituting HSC, which have a limited self-renewal potential and arise from long-term reconstituting HSC [2, 3]. The short-term reconstituting HSCs give rise to multipotent progenitors (MPPs), which, in turn, generate lineage-committed oligopotent progenitors, including (i) common lymphoid progenitors (CLPs) and (ii) common myeloid progenitors (CMPs) [2]. The CLPs differentiate into precursors of T and B lymphocytes, natural killer cells and subtypes of dendritic cells. The CMPs evolve into

precursors of mature erythrocytes, platelets, granulocytes, and monocytes/macrophages [2, 3]. Most dendritic cells arise from CMP progenitors.

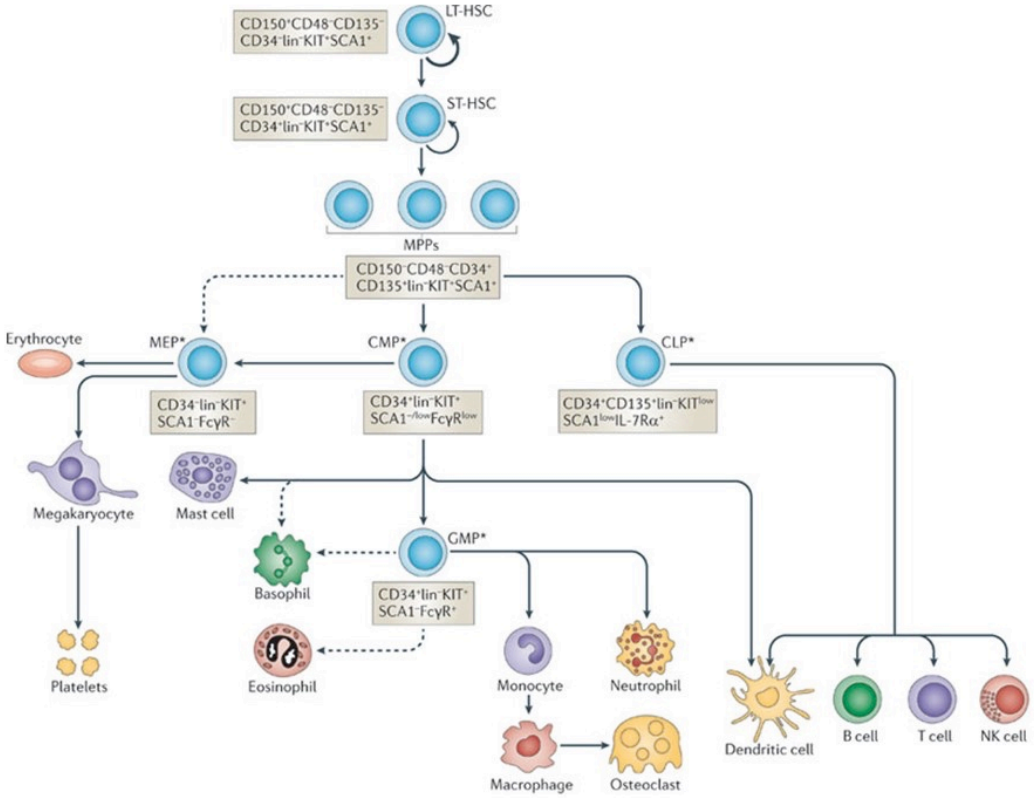

Figure 1. Diagram of the hematopoiesis scheme. Hematopoietic stem cells are generated from a small population of hematopoietic stem cells (HSCs). HSCs can be divided into long-term (LT-HSC) and short-term reconstituting HSCs (ST-HSC). ST-HSCs maintain multipotency and give rise to multipotent progenitors (MPPs), which, in turn, generate lineage-committed oligopotent progenitors, including common lymphoid progenitors (CLP) and common myeloid progenitors (CMP). The precursors of megakaryocyte-erythrocyte progenitors (MEP) and granulocyte-monocyte progenitors (GMP) give rise to erythrocytes or granulocytes. Figure adapted from [2].

2. The Immune System

The immune system can be divided into the innate (natural) and adaptive (acquired) immune system. Failure in one of these systems will greatly increase the susceptibility to infection.

Anatomic and physical barriers provide the crucial first line of defense against pathogens and can be regarded as part of the innate immune system. An intact skin, mucociliary clearance mechanisms, low stomach pH, saliva, and other enzymatic-enriched secretions belong to this group.

2.1. The innate immune system

The innate immune system consists of hematopoietic-derived cells, which can be further classified into polynuclear granulocytes (neutrophils, eosinophils, basophils, and mast cells), mononuclear granulocytes (monocytes and tissue-resident macrophages), Langerhans cells, dendritic cells, natural killer (NK) cells and innate lymphoid cells (ILCs), and natural killer (NK) T cells. Most innate immune cells function as sentinel cells and populate the sites of body barriers. Innate immune cells possess a repertoire of pattern recognition receptors (PRRs), including Toll-like receptors (TLRs), NOD-like receptors (NDRs), complement receptors (CR), and killer-cell immunoglobulin-like receptors (KIRs) [4, 5].

2.2. The adaptive immune system

The adaptive immune system is composed of highly-specialized systemic T and B lymphocytes. The adaptive immune response holds an extremely diverse and randomly generated collection of cell receptors (T cell receptor (TCR) and B cell receptor (BCR)) produced by a somatic recombination mechanism, which, in turn, leads to the antigen-dependent and antigen-specific functionality of this system [6]. Antigen presentation plays a central role in generating adaptive immunity and is performed by antigen-presenting cells (APCs) of the innate immune system, mainly dendritic cells and macrophages as well as by B cells [7].

Taken as a whole, the different immune cells orchestrate barrier surveillance by an interaction of the innate and adaptive immune system.

2.3. Innate immune cells

Monocytes are completely dependent on macrophage colony-stimulating factor (M-CSF) for their development and survival especially in mice. Monocytes are heterogeneous and consist of different subsets distinguishable by their surface markers and functions [8]. In mice, the "classical monocytes" are defined by CD11b, a glycoprotein also known as integrin alpha M, and by high lymphocyte antigen 6 C expression ($Ly6C^{Hi}$), a part of the granulocyte differentiation antigen 1 (Gr-1). These

monocytes are rapidly recruited to the site of infection or tissue injury and can act as precursors of peripheral mononuclear phagocytes by differentiating into macrophages and dendritic cells [9].

Macrophages represent the mature form of monocytes and are resident in almost all tissues, where they take various forms (with various names) in a highly heterogeneous manner with a multifunctional character [10-12]. One major function of macrophages is to ingest and kill microbes by fusing the trapped microbe in the phagosome with a lysosome, harboring enzymes and free radicals, which help to destroy the microbe [13]. On the other hand, macrophages display also regulatory and protective roles [13]. Inflammation-induced macrophages (by LPS or Interferon-γ (IFN-γ)) are called "classically activated" macrophages (M1 macrophages) [14]. They defend the host from a variety of pathogens and have roles in antitumor immunity. Macrophages stimulated by interleukin-4 (IL-4) or IL-13, referred to as M2 macrophages, have immunosuppressive and anti-inflammatory roles and are important in wound healing [14]. They sense signals, which are associated with invading pathogens and dying or dead cells, through pattern-recognition receptors including Toll-like receptors or C-type lectin receptors, and they play an important role in the clearance of apoptotic cells (termed efferocytosis), and in the remodeling of the extra cellular matrix, which has been described in detail [13, 15]. Most murine macrophages are defined by the expression of CD11b in combination with F4/80, a member of the epidermal-growth-factor (EGF)-transmembrane 7 family. Different expression intensities define varying macrophage subtypes within a tissue.

Eosinophils are granulocytes that express cytoplasmic granules containing cytotoxic enzymes and are important for parasite defense. Under baseline conditions, they are mostly found in mucosal linings of the respiratory and gastrointestinal tracts. Their number can massively increase at the site of inflammation, where they then release their cytotoxic granules in "bit-by-bit" degranulation steps into the extracellular space. Upon immunoglobulin, complement and particularly IL-5 activation eosinophils secrete various pro-inflammatory cytokines and chemokines [16, 17]. In general, IL-5 has a central role in maturation and differentiation of eosinophils [18]. Along with other

surface markers, eosinophils in mice can be defined by the expression of $CD11b^+$ Siglec F^+ (CD170).

Basophils represent the smallest subset of granulocytes. They differentiate from the granulocyte-monocyte progenitors and fully mature in the bone marrow. Under normal conditions, they are found the in the periphery. During parasitic infections or allergies they migrate into the affected tissue [19, 20]. Basophils are a major source of IL-4 and can even function as antigen-presenting cells inducing differentiation of naïve T cells into T helper 2 (Th2) cells [21].

Mast cells arise from common myeloid progenitors. Mast cells mature under the influence of the c-kit receptor (CD117) and the stem cell factor (SCF), which is mainly produced by fibroblasts, while IL-3 plays another supportive role in growth and differentiation [22]. Mast cells reside in connective tissue at sites that are exposed to the external environment, such as the skin, the airways and the intestine. They patrol in areas below the epithelium and are placed to function as sentinel cells in host defense against microbes and parasites. The most common way to activate mast cells is by crosslinking IgE-Fcε Receptor 1 (Immunoglobulin E; FcεR1) with an antigen (such as an allergen) [23]. Mast cells are also involved in physiological functions, including vasodilation and angiogenesis [24]. Mast cells store granules with a combination of inflammatory mediators including histamine, heparin, and a variety of cytokines, chemokines, growth factors and antimicrobial peptides [25]. In mice mast cells can be defined by the surface expression of c-kit and FcεR1.

Neutrophils play a major role in the first line of defense against invading pathogens. The granulocyte colony-stimulating factor (G-CSF) is the predominant factor regulating proliferation, survival, differentiation, and trafficking/mobilization [26]. Also, IL-3 and IL-6 play an additional role for proliferation and granulocytic differentiation [27]. Neutrophils are the most abundant and important factors in the innate immune response [28]. Neutrophil effector functions include phagocytosis, the formation of effector granules, respiratory burst, NETosis (neutrophil extracellular trap — NET), and cytokine production [29]. Neutrophils are defined by the expression of CD11b together

with the lymphocyte antigen 6 complex – locus G (Ly6G), a part of the granulocyte differentiation antigen 1 (Gr-1) [30].

Dendritic cells (DCs) play an important role in the innate and adaptive immune system. DCs can be divided into three groups: (1) the conventional DCs (cDCs), (2) plasmacytoid DCs and the (3) inflammatory DCs [31]. Dendritic cells are rare cells but widely distributed in the majority of tissues. Dendritic cells are equipped with various pathogen-recognition receptors, allowing them to sense the environment, and express major histocompatibility complex (MHC) class I and class II molecules to present antigens. In general, DCs are specialized in the capture, processing, and presentation of antigens to naïve $CD4^+$ T cells. Depending on the type of DC and its activation state, the DC-T cell interaction leads to the initiation of an immune response or to T-cell tolerance [31, 32]. In mice, classical DCs are defined as $CD11c^{Hi}$ MHC class II^+ cells [33].

Natural Killer cells – Innate Lymphoid cells arise from the common-myeloid progenitor and represent a diverse population of cells that have lymphoid characteristics but lack the V(D)J-rearranged antigen receptors [34]. They play a role in the innate immune system. ILCs can maintain homeostasis in epithelial surfaces (e.g. skin, gastrointestinal tract, and respiratory tract) by responding to locally produced cytokines [34].

ILCs have been classified into three groups:

(1) ILC1 cells, which include conventional NK cells, express the transcription factor T-bet, which cooperates with eomesodermin — the transcription factor of NK cells [35]. ILC1 cells produce the T helper type 1 cytokine IFN-γ [36].

(2) ILC2 cells, which include nuocytes and natural helper cells, express the transcription factor GATA-3 and produce typical T helper type 2 cytokines IL-5 and IL-13 [36].

(3) ILC3 cells, which include lymphoid tissue-inducer cells (LTi), are crucial for lymph node development, express the transcription factor RORγt and produce effector molecules IL-17, IL-22, and they may also secrete IFN-γ and IL-13 [36].

Altered epithelial barrier function seems to be a key point in activation of ILCs to promote inflammatory responses [37]. The ILCs take part in the initiation and maintenance of defense against infections as well as immune-mediated diseases. Also,

NK cells have been described to act against viral infections and are involved in tumor immune surveillance. The development and functional activities of ILCs and NK cells are controlled by several factors among which the usage of the common cytokine-receptor gamma chain (γ_c or CD132; part of the IL-2 Receptor — IL2RG) plays a major role. In particular, IL-2, IL-7, IL-9, IL-15 and IL-21 are the members of this family predominately involved in the biology of NK and ILCs, respectively [38].

The **Natural Killer T cells** carry a TCR with an limited diversity of the TCRα chain and a restricted-assortment of TCRβ chains which are generated by somatic V(D)J gene rearrangement in the thymus [39]. These Type 1 Natural killer T cells are also called invariant natural killer T cells (iNKT) and are classified as CD1d-restricted T cells. The ability of these cells is to recognize alpha-galactosylceramide (α-GalCer) in association with CD1d-mediated presentation [40]. CD1d – a non-polymorphic major histocompatibility complex (MHC) class I-like molecule – is expressed by several cells of hematopoietic origin. NK T cells act at the interface between innate and adaptive immune response [40].

2.4. Adaptive immune cells

Both, T and B lymphocytes are the key players of the adaptive immune system. In response to pathogens, naïve T and B lymphocytes undergo activation and proliferation, giving rise to progeny with effector and memory fates that are able to mediate immediate long-term protection.

T Lymphocytes

The progenitors of the immature form of T lymphocytes develop in the bone marrow and mature in the thymus, where they become naïve T cells [41]. The thymus represents an epithelial-mesenchymal tissue, anatomically structured into cortical and medullary regions that contain stromal cells and epithelial cells, and the thymus supports the differentiation and selection of T cells [42]. The cortical thymic epithelial cells (cTECs) and medullary thymic epithelial cells (mTECs) interact with developing thymocytes and provide essential signals during thymopoiesis [43]. Lymphoid progenitors enter the thymus through blood vessels at the cortico-medullary junction, and then migrate

through the cortex to the subcapsular zone as $CD4^-CD8^-$ double negative (DN) thymocytes. Following pre-T-cell receptor (TCR)-mediated selection, DN thymocytes mature into $CD4^+CD8^+$ double positive (DP) thymocytes that accumulate in the outer cortex. The positive selection of DP thymocytes in the cortex results in further maturation to $CD4^+$ and $CD8^+$ single positive (SP) thymocytes that migrate back across the cortex toward the thymic medulla where positively selected SP cells interact with mTECs to complete thymocyte development and ensure central tolerance. During T cell development, T cells undergo TCR gene rearrangements – V(D)J recombination process – to form their lineage-specific TCR, upon which their function will depend. [41]. These cells are divided into two groups: (1) αβ-recombined TCR T cells or (2) γδ-recombined TCR T cells [44]. αβ T cells additionally express CD4 or CD8 glycoproteins [45]. The CD3 complex associates non-covalently with the T cell receptor of αβ T cells and γδ T cells [46].

Depending on molecular signals present in their milieu in peripheral lymphoid organs, different subpopulations of effector helper αβ T cells can develop. The T helper cells express CD4, and the TCR binds antigens presented with MHC class II molecules. Each sublineage secretes a unique pattern of cytokines and generates a specific function to regulate immune responses (summarized in **Figure 2**) [47].

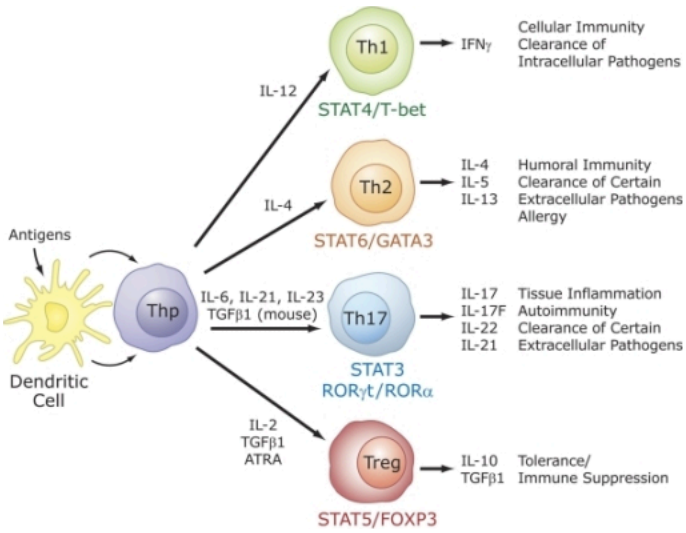

Figure 2. αβ T helper subtypes. Activation and differentiation of naïve T helper progenitors (Thp) into different subtypes of effector T helper cells. Corresponding transcription factors and signal transducer and activator of transcription (STAT) are marked below each T helper cell. Priming cytokines to induce differentiation are written along black arrows. The unique cytokine pattern and function of each T helper effector cell are noted next to each T cell. Figure adapted from www.open.nil.nih.gov.

Activated **CD8⁺ T cells** are also called **cytotoxic T cells** (CTLs). The TCR of CD8⁺ T cells bind antigens presented with MHC class I molecules, which are expressed on every cell [48]. The transcription factors T-bet and eomesodermin are involved in the fine-tuning of CD8⁺ effector (CLTs) and memory T cell differentiation. IL-2 promotes proliferation and differentiation of CD8⁺ T cells into CTLs and memory cells. IL-15 is important for the survival of memory CD8⁺ T cells. After clonal expansion, activated CD8⁺ T cells patrol the internal environment in search of infected cells. CD8⁺ T effector cells secrete tumor necrosis factor alpha (TNF-α) and IFN-γ, which have anti-tumor and anti-microbial effect [49]. Cytotoxic effector T cells can kill by permeabilizing the membrane of malignant cells with the help of perforin — which is stored in granules — and induce apoptosis via granzyme-induced caspase activation or the Fas/FasLigand pathway.

γδ T cells are a subset of effector lymphocytes with a unique TCR comprising variant combination of a γ-chain and δ-chain. They play a pivotal role in the first line of defense against microbes in epidermal and mucosal barriers and are therefore important for the surveillance of body barriers. Effector IFN-γ-producing γδ T cells express the transcriptional regulator T-bet, whereas IL-17-producing γδ T cells development involves RORγt [44].

T cell-mediated immune responses to an antigen usually result in the generation of memory T cells specific for that antigen, which may persist for years, even a lifetime. The transcription factor Blimp-1 and the cytokines IL-7 and IL-15 are important for the generation and maintenance of memory T cells.

B Lymphocytes

The maturation of B cells from progenitors committed to this lineage occurs mostly in the bone marrow and before birth in the fetal liver. Fetal liver-derived stem cells give rise mainly to B-1 cells with less diverse antigen receptors. In the bone marrow B precursor cells form a premature functional B cell antigen receptor (BCR) — generated by V(D)J recombination — and are tested for autoreactivity to maintain central tolerance mediated by receptor editing and negative selection [50]. Immature transitional B-2 cells then migrate into peripheral lymphoid organs (lymph nodes and spleen) and develop into (i) marginal-zone B cells or (ii) follicular B cells. In contrast to

follicular B cells, marginal-zone B cells produce antibodies with very limited diversity. With the help of follicular dendritic cells and follicular helper T cells — together with activated B cells — germinal centers (GCs) are formed and maintained in secondary lymphoid organs [51]. Within GCs, memory B cells are generated, and B cells secreting high-affinity immunoglobulins (Ig) (affinity maturation) develop and differentiate into specific antibody-producing plasma cells, diversified by somatic hypermutation of the immunoglobulin variable gene segments [52-54]. Helper T cell-derived signals, including CD40L and different cytokines, induce isotype switching in B cells. Upon activation, B cells have the capacity to produce different antibody isotypes, which provide a remarkable plasticity to perform distinct effector functions. The outcome of B cell differentiation is regulated by the induction and activation of different transcription factors and transcriptional activators. The transcription factors Blimp-1 and IRF4 commit activated B cells to plasma cells, and Pax5 is required for the maintenance of mature B cells.

B cells can be defined by the expression of CD19, which assembles with the BCR and regulates B cell development, activation, and differentiation [55].

The function of immune cells of the innate and adaptive immune system is rather complementary so that defects in either system results in the host's vulnerability.

3. Primary Immunodeficiency

Primary immunodeficiency diseases (PIDs) are a group of rare diseases caused by genetic defects. The clinical features are highly variable, but they all result from a defect in one of the functions of the body's normal immune system. Most primary or congenital immunodeficiencies result in an increased susceptibility to infections and may lead to immune dysregulation. Most PIDs are diagnosed in infancy and early childhood, but sometimes they are clinically detected later in life.

Today, over 300 different single-gene inborn errors have been described, and they are characterized by genetic mutations. PIDs are classified according to the component of the immune system that is primarily involved into 1. immunodeficiencies affecting cellular and humoral immunity, 2. combined immunodeficiencies with syndromic

features, 3. predominantly antibody deficiencies, 4. diseases of immune dysregulation, 5. congenital defects of phagocyte number, function or both, 6. defects in intrinsic and innate immunity, 7. autoinflammatory disorders, and 8. complement deficiencies [56, 57]. The immunodeficiencies affecting "cellular and humoral immunity" arise from defects affecting T lymphocytes. Severe combined immunodeficiencies (SCIDs) arise from a complete lack in T cell development and, in some cases also block other lymphoid lineages. The study of human T-cell PIDs with Mendelian inheritance has enabled the molecular characterization of important key functions and pathways in T-cell biology. Mutations in the recombinase activating genes (RAG1/2) — RAG1/2 genes are important to form functional T cell receptors during thymopoiesis — and (ii) mutations in the common cytokine receptor gamma chain (IL2RG) lead to defects in T-cell differentiation and the premature death of progenitor cells resulting in the typical SCID phenotype, characterized by a virtual lack of circulating autologous T lymphocytes and absence of functional T-cell responses. Not only lymphoid cells can be affected; for instance, in the case of reticular dysgenesis, mutations in the adenylate kinase 2 (AK2) gene lead to maturation defects in lymphoid and myeloid cells [58].

3.1. Thymic defects — treatment

Most of these severe primary immunological diseases are commonly treated by allogeneic hematopoietic stem cell transplantation (HSCT) or, in some cases, by gene therapy with re-infusion of genetically modified autologous hematopoietic cells. Instead, thymus transplantation is a therapeutic option for infants with DiGeorge Syndrome (22q11.2 deletion syndrome; deletion of genes required for thymus development) and Winged helix deficiency (mutation in *FOXN1* gene; important for thymus development).

Although, these procedures have been successful in treating some immunodeficiencies, but they have not been so in treating diseases affecting multiple organs alongside the hematopoietic system. These challenges ask for new approaches to discover treatments for rare diseases affecting multiple organs, and individually optimized therapy concepts have to be targeted. The target-specific therapeutic agents must be able to trigger cellular functions that are enhanced or suppressed to compensate for imbalanced or missing functionality of the affected gene.

4. The Non-Hematopoietic System

Hematopoietic cells are also strongly influenced by the surrounding non-hematopoietic cells, which consist of tissue-forming cells (fibroblasts, endothelial cells, epithelial cells, nerve cells, etc.) that form the environment in which immune responses can occur [59]. Not only failures in the hematopoietic system can lead to life-threatening disorders, defects in the non-hematopoietic system can also be the cause for a disease.

In vertebrates, after fertilization, the development of a multicellular organism begins from a single-celled zygote [60]. A zygote undergoes rapid cell division to form a spherical ball of cells, the blastula. At this stage in mammals, they are called blastocytes [60]. The next step in embryonic development is the formation of the gastrula. During triploblastic gastrulation, three germ layers, the ectoderm, endoderm and mesoderm layers, are formed [60]. Each of these germ layers develops into different organs or tissue systems (**Figure 3**). This involves the coordination of multiple complex developmental processes, such as embryonic induction, pattern formation, morphogenesis, cell proliferation, and differentiation.

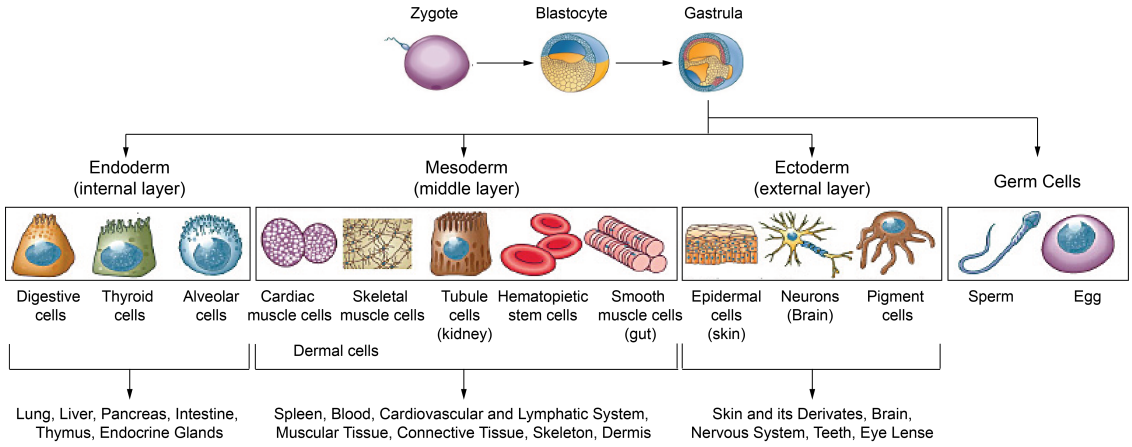

Figure 3. The three germ layers during embryogenesis. The three germ layers endoderm, mesoderm and ectoderm give rise to all of a vertebrate's tissues and organs [60]. Figure adapted and adjusted from threesology.org.

4.1. The skin

The skin is the largest organ of the body. It is a constantly renewing organ that provides a protective covering essential for thermal and osmotic regulation in preventing unregulated loss of water and solutes. It also functions as an effective barrier between an organism and the environment, protecting against invasion by pathogens and fending off chemical and physical injuries. The skin consists of two major components: a

stratified squamous epithelium and the dermis. The dermis is part of the connective tissue and is a highly vascularized region, drained by lymphatic vessels, equipped with sensing nerve ends and hair follicles, composed of mesenchymally derived fibroblasts, rich in collagen, elastin and fibers, and other components of the extra cellular matrix (ECM) (**Figure 4**) [61]. Draining lymphatics begin in the dermis and traverse the deeper layers of the skin to eventually access lymph nodes. An accurate interplay between the cells of the epidermis and dermis is needed to establish a proper dermo-epidermal architecture, a polarized pattern of epithelial growth, and differentiation of the basal layer of proliferating keratinocytes, and the formation of dermal-resident fibroblasts [61].

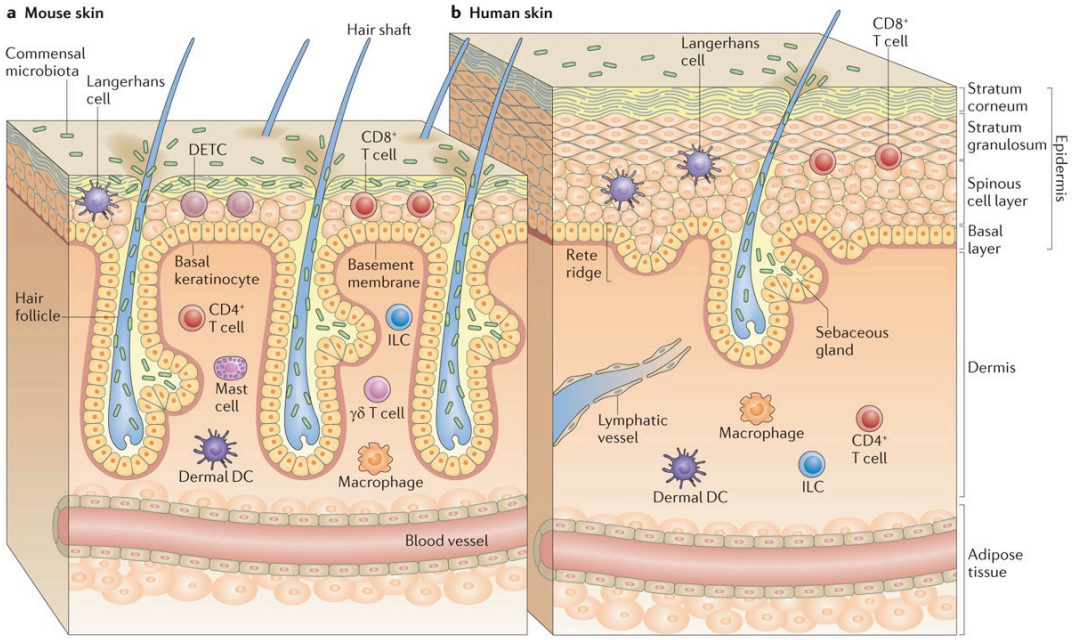

Figure 4. Difference in structure and cellular components between mouse and human skin. (**a**) Mouse skin is densely packed with hair follicles and has a thin epidermis. In the epidermis, the most prominent population is dendritic epidermal T cells (DETCs). Recruited γδ T cells play an important role in skin immune surveillance and IL-17 and IL-22 production. (**b**) The human epidermis has larger areas of interfollicular skin with sparse hair follicles and a thick epidermis with more cell layers. The most prevalent immune cells in the epidermis are Langerhans cells and $CD8^+$ T cells. In both, mouse and human, the dermis is populated by macrophages, mast cells, conventional αβ T cells, and some innate lymphoid cells (ILCs). Figure adapted from [62].

Skin homeostasis and immunity are mainly controlled by the crosstalk between immune cells, vascular endothelial cells, fibroblasts, and keratinocytes. This epidermal-dermal cell interaction is driven by cytokines, chemokines, antimicrobial peptides (AMPs), and growth factors [63, 64]. Many different populations of myeloid and

lymphoid immune cells either reside in or traffic into the dermis. These immune cell populations are dynamic and change during immune responses.

4.1.1. Keratinocytes

Skin epidermis can be divided into a viable stratified squamous part and a dead layer — the stratum corneum (**Figure 5**). The latter consists of additional 3 diversified layers/strata: (1) stratum basale (basal layer), (2) stratum spinosum (spinous layer), and (3) stratum granulosum (granulose layer). The stratum basale, or basal layer, harbors proliferative self-renewing cells — rapidly dividing progeny stem cells. These are undifferentiated basal keratinocytes that undergo a limited number of divisions — this is referred to as transit amplifying [65]. Before keratinocytes withdraw from the cycle to become differentiated, they detach from the basement membrane to begin a maturation process during which they migrate toward the surface of the skin. Keratinocytes in the stratum granulosum are characterized by dark clumps and produce keratin proteins and lipids [66]. Keratinocytes that reach the body surface are the ultimate product of maturing keratinocytes. These are dead, enucleated, flattened keratinocytes (squames) that are subsequently sloughed and are continually replaced by inner cells that move outwards. The keratinocytes in this layer are called corneocytes and form the outermost layer — the stratum corneum. The stratum corneum builds a permeability barrier to prevent excessive water loss and penetration of water-soluble substances. Each corneocyte is surrounded by a protein shell called cell envelope. The cell envelope is composed of two proteins, loricrin and involucrin. These proteins contain extensive links between each other, making the cell envelope the most insoluble structure of the corneocytes. Attached to the cell envelope is a layer of ceramide lipids that repel the water. Corneocytes are held together by corneodesmosomes. The corneal layer is a unique layer to the skin and not present in other epithelia (such as in the gut or the lungs).

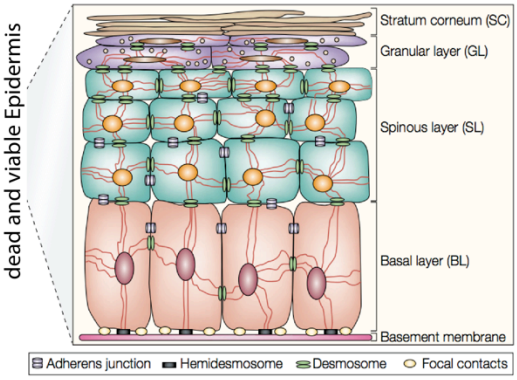

Figure 5. Layers of the dead and viable epidermis. The viable mammalian epidermis is a stratified squamous epithelium that can be divided into different cell layers. Resting on the basement membrane is the basal layer (BL) consisting of proliferating, transit-amplifying cells (dividing progeny of stem cells). The basal layer stratifies to give rise to differentiated cell layers of the spinous layer (SL), granular layer (GL), and a layer containing dead cells — the stratum corneum (SC). Figure adapted from [61].

The stratum corneum and tight junctions within the stratum granulosum ensure an effective physical barrier. The corneal layer also provides a scaffold function for microflora (antimicrobial activity). Keratinocytes express many pattern-recognition receptors, such as functional TLRs and NLRs, which make them able to respond to stimulation by pathogens or stress factors, and therefore able to induce immune responses [66].

In the skin, keratinocytes are an important source of cationic antimicrobial peptides (AMPs), such as β-defensins and cathelicidins [67, 68]. In addition to AMPs, keratinocytes constitutively secrete, or can be induced to release, a wide range of cytokines, including IL-1, IL-6, IL-10, IL-18, IL-33 and TNF-α [69, 70]. Thus, keratinocyte-intrinsic pathways play a key role in regulating immune homeostasis and inflammation in the skin. Conversely, inflammation does also regulate keratinocyte proliferation [71].

4.1.2. Fibroblasts and the extracellular matrix (ECM)

The dermis consists of mesenchymally derived fibroblasts, and a mixed population of innate and adaptive immune cells. Fibroblasts are the most common cells that make up the structural framework of connective tissues. Fibroblasts are the primary cells that build and maintain the ECM [72, 73].

Fibroblasts play a pivotal role in regulating the skin physiology, and they are usually quiescent and become activated in wound healing processes [74]. Once activated, the functions of fibroblasts include synthesizing the extra cellular matrix, generating

cytokines and chemokines, recruiting immune cells and exerting physical forces to modify tissue architecture [75]. Fibroblasts can produce TNF-α, IL-6, IL-8 and diverse set of growth factors, including epidermal growth factor (EGF) and fibroblast growth factors (FGFs) [76]. FGFs are polypeptide growth factors with diverse biological activities, and induce positive and negative regulation of proliferation, survival, migration, and differentiation [77]. For instance, FGF3, FGF7, FGF10 and KGF1 (keratinocyte growth factor 1) are known to induce keratinocyte proliferation [78, 79].

The extracellular matrix is highly conserved among species and is assembled into diverse structures depending on the tissue and its particular composition of the ECM proteins [80]. The ECM consists of a diverse set of metalloproteinases, growth factors, as well as fibrous proteins, such as collagens, elastin, fibronectin, glycosaminoglycans, and many others [80]. The ECM is involved in many developmental, physiological and pathological processes, including cell proliferation, tissue homeostasis, differentiation, cell adhesion and cell migration [81-83]. Cell migration and adhesion are controlled by integrins and the components of the ECM [84, 85] (**Figure 6**). Cell-ECM interactions are crucial in angiogenesis and the formation of the cardiovascular system.

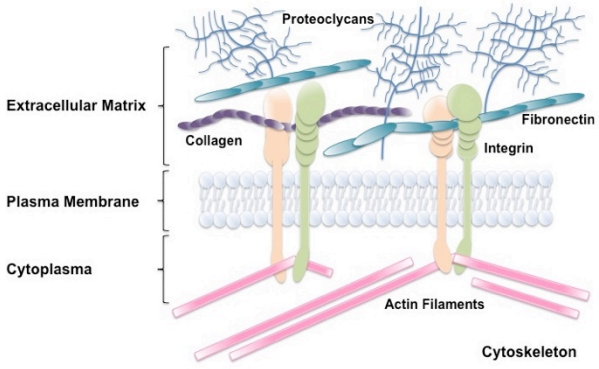

Figure 6. Components of the extra cellular matrix. The extra cellular matrix is the non-cellular component present within in all tissues and organs [86]. For instance, collagen, proteoglycans, fibronectin and other compounds play an important role for cell adhesion and migration. Integrins expressed on the cell surface can interact with the ECM components to perform motility [84].

The ECM directs essential morphological organization and physiological function by binding growth factors to elicit signal transductions [77]. Consequently, the ECM plays a fundamental role in the dermis and other tissues.

It is the organization of the stromal cell network that provides support for adaptive and innate immune cells to drive efficient immune responses. This interdependence of

stromal cells of different lineages with all types of hematopoietic cells plays, therefore, an integral part in forming skin immunity. Even in healthy tissue, the type of stroma and its cellular activity influence its hematopoietic composition.

4.2. Skin disorders

Numerous skin disorders, such as psoriasis, atopic dermatitis, or contact dermatitis are associated with dysregulation of immune responses in the skin.

4.2.1. Psoriasis

Psoriasis is a chronic lifelong inflammatory skin disease that develops in genetically susceptible individuals upon unknown initial environmental, pathogenic, or internal triggers. Psoriatic skin is characterized by keratinocyte hyperproliferation, leading to thickening of the epidermis (acanthosis), combined with dysregulated keratinocyte differentiation resulting in altered protein expression, loss of a mature granular layer and retention of keratinocyte nuclei (parakeratosis) (**Figure 7**). These changes are accompanied by increased dermal vascularity and accumulation of inflammatory infiltrates of T cells, neutrophils, and macrophages [64]. The immunopathogenesis of psoriasis is a close interdependence of the epidermis and dermal inflammatory infiltrates, as well as a balance between innate and adaptive immune system.

By analogy with autoimmune-type diseases, psoriasis has been considered a Th1-type disease, where TNF-α, IL-2, and INF-γ play a role [87]. The current view involves Th1, Th17 and Th22 cells and proposes a model in which activated dendritic cells and macrophages express IL-12 and IL-23, which causes T cells to differentiate toward effector cell activity [88-90]. Data from clinical studies and experiments in mouse models describe the IL-23/IL-17 axis as the essential pathway in the pathogenesis of psoriasis [91-93].

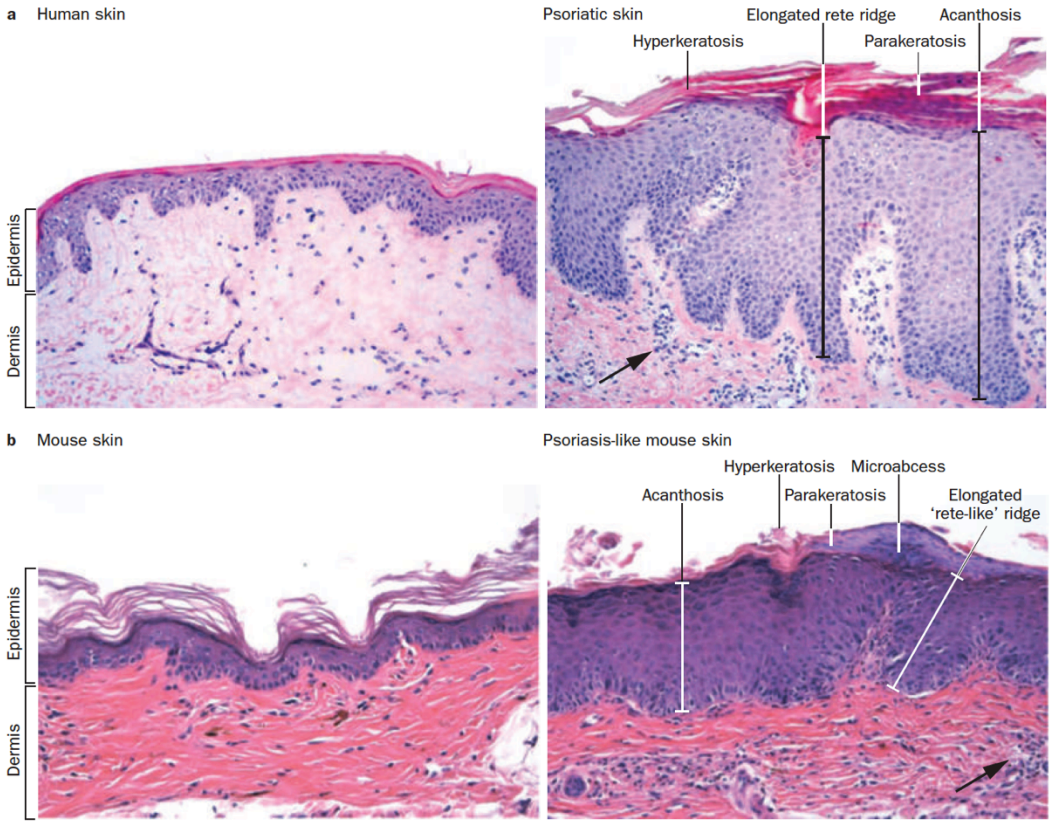

Figure 7. Difference between human and mouse skin. (**a**) Histological overview of human healthy (left) and psoriatic (right) skin (hematoxylin-eosin (H&E) staining; Magnification: x20). Acanthosis (epidermal thickening) is accompanied with elongated rete ridges. Hyperkeratosis of the stratum corneum (cornified layer thickening). parakeratosis (presence of nuclei in cornified layer) and scales peeling off are shown. The black arrow indicates dermal inflammatory infiltrates. (**b**) Histological features of murine healthy (left) and psoriasis-like (right) skin (H&E; Magnification: x20). Acanthosis with elongation of rete-like ridges, hyperkeratosis with microabscesses of inflammatory cells (neutrophils), parakeratosis, and scales peeling off are shown. The black arrow indicates dermal inflammatory infiltrates. Figure adapted from [94].

In the Aldara-treated mouse model, it has been shown that formation of psoriatic lesions depends on γδ T cells (Vγ4+ TCR) in the absence of Th17 and Th22 cells. These γδ T cells together with type 3 innate lymphoid cells (ILC3) are the main source of IL-17A, IL-17F and IL-22 [95]. IL-17 regulates antimicrobial peptides (AMPs), whereas IL-22 acts on keratinocytes to induce hyperproliferation [96]. Therapeutic studies of psoriasis are based on clinical observations in humans [97]. Today, anti-IL17A antibodies and anti-IL12/23p40 antibodies are used to treat psoriasis [98, 99].

4.2.2. Atopic Dermatitis

Atopic Dermatitis (AD) is the most common inflammatory skin disease worldwide. Impaired skin barriers with increased trans-epidermal water loss and sensitization to

allergens often caused by filaggrin deficiency and Th2/Th22-skewed inflammation are critical biological features observed in the majority of patients [100-102]. There is a consensus that the leaky epithelial barrier facilitates allergen sensitization and promotes exposure to infectious agents [103]. The magnitude of skin barrier dysfunction correlates with AD disease severity. Acute AD skin lesions are characterized by thickening of the epidermis and dermis, dermal infiltration of $CD4^+$ T cells and eosinophils, increased expression of Th2-related cytokines IL-4 and IL-13, and Th22-related cytokine IL-22. A recent study did focus on the mechanism of cutaneous sensitization driven by IL-23-producing dendritic cells in a mouse model with similar features to AD. The results describe a novel pathway in which IL-23 released by keratinocytes after mechanical skin injury targets skin dendritic cells, up-regulating their endogenous IL-23 production and polarizing them to drive an IL-22 response in naïve $CD4^+$ T cells, which, in turn, mediates epidermal thickening [104]. An ongoing trial is also testing the utility of IL-23 and IL-22 blockade in AD.

5. *TTC7A* Mutations in Humans

Mutations in the tetratricopeptide repeat (TPR) domain 7A gene (*TTC7A)* cause an autosomic recessive multi-organ disease. The disease is caused by homozygous or compound heterozygous mutations spread along the *TTC7A* gene localized on chromosome 2p21 (**Figure 8**). *TTC7A* deficiency is a rare devastating disease where less than 50 patients have been described so far. The disorder presents with immune defects ranging from severe combined immunodeficiency (SCID) to hypogammaglobulinemia and autoimmunity [105-113]. Most patients suffer from MINAT (OMIM #243150), which is known as multiple intestinal atresia, or GIDID (OMIM #243150), which stands for gastrointestinal defects and immunodeficiency syndrome. In some cases, patients present with a very early onset inflammatory bowel disease (VEOIBD), and enteropathy-lymphocytopenia-alopecia (ELA) syndrome have been described [105, 107-114].

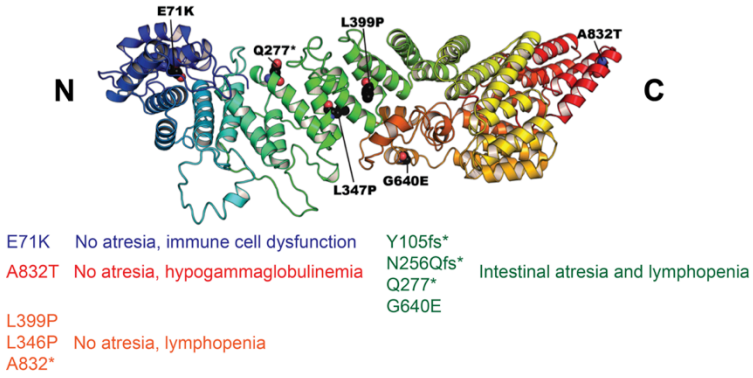

Figure 8. Overview of all known homozygous disease causing mutations in TTC7A deficiencies. The TTC7A crystal structure was predicted based on the available structure of TTC7B (over 95% structural similarity). The C- and N-terminus are given in black capital letters. The position of amino acids affecting disease-causing mutations is given in small black letters and described below the protein structure. "*" = stop codon, "fs*" = frame shift lead to stop codon. This figure was drawn in collaboration with Prof. Sebastian Hiller, Biozentrum, Basel.

Overall, the gut is the most affected organ — ranging from intestinal atresia at birth to inflammatory bowel disease. Despite successful hematopoietic stem cell transplantation in combination with surgical outcomes in patients with atresia are often poor. Unfortunately, the ongoing progression of gastrointestinal disease can be life-threatening. This observation indicates that the loss of TTC7A function does not only affect immune homeostasis but also the stromal compartment. Epithelial cell-intrinsic effects have been suspected to link *TTC7A* mutations with disrupted apicobasal polarity of the intestinal epithelium. Pathological examination of gut biopsies from *TTC7A*-deficient patients affirmed an inverted enterocyte polarity in patient-derived gut organoid cultures [107, 108].

5.1. Spontaneous gene mutations in murine *Ttc7*

Based on gene homology, three mouse strains are known and commercially available, carrying spontaneously occurring mutations in *Ttc7,* the orthologous gene to *TTC7A* in humans. *Ttc7* is localized on chromosome 17 and contains 20 exons. The hereditary erythroblastic anemia (*hea*) mutant mouse (*Ttc7*$^{hea/hea}$) carries a large deletion of exons 1–14 in *Ttc7*. The mutation is inherited in an autosomal recessive manner. Affected homozygous *Ttc7*$^{hea/hea}$ mice have hematological abnormalities, a severe anemia since birth, and die at around 1 week of age [115]. An atrophic thymus and defective T-cell differentiation during thymocyte development have been reported [116]. The mutation in homozygous *Ttc7*$^{jic/jic}$ mice is caused by a genomic in-frame deletion, resulting in two

different but equally produced amplicons. Transcript 1 is missing exons 9 to 10, and transcript 2 lost exons 9 to 11. *Ttc7*$^{hea/hea}$ and *Ttc7*$^{jic/jic}$ mice show a similar phenotype, but *Ttc7*$^{jic/jic}$ mice have a longer life expectancy and die at around 2 weeks of age [117]. The flaky skin (*fsn*) mutant mouse (*Ttc7*$^{fsn/fsn}$) bears an insertion of an endogenous retrovirus-like element (ETn) between exons 14 and 15 [118]. This 183bp-long element leads to an enlarged protein of 858 amino acids. Studies using *Ttc7*$^{fsn/fsn}$ mice have focused on immunological dysfunction and autoimmunity [119-122]. We therefore decided to work with the flaky skin mutant mouse model, which results in a life expectancy of 3 months.

5.2. Flaky skin (*fsn*) mutant mouse model – *Ttc7*$^{fsn/fsn}$

In contrast to humans with intestinal disease, *fsn* mutant mice develop a severe hyperplastic dermatitis as the main feature associated with pleiotropic abnormalities, including a hyperproliferative immune disorder (splenomegaly and lymphadenopathy), gastric forestomach papillomas, anemia and autoimmunity [119, 121, 123-128]. The autoimmunity is presented by a hyperactivation of CD22^{Low} B cells (immature B cells) in the spleen, including a fraction of autoreactive B-1 cells [129]. This expansion and activation of autoreactive plasma cells leads to the production of circulating antinuclear autoantibodies, which is likely associated with a chronic IL-4 exposure. An overproduction of IL-4 has been described in hyperactivated splenic lymphocytes due to constitutive STAT6 activation, hyperresponsiveness to IL-2, IL-4, and IL-7, and enhanced IgE production in responses to ovalbumine [121].

The *Ttc7*$^{fsn/fsn}$ mouse has been regarded as a model for human psoriasis because of patchy, thick, white scales on the skin with microscopically evident acanthosis, parakeratosis and hyperkeratosis, mononuclear dermal infiltrates with increased amount of mast cells, and dilation of dermal capillaries [125-127].

The *Ttc7*$^{fsn/fsn}$ mouse strain shows some immune-related phenotypes that resemble those in humans with mutations in *TTC7A*. A study comparing the skin of patients with *TTC7A* mutations and that of *Ttc7*$^{fsn/fsn}$ mice reported on clinical, functional, and histopathological findings consistent with abnormal epidermal maturation and epidermal barrier dysfunction [130].

However, the *Ttc7* mutation in the flaky skin mutant mouse differs from the ones described in *TTC7A* in humans. The *Ttc7* mutation is based on an insertion, which

disrupts a tetratricopeptide repeat (TPR) domain. TPR-motifs are known to mediate protein–protein interactions and are essential for multi-protein complexes [131]. The mutation leads to reduced levels of wild-type transcripts. Ttc7 is expressed in many different tissues. Microarray analysis of mouse tissues has shown similar relative levels of *Ttc7* expression in bone marrow, lymph nodes, and various T and B cell subsets [117, 127].

6. TTC7 is a scaffold protein — A chaperone

TTC7 is ubiquitously expressed and functions as a scaffold protein known to play an essential role in localizing phosphatidylinositol 4-Kinase-IIIα (PI4KIIIα) to the inner leaflet of the plasma membrane [132]. PI4KIIIα is responsible for localization-specific phosphorylation of the hydroxyl group at the 4th position of the inositol ring to generate the most abundant monophosphorylated phosphatidylinositol 4-phosphates (PI4P). In the assembly, TTC7 plays a central role in bridging PI4KIIIα to EFR3B (membrane-resident anchor protein) and FAM126A, via direct interaction (similar to human TTC7A and TTC7B) (**Figure 9A**); this results in PI4P synthesis at the plasma membrane [133].

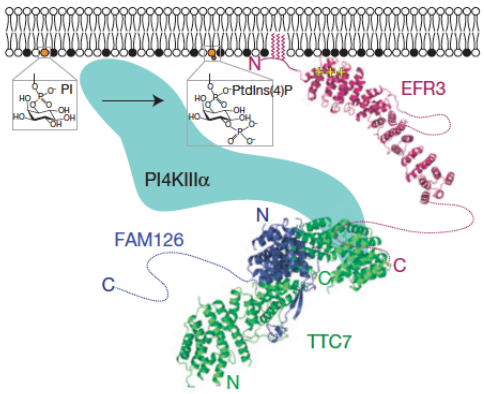

Figure 9A. **TTC7 act as scaffold protein in bridging PI4KIIIα to EFR3B at the plasma membrane via binding to FAM126**. PI4KIIIα phosphorylates phosphatidylinositol (PI) at the 4th position of its inositol ring to generate phosphatidylinositol 4-phosphate (PtdIns4P = PI4P). EFR3 — palmitoylated resident anchor protein (red), FAM126 (blue), PI4KIIIα (turquois), and TTC7 (green). Figure adapted from [133].

PI4P is the metabolic precursor of phosphatidylinositol 4,5-biphosphate (PI(4,5)P_2), the major substrate for receptor-linked phospholipase C and phosphatidylinositol 3-kinase (PI3K), and thereby it is essential in regulating a variety of signaling pathways in

different cell types. Furthermore, $PI(4,5)P_2$ plays a general role in actin polymerization at the plasma membrane, vesicular trafficking (endocytosis/exocytosis), cell motility, the formation of the immunological synapse, and other cellular processes [134-138] (**Figure 9B**).

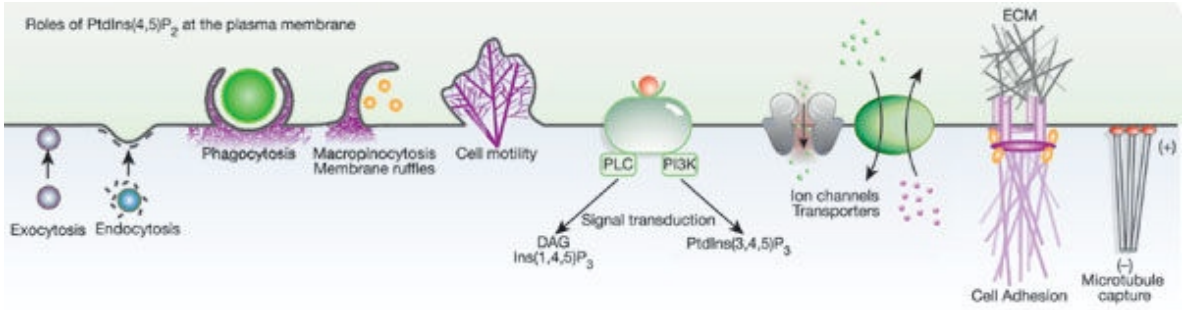

Figure 9B. Roles of $PI(4,5)P_2$ at the plasma membrane. (**B**) Examples of cellular processes regulated by $PI(4,5)P_2$ (= $PtdIns(4,5)P_2$) at the plasma membrane. PLC = phospholipase C; ECM = extracellular matrix. Figure adapted from [139].

Further synthesis of phosphoinositides have been widely implicated in receptor signalling and as anchors for structural proteins, therefore controlling a wide range of cellular processes, including cytokinesis, cell polarization, migration, adhesion, formation of the lamellipodium for cell motility, and morphogenesis [139]. The synthesis and turnover of phosphoinositides are spatially and temporally tightly regulated processes [21]. Dysfunctions in the control of the phosphoinositide levels often lead to pathologies [139].

6.1. *TTC7A* deficiency — a primary immunodeficiency combined with multisystemic disease

Genetic diseases with multisystemic outcomes, such as seen in *TTC7A* deficiencies, require a deeper understanding of the leading mediator(s) and mechanisms involved the pathogenesis of the disease. Dissecting the effect that a genetic mutation has on multiple-organs requires studies of each system separately.

Until now, it has not been clear whether the disease results primarily from intrinsic T cell defects, thymic epithelial defects, or both. Thus, the value of HSCT in patients carrying *TTC7A* mutations is subject to debate. Mouse models are of great benefit to study such multisystemic diseases.

The flaky skin mutant mouse model presents a multifactorial disorder with a striking hyperplastic skin phenotype. The overview of the pathophysiology of the flaky skin mutant mouse is still elusive. We do not know whether an intrinsic epidermal-barrier dysfunction is the initial insult that precedes dysregulated immune activation or if altered immune activation leads to reactive epidermal hyperplasia.

Considering the multisystemic disease in patients and the flaky skin mutant mouse with an evident skin pathology, we aimed to study the skin in different mouse strains carrying the flaky skin mutation with the focus to investigate whether cells of non-hematopoietic or hematopoietic origin trigger the development of the hyperplastic skin phenotype.

IV. MATERIAL and METHODS

1. Animals

All mouse experiments were performed in accordance with the Swiss Federal Veterinarian Office and Cantonal Veterinary Office guidelines.

1.1. The flaky skin mutant mouse – *Ttc7*$^{fsn/fsn}$

BALB/cBy.A-fsn/+ mice (termed *Ttc7*$^{fsn/+}$, CD45.2) were obtained from The Jackson Laboratory (Bar Harbor, ME, USA) and maintained under specific pathogen-free conditions at the Laboratory Animal Services Center (University of Zurich, Zürich, Switzerland). Given that neither female nor male *Ttc7*$^{fsn/fsn}$ mice will mate, heterozygous *Ttc7*$^{fsn/+}$ mice were used to obtain wild-types (WT), heterozygous and homozygous mutant flaky skin mice for experiments. The mice used in these experiments were 2- to 14-weeks old. All mice were maintained and handled in accordance with Swiss Federal Veterinarian Office and Cantonal Veterinary office guidelines. The presence of the flaky skin was confirmed by a restriction site analysis of the PCR products of mouse ear DNA. Briefly, a punched sample (diameter: 1.5mm) from the mouse ear was incubated at 55°C in a lysis reagent (catalog 31-402-E) (Peqlab, VWR, Erlangen, Germany) containing proteinase K (0.2mg/mL) (catalog P4850) (Sigma Aldrich) for 5 to 16h. Proteinase K was inactivated by incubation at 85°C for 45 min. The resulting DNA-containing solution was then directly used for PCR assays with the following primers: WT: 5'-GAAGAGCAGCGCTAGCAAGT-3'; forward Ttc7: 5'-CAA GATGCTTGCTTCTGG-3'; reverse ETn: 5'-CCGATACGAAGATCCTTTCC-3' (94°C for 3min; 94°C for 30sec, 60°C for 30sec, 73°C for 45sec, 73°C for 5min; x40). The DNA samples were separated on a 1.5% agarose gel containing SYBR® Safe DNA Gel Stain (Invitrogen by Thermo Scientific) DNA from WT mice produced a single 450bp band only for the WT-DNA strain, DNA from *Ttc7*$^{fsn/fsn}$ mice produced a single 450bp band only for the mutant-DNA strain, and DNA from heterozygous mice produced a single 450bp band for the WT-DNA strain and a single 450bp band for the mutant-DNA strain.

1.2. Ly5.1 Balb/c mice

CBy.SJL(B6)-Ptprc<a>/J (Balb/c; CD45.1) mice were purchased from The Jackson Laboratory and used as controls for adoptive hematopoietic stem cell transfer (license No. 65/2014).

1.3. Rag2-deficient and Rag2-IL2rg-deficient mice

The C.129S7-Rag2<tm1Mom> (*Rag2*$^{-/-}$; Balb/c; CD45.2) mice and the Balb/c-IL2rg<tm1>B6.129S6-Rag2<tm1Fwa> (*IL2rg*$^{-/-}$, *Rag2*$^{-/-}$; CD45.2) mice were a generous gift from Professor Burkhard Becher (University of Zurich). These mice were crossed with *Ttc7*$^{fsn/+}$ mice for the generation of the double and triple homozygous mutant mice. The offspring of double and triple homozygotes were genotyped by using the following primer combinations. For the Rag2-knockout, the following primer combination was used: forward primer Rag1 5'-GGG AGG ACA CTC ACT TGC CAG TA-3', Rag2 5'-AGTC AGG AGT CTC CAT CTC ACT GA-3' and reverse Rag_{neo} 5'-CGG CCG GAG AAC CTG CGT GCAA-3' (94°C for 3min; 94°C for 30sec, 55°C for 30sec, 72°C for 45sec, 72°C for 5min; 35x; WT: 263bp, mut: 350bp).

The primer combinations for IL2rg-knockout were as follows: forward primer P5 5'-CCT GCG TGC AAT CCA TCT TGT TCA AT-3', reverse primer P7: 5'-CTGCTCAGAATGCCTCCAATTCC-3', and primer pNeo: 5'-CCT GCG TGC AAT CCA TCT TGT TCA AT-3' (94°C for 3min; 94°C for 30sec, 55°C for 30sec, 72°C for 45sec, 72°C for 5min; 35x; WT: 650bp, mut: 400bp).

All mice used in subsequent experiments were identified by genotyping with the specific primer combinations listed above.

2. Hematopoietic Stem Cell Transfer (HSCT)

2.1. Bone marrow isolation

Femur, tibia and fibula were collected from CO_2 euthanized mice and stored in PBS. Bone marrow was flushed with a 29G syringe and 1x phosphate buffer saline (PBS) (Gibco by Life Technologies™) supplemented with 2% fetal bovine serum (FBS, heat-

inactivated) (Sigma Aldrich) and 2.5mM EDTA (Sigma Aldrich). Whole bone marrow – Lin- and Lin+ cells – were purified with PBS and counted with Neubauer Improved chips, disposable hemocytometer (C-Chip, NanoEnTek). Bone marrow chimeras were generated by transplanting fresh 5 x 10^6 wild-type (Balb/c CD45.2) or 5 x 10^6 *Ttc7*$^{fsn/fsn}$ (Balb/c CD45.2) cells sampled from whole bone marrow. Cells were stored in an appropriate volume of sodium chloride solution (0.9%, B. Braun Medical AG) prior to tail-vein injection.

2.2. Irradiation

Mixed Lin- and Lin+ bone marrow cells were injected intravenously (i.v.) into total-body-irradiated female wild-type CD45.1–congenic host mice (Balb/c) receiving two 400 rad doses with a 24h inter-dose interval (225kV, 17.7mA) (RS-2000, Rad Source Technologies, Inc.). Bone marrow chimeric mice were allowed to reconstitute for 10 to 12 weeks without further treatment. Irradiated mice received a 1:250 dilution of 24% Borgal in their drinking water for 14 days.

3. Organ and Tissue Preparation

Mice were euthanized by CO_2 inhalation. Peripheral blood was immediately collected by cardiac puncture and kept in EDTA-coated tubes under rotation at room temperature (K2E BD Microcontainer, BD Biosciences™). Thymus, axillary and inguinal lymph nodes, spleen, skin (shaved areas) and gastrointestinal tract were isolated and stored in cold 1x phosphate buffer saline (PBS) (Gibco by Life Technologies™) supplemented with 2% fetal bovine serum (FBS) (Sigma Aldrich).

3.1. Histopathology

For histopathologic examination tissues (thymus, spleen, axillary and inguinal lymph nodes, skin, and gastrointestinal tracts – forestomach, duodenum, and colon) were fixed in 4% paraformaldehyde and embedded, following standard protocols. Deparaffinized

sections were stained with hematoxylin-eosin reagent according to standard protocols. Further, immunohistochemical stainings with anti-CD45/LCA (30-F11, 1:150, BD Bioscience), anti-CD3 (Rabbit Mab RMAB 005, 1:150, Diagnostic Biosystems), anti-CD4 (4SM95, 1:150, eBioscience™), anti-CD19 (pY531, 1:150, Abcam), anti-B220 (RA3-6B2, 1:150, BD Biosciences), anti-IL-17 (ab79056, 1:150, Abcam), anti-IL-22 (NB100-738, 1:150, Novus Biologicals, Biotechne brand), and anti-CD11c (HL3, 1:150, BD Biosciences) according to manufacturer's instructions were performed followed by counterstaining with hematoxylin and a BOND™ Bond Polymer Refine Detection Kit (Leica Biosystems, Newcastle, United Kingdom). The images were acquired with a bright field light microscope (Zeiss Axio Observer, Carl Zeiss AG, Switzerland) at a magnification of 5x or 10x.

4. Flow Cytometry

4.1. Cell preparation

4.1.1. Thymus, spleen, skin-draining lymph nodes

Single-cell suspensions were prepared from thymus, spleens, and skin-draining lymph nodes (axillary, brachial and inguinal lymph nodes = pLN). Thymus, spleen, and lymph nodes were harvested, cut into small pieces, and digested in Hank's Balanced Salt Solution (Ca^{+2}, Mg^{+2}, HBSS) (Gibco byLife Technologies™) supplemented with 10% fetal bovine serum (FBS) (Sigma Aldrich), 0.2U/mL Liberase TM (Roche Applied Science), and 0.1mg/mL DNAse (Roche Applied Science) for 5 – 10min at 37°C. Afterwards, the tissue fragments were passed through a 40µm wire mesh. Erythrocytes in splenocyte and lymph node cell suspensions were lysed with Red Blood Cell Lysis buffer (Sigma Aldrich) for 2min at room temperature. Purified cells were then counted prior to antibody staining for flow cytometry analyses.

4.1.2. Skin

For leukocyte isolation fat tissue and hair were removed from skin, cut into small pieces, and digested in an enzymatic cocktail consisting of 10% FBS (Sigma Aldrich), 0.25U/mL Liberase DL (Roche Applied Science), and 0.1mg/mL DNAse (Roche) added to HBSS

(Ca^{+2}, Mg^{+2}) (Gibco by Invitrogen) for 2h at 37°C with repetitive pipetting to disrupt skin architecture. The tissue fragments were then passed through a 40µm wire mesh and purified. The cell suspension was magnetically labeled with CD45 MicroBeads (MACS, Miltenyi Biotec, Bergisch Galdbach, Germany), loaded onto a MACS column, and separated into $CD45^{negtive}$ and $CD45^{positive}$ fractions (MACS, Miltenyi Biotec). Collected $CD45^{positive}$ cells were purified and blocked with anti-mouse CD16/32 (93; TruStain fcX™, BioLegend) prior to antibody staining for flow cytometry analyses.

4.2. Staining antibodies

For surface and intracellular staining, the following dyes and fluorochrome-coupled antibodies were used at saturating concentrations: Zombie Aqua (amine reactive-fluorescent dye for live/dead stain, BioLegend; 1:100), rat anti-mouse Per-CP-anti-CD45.1 (A20; BioLegend; 1:50), APC-anti-CD45.1 (A20; BioLegend; 1:50), Pacific-Blue-anti-CD45.2 (104; BioLegend; 1:50), PE/Cy7-anti-CD19 (6D5; 1:50, BioLegend), Alexa-Fluor-700-anti-CD3 (17A2; BioLegend; 1:50), FITC-anti-CD4 (GK1.1; eBioscience; 1:50), PE-anti-CD8a (53-6.7; eBioscience; 1:50), FITC-anti-CD11b (M1/70; BioLegend; 1:50), PE-anti-Ly6G (1A8; BioLegend; 1:50), APC-Cy7-anti-Ly6C (HK1.4; BioLegend; 1:50), primary Biotin-anti-Siglec F antibody (MACS, Miltenyi Biotec; 1:10), in combination with secondary Alexa-Fluor-700-Streptavidin antibody (MACS, Miltenyi Biotec; 1:200), and APC-anti-F4/80 (BM8; BioLegend: 1:50). Measurements were performed using a Gallios flow cytometer (Beckman Coulter), and the data were analyzed with Flow Jo software (Version 10.2, Graphpad Software).

4.3. Blood — Hemogram

4.3.1. Blood

Peripheral blood was immediately collected after CO_2 asphyxation from mice by cardiac puncture and kept in EDTA-coated tubes (K2E BD Microcontainer, BD Pharmingen). Blood samples were then filtered through 70µm nylon wire mesh and diluted with 1x PBS in a 1:5 ratio. Blood counts were performed using the ADVIA 120 Hematology System (Siemens).

4.3.2. Serum cytokines

Peripheral blood was collected into regular 1.5mL Eppendorf tubes post mortem by cardiac puncture from mice. Blood samples were left for 30 – 60min at room temperature for blood coagulation. Then, the samples were centrifuged at 3,000rpm (1500 x g) for 20min at room temperature. The supernatant (serum) was carefully transferred into new Eppendorf tubes and prepared for multiplex assay analysis or stored at -80°C.

4.3.3. Multiplex assay technology combined with flow cytometry analysis

After spinning color-coded beads pre-coated with analyte-specific capture antibodies for IL-2, IL-4, IL-5, IL-6, IL-10, IL-15, IL-17, IL-22, EPO, TNF-α, TGF-β and IFN-γ kit (Bead-Kits from Luminex, ProcartaPlex) were used to measure serum cytokine levels using a Guava EasyCyte flow cytometer (Merck Millipore).

5. Organoid Culture

5.1. Three-dimensional intestinal organoid cultures of the gastro-intestinal tract (GI)

Organoids of small intestine, stomach corpus and forestomach were established from freshly isolated glands from each organ. Incubation in 1x PBS (ph 7.4) containing 2mM EDTA (from the small intestine) or 5mM EDTA (for the stomach and colon) was used for the isolation of glands. Biopsy specimens were manually dissected, and the mucosal layer was cut into small pieces that were washed, embedded in Matrigel (BD Biosciences), and cultured in conditions, as previously described [140].

6. Next Generation Sequencing (NGS)

6.1. Primary fibroblast cell culture

RNA was isolated from primary mouse fibroblast cultures from wild-type and *Ttc7*$^{fsn/fsn}$ mice. From shaved back skin fatty tissue and hairs were carefully removed under sterile

conditions. After cutting the skin into small pieces, the dermal side of the skin was attached on cell culture plates. After adherence, skin pieces were covered and cultured in Dulbecco's Modified Eagle Medium (DMEM, Gibco by Life Technologies™) supplemented with 15% FBS (Gibco by Life Technologies™), 1% sodium pyruvate (Gibco by Life Technologies™), 1% Glutamax (Gibco by Life Technologies™), 1% non-essential amino acids (Gibco by Life Technologies™), 2mM stable glutamine (Gibco by Life Technologies™), 1% Kanamycin (Gibco by Life Technologies™), 5mg gentamicin (Gibco by Life Technologies™), and 1x Anti-Anti (Gibco by Life Technologies™). After 14 days primary fibroblast culture plates were flushed with 1x PBS and directly lysed and stored in TRIzol Reagent (Ambion by Life Technologies™). Total RNA was isolated using a PureLink RNA Mini Kit (Invitrogen by Life Technologies™) according to the manufacturer's instructions.

6.2. NGS of RNA from *Ttc7*$^{fsn/fsn}$ and wild-type fibroblasts

Next generation sequencing (NGS) of purified total RNA isolated from fibroblasts from wild-type and *Ttc7*$^{fsn/fsn}$ mice was performed by the Functional Genomic Center Zurich (ETH Zurich and University of Zurich, Zurich, Switzerland).

NGS of purified total RNA isolated from Fibroblast of wild-type in triplicates and *Ttc7*$^{fsn/fsn}$ mice in quadruplicates were performed by the Functional Genomic Center Zurich. The TruSeq stranded mRNA Sample Prep Kit (Illumina, Inc, California, USA) was used with a starting amount of 500ng total RNA per sample [141]. Libraries were sequenced on HiSeq4000 in single read mode at 1x125 bp and NGS reads were quality-checked with FastQC (http://www.bioinformatics.babraham.ac.uk/projects/fastqc/). Reads were trimmed with Trimmomatic (v0.33, 4 bases hard-trimming from the start, and adapter trimming at the end) [141]. We aligned the trimmed reads to the reference genome and transcriptome (FASTA and GTF files, respectively, Ensembl GRCm38) with STAR version 2.5.1b [142]. Gene expression was quantified using RSEM (version 1.2.22) [143]. To detect differentially expressed genes, we applied the count based negative binomial model implemented in the R/Bioconductor package edgeR (R version: 3.3.2, edgeR version: 3.16.5), in which the normalization factor was calculated by the trimmed mean of M values (TMM) method [144, 145].

The unsupervised hierarchical cluster analysis of RNA-seq data is based on normalized counts after log transformation with an offset of 10 counts added. The 2,500 genes with the biggest variance across all samples were used.

6.2.1. MetaCore™

The NGS data was studied and quantified by using analytical MetaCore™ tools for functional analysis. MetaCore™ is based on a high-quality, manually-curated database of transcription factors, receptors, ligand, kinases, drugs, and endogenous metabolites and other molecular classes. Signaling and metabolic pathways were represented in tables and maps.

7. Dermal-Epidermal Skin Substitute (DESS)

7.1. Primary mouse fibroblast cell culture

To isolate fibroblasts, mouse skin samples were cut into small (1cm^2) pieces and digested overnight at 4°C in 12U/ml Dispase (Corning). Next, the dermis and the epidermis were separated using a forceps. The dermal compartment was further digested with 2mg/ml collagenase for 1h at 37°C. Isolated fibroblasts were then seeded on tissue culture plates and grown in Dulbecco's Modified Eagle Medium (DMEM) (Gibco by Invitrogen) supplemented with 10% FBS, 1% HEPES, and 5mg/mL gentamicin.

7.2. Primary human keratinocyte cell culture

To isolate human keratinocytes, foreskin samples were cut into small (1cm^2) pieces and digested overnight at 4°C in 12U/ml Dispase (Corning). Afterwards, the dermis was separated from the epidermis using forceps. The epidermal compartment of the skin was further digested in 0.5% trypsin (Gibco by Invitrogen) for 2min at 37°C. Isolated keratinocytes were cultured in serum-free medium (CellnTec) supplemented with 25mg/mL bovine pituitary extract, 0.2ng/mL epidermal growth factor, and 5mg/mL gentamicin.

7.2.1. Preparation of DESS containing skin fibroblasts isolated from *Ttc7*$^{fsn/fsn}$ and wild-type mice.

The DESSs were prepared using 3ml of bovine collagen type I (5mg/mL, Symatese Biomateriaux) mixed with 2 x 10^5 mouse fibroblasts isolated from *Ttc7*$^{fsn/fsn}$ (*Ttc7*$^{fsn/fsn}$ DESS) or wild-type skin (WT DESS) and cultured in six-well cell culture inserts (pore size: 3.0µm; BD Biosciences, Allschwil, Switzerland). The prepared dermal equivalents were cultured in DMEM (Gibco, Invitrogen, Carlsbad, USA) supplemented with 10% FBS, 1% HEPES, and 5mg/mL gentamicin for 7 days following seeding of 7 x 10^5 keratinocytes isolated from human foreskin and DESS were cultured for five addition days and subsequently transplanted onto immunocompromised rats (athymic nude rats, *Foxn1*$^{rnu/rnu}$).

7.3. Transplantation of DESS

The surgical protocol was approved by the local Committee for Experimental Animal Research (authorization number: ZH090/15). Immunocompromised female nude rats aged eight to ten weeks (Harlan Laboratories) were prepared and anesthetized as previously described [146]. DESSs were transplanted into full-thickness skin wounds created surgically on the animal's back. The protection from wound closure was provided by suturing steel surgical rings (diameter: 26mm) to the skin defects using non-absorbable polyester sutures (Ethibond®; Ethicon). The DESSs were covered with silicon foil (Silon-SES; BMS), a polyurethane sponge (Ligasano, Ligameda bandage (Sincohaft, Theo Frey AG), and tape as a wound dressing. Photographs were taken weekly when the wound dressing was changed. Three weeks after the transplantation, the DESSs were excised and processed for cryosection analysis.

7.4. Immunofluorescence staining of transplanted DESS

12µm cryosections were fixed with 1:1 acetone/methanol for 5min at -20°C, air-dried, washed three times in PBS, blocked in 2% bovine serum albumin in PBS solution for 30min, and incubated overnight at 4°C with diluted primary antibodies. Thereafter, slides were washed three times in PBS, blocked for an additional 15min, and incubated

with an appropriate secondary antibody for 45min at room temperature. Lastly, the slides were incubated for 5min in PBS containing 1µg/ml Hoechst reagent (Sigma Aldrich), washed once using PBS, mounted with mounting medium (Dako, Baar, Switzerland), and covered with coverslips. Immunofluorescence pictures were taken using a DXM1200F digital camera connected to a Nikon Eclipse TE2000-U inverted microscope equipped with Hoechst 33342-, Fluorescein Isothiocyanate (FITC)-, and Tetramethylrhodamine Isothiocyanate (TRITC)-filter sets (Nikon AG; Software: Nikon ACT-1 version 2.70). Images were processed with Photoshop software (version 10.0, Adobe Systems, Inc.). The following primary antibodies were used: anti-loricrin (polyclonal, 1:200, Abcam), Alexa Fluor 488 anti-E-cadherin (clone 67A4, 1:50, BD Pharmingen), and anti-Ki67 (clone SP6, 1:100, Abcam).

7.4.1. Quantification of cell proliferation in DESS *in vivo*

Transplanted skin grafts were stained with an anti-Ki-67 antibody. The number of Ki-67 positive cells in the basal cell layer was quantified in three separate areas of two representative sections from each DESS. The results were analyzed using GraphPrism6 software and expressed as the mean ± SD count.

8. Statistics

A clinical monitoring score sheet was used to rate disease severity. Differences between two groups or two datasets were examined for statistical significance by using unpaired two-tailed Student's *t* test. Data were quoted as the mean ± standard deviation (SD). The correlation between two parameters was estimated by calculating Pearson's *r*. Statistical significance was expressed as follows: $*p<0.05$, $**p<0.01$, $***p<0.001$, ns: not significant, and nd: not detected. All statistical analyses were performed with Prism Software (Version 6, GraphPad Software, Inc).

9. Data availability

Sequence data that support the findings of this study have been deposited in the European Nucleotide Archive with the primary accession ID PRJEB21496. The authors declare that all other data supporting the results of this study are available on request.

10. Study approval

Human keratinocytes were isolated from foreskin samples from children 1 – 16 years of age. This part of the study was performed in accordance with the tenets of the Declaration of Helsinki and after approval by the local investigational review board of the ethics commission in Canton Zurich, Switzerland. Parents and/or patients were provided with information about the study and gave their written consent. All animal experiments were approved by the Cantonal Veterinary Office (Zurich, Switzerland; approval number: 65/2014).

V. RESULTS

1. Phenotype of the *fsn* mutant (*Ttc7*$^{fsn/fsn}$) mouse

1.1. Anemia

In previous studies on the homozygous *fsn* mutant mouse, a hypochromic microcytic anemia has been described, which is obvious at birth and becomes more severe with increasing age [123, 127]. The anemia is the most probable reason why the *Ttc7*$^{fsn/fsn}$ mice die at the age of 12 to 14 weeks. We measured red blood cells counts and hemoglobin content in *Ttc7*$^{fsn/fsn}$ mice and could confirm these findings (**Figures 10A, 10B)**. Additionally, we measured serum levels of erythropoietin (EPO). This glycoprotein hormone is synthesized by the kidney-resident fibroblasts and fetal liver and promotes the survival, proliferation, and differentiation of erythrocytic progenitors of red blood cells. Synthesis of EPO relies on a feedback mechanism based on tissue O_2 pressure, which depends, among other factors, on hemoglobin concentration and iron availability [147]. *Ttc7*$^{fsn/fsn}$ mice have the unique ability to excrete elevated levels of iron through the urine [123, 148]. We observed significantly higher serum EPO levels, which increased with age in *Ttc7*$^{fsn/fsn}$ mice when compared with WT littermates (**Figure 10C**), consistent with an iron-deficient anemia. Taken together, anemia in *Ttc7*$^{fsn/fsn}$ mice is based on elevated urinary iron excretion, pointing out an altered epithelial function of renal tubular cells. This is associated with increased EPO concentrations in blood.

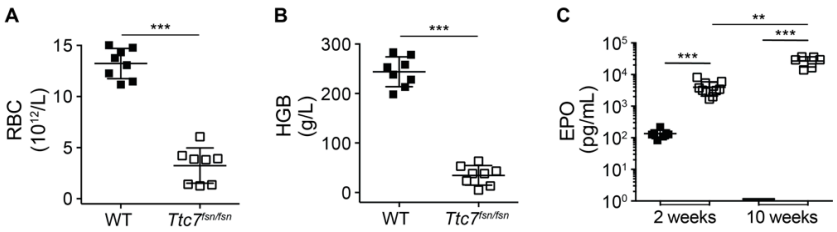

Figure 10. Decreased RBC counts and HGB levels are accompanied by elevated serum EPO levels in *Ttc7*$^{fsn/fsn}$ mice. (**A** and **B**) Red blood cell (RBC) counts and hemoglobin (HGB) levels in peripheral blood of gender-matched wild-type (WT) and *Ttc7*$^{fsn/fsn}$ mice at the age of 10 weeks. (**C**) Serum erythropoietin (EPO) levels measured in 2- and 10-week old WT and *Ttc7*$^{fsn/fsn}$ mice. Scatter plots indicate pooled data with average mean ± standard deviation (SD) from >3 independent experiments. Each symbol represents one individual mouse (n = 6–10).

1.2. Splenomegaly

Another hallmark of the flaky skin mutant mouse is the hyperplasia of the spleen [128]. We assessed the severity of the splenomegaly relative to body weight at different ages of the mice. Spleens of *Ttc7*$^{fsn/fsn}$ mice were not enlarged compared to wild-type littermates at 2 weeks, but with increasing age, the splenomegaly became apparent (**Figures 11A, 11B**).

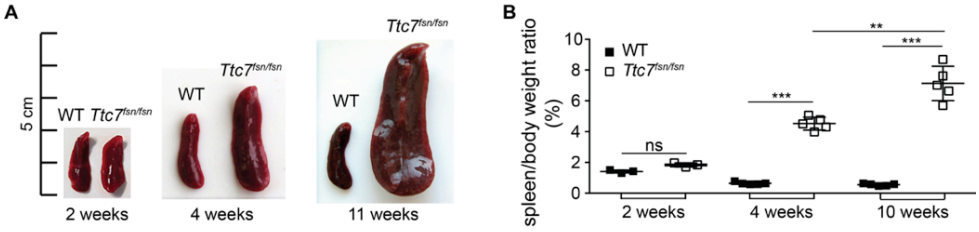

Figure 11A-B. Splenomegaly aggravates with increasing age. (**A**) Photos of spleens from female WT and *Ttc7*$^{fsn/fsn}$ mice at the age of 2, 4 and 10 weeks. (**B**) Spleen to body weight ratios. (**A**) Photos are representative of 3–4 independent experiments. (**B**) Scatter plots indicate pooled data with average mean ±SD from 3–4 independent experiments. Each symbol represents one individual mouse (n = 3–5).

Histopathology revealed enlarged red pulp in spleens from *Ttc7*$^{fsn/fsn}$ mice at 4 and 10 weeks, when compared with age-matched WT littermates (**Figures 11C, 11D**). This observation was accompanied by higher numbers proliferating Ki-67 positive cells (**Figure 11E**) and a higher number of total splenocytes (**Figure 11F**).

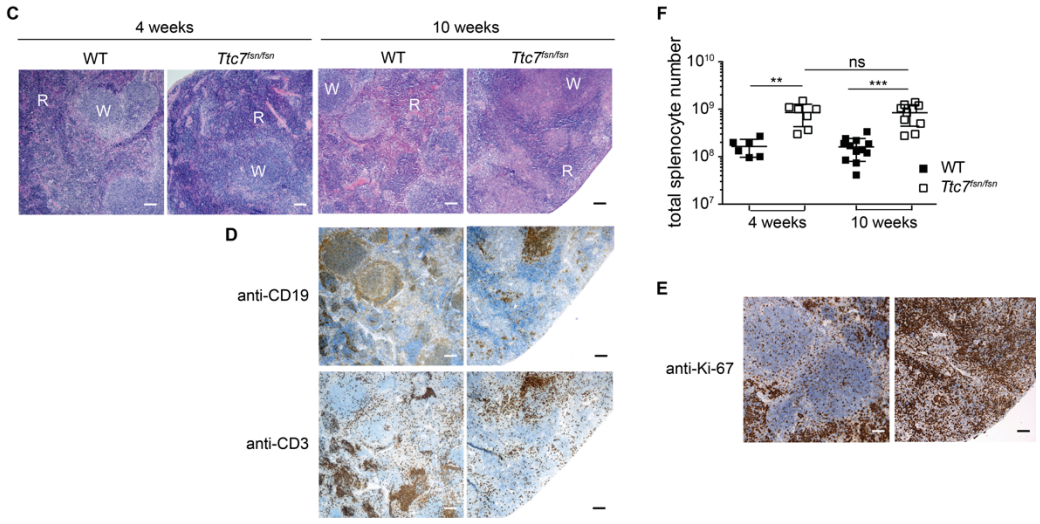

Figure 11C-F. Enlarged red pulp and higher numbers of proliferating splenocytes in *Ttc7*$^{fsn/fsn}$ mice. (**C**) Hematoxylin-eosin staining of splenic sections from 4- and 10-week old female WT and *Ttc7*$^{fsn/fsn}$ mice (Magnification: x5). White and black scale bars correspond to 100µm; "W" = white pulp; "R" = red pulp. (**D**) Immunohistochemical stainings of splenic sections with anti-CD20 and anti-CD3 antibodies in 10-week old WT and *Ttc7*$^{fsn/fsn}$ mice (Magnification: x5). White and black scale bars correspond to 100µm. (**E**) Immunohistochemical staining of splenic

sections with anti-Ki-67 antibodies from 10-week old wild-type and *Ttc7*$^{fsn/fsn}$ mice (Magnification: x20). White and black scale bars correspond to 50µm. Representative microscopic images of >3 independent experiments. (**F**) Total splenocyte numbers of 4- and 10-week old WT and *Ttc7*$^{fsn/fsn}$ mice quantified by flow cytometry. Each symbol of the scatter plot represents one individual mouse (n = 6–8); mean ±SD from >3 independent experiments are indicated.

In order to analyze what cells the spleens consist of, we performed further measurements by flow cytometry. We found mainly an increased number of cells deriving from the erythroid lineage (data not shown). However, we also observed a significantly higher number of CD45-positive cells (a leukocyte-common antigen) in *Ttc7*$^{fsn/fsn}$ spleens when compared with spleens from WT littermates (**Figure 11H**). CD19$^+$ B cells were lower in frequency, but the total number did not differ between *Ttc7*$^{fsn/fsn}$ and WT mice (**Figures 11G, 11I)**. Instead, we found a decreased frequency and total number of CD3$^+$ T cells in *Ttc7*$^{fsn/fsn}$ mice (**Figures 11G, 11J**). Within in this cell group, CD4$^+$ T cells were lower in frequency and total numbers, and CD8$^+$ T cells were lower in frequency but similar in total numbers compared to wild-type littermates (**Figures 11K-M).** Overall, the lymphocyte cell counts did not significantly differ between *Ttc7*$^{fsn/fsn}$ and WT spleens. These observations are consistent with previous publications [119, 121, 128].

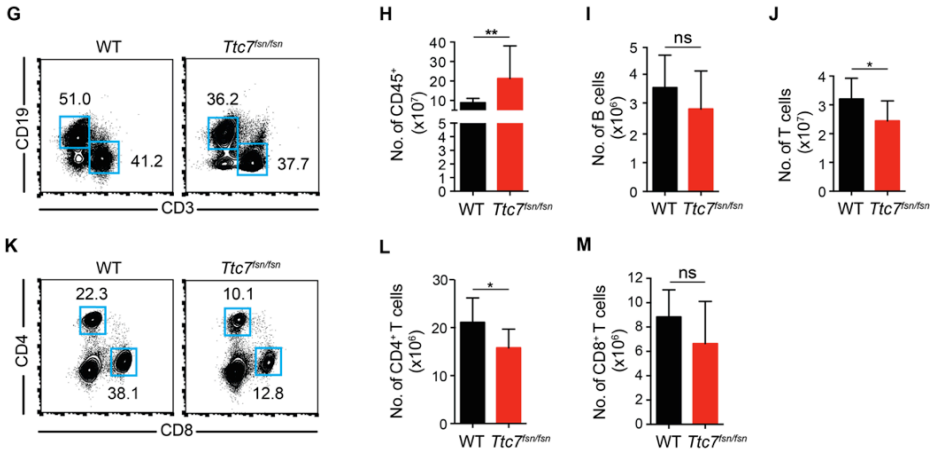

Figure 11G-M. The spleens of *Ttc7*$^{fsn/fsn}$ mice contain more leukocytes but similar total numbers of B and T cells. (**G**) Representative flow cytometric dot plots of CD19$^+$ B cells (CD19$^+$/CD45$^+$ cells) and CD3$^+$ T cells (CD3$^+$/CD45$^+$ cells) in spleens of 10-week old female WT and *Ttc7*$^{fsn/fsn}$ mice. (**H**) Total number of CD45$^+$ cells, (**I**) CD19$^+$ B cells, and (**J**) CD3$^+$ T cells. (**K**) Representative flow cytometric dot plots of CD4$^+$ (CD3$^+$CD4$^+$/CD45$^+$ cells) and CD8$^+$ T cells (CD3$^+$CD8$^+$/CD45$^+$ cells) in spleens of WT and *Ttc7*$^{fsn/fsn}$ mice. (**L**) Total number of CD4$^+$ T cells and (**M**) CD8$^+$ T cells. (**H-J, L-M**) The bars indicate pooled data as the mean +SD from >3 independent experiments (n = 8–12 mice).

In contrast to the equal numbers of lymphocytes, the myeloid cell compartment in spleens of *Ttc7*$^{fsn/fsn}$ mice significantly differed between *Ttc7*$^{fsn/fsn}$ and WT spleens; higher

frequencies and total numbers of eosinophils, neutrophils, and monocytes were found (**Figures 11N-P**). Interestingly, some *Ttc7*$^{fsn/fsn}$ mice showed a higher frequency of CD11b^{Low} macrophages whereas other mutants had higher frequencies in CD11b^{High} macrophages, but in total, the numbers of these two macrophage populations were not significantly different compared to the wild-type numbers (**Figure 11Q**). The severity of the anemia in *Ttc7*$^{fsn/fsn}$ mice can differ. Macrophages tightly control the production and clearance of red blood cells during healthy and disturbed erythropoiesis [149]. An increased clearance of apoptotic cells in the *Ttc7*$^{fsn/fsn}$ mice could explain the elevated numbers of CD11b^{High} and CD11b^{Low} macrophages that we observe in the spleen of these mice.

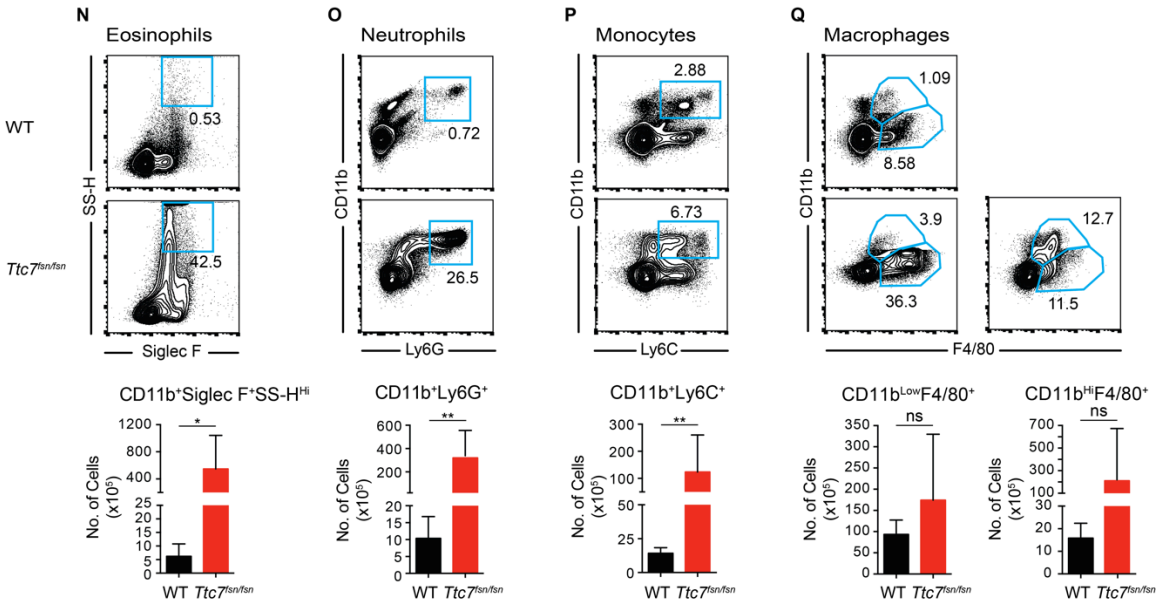

Figure 11N-Q. Increased numbers of eosinophils, neutrophils, and monocytes in *Ttc7*$^{fsn/fsn}$ mice. (**N-Q**) Representative flow cytometric dot plots of eosinophils, neutrophils, monocytes, and macrophages in spleens of 10-week old female WT and *Ttc7*$^{fsn/fsn}$ mice. (**N**) Eosinophils (CD11b^{+}, Siglec F^{+} and SS-H^{Hi}/CD45^{+}), (**O**) neutrophils (CD11b^{+}, Ly6G^{+}/CD45^{+} Siglec F^{+} and SS-H^{Hi}), (**P**) monocytes (CD11b^{+}, Ly6C^{+}/CD45^{+} Siglec F^{+} SS-H^{Hi} and Ly6G^{+}), (**Q**) CD11b^{Low} macrophages (CD11b^{Low}, F4/80^{+}/CD45^{+} Siglec F^{+} SS-H^{Hi} Ly6G^{+} and Ly6C^{+}), and CD11b^{Hi} macrophages (CD11b^{Hi}, F4/80^{+}/CD45^{+} Siglec F^{+} SS-H^{Hi} Ly6G^{+} and Ly6C^{+}) are given as total number per lymph node of the indicated gate. The bars represent pooled data as the mean +SD from >3 independent experiments (n = 8–12 mice).

In mice, the spleen plays a crucial role in erythropoiesis outside the bone marrow, even in healthy adult animals. Extramedullar production, particularly in the spleen, is part of the physiological erythropoiesis. Under erythroid stress conditions, such as iron deficiency, the spleen is used to expand the erythropoietic capacity, which takes place in an impressive way in the *Ttc7*$^{fsn/fsn}$ mice. Red blood cells accumulate in the red pulp

compartment and lead to severe splenomegaly, as has been described in the literature. Correspondingly, our findings led us to conclude that we could reconfirm published data, revealing hyperplasia of the spleen, because of greatly increased red pulp due to accumulation of immature erythroid cells characterizing the anemia [119, 123, 127].

1.3. Axillary, brachial and inguinal lymphadenopathy

All major epithelial barriers of the body, including the skin, as well as the gastrointestinal and bronchial mucosa, have their own system of lymph nodes. The axillary, brachial and inguinal lymph nodes are important skin-draining lymph nodes. They play a major role in activating immune responses in the *Ttc7*$^{fsn/fsn}$ mouse. The work of Abernethy and Pelsue shows histological and immunological data on lymph node alterations observed in *Ttc7*$^{fsn/fsn}$ mice [119, 128, 150]. Based on these publications, we wanted to ascertain at which age these abnormalities initially develop. We assessed the extent of lymphadenopathy at ages of 2, 4, and 10 weeks. On a macroscopic level, the *Ttc7*$^{fsn/fsn}$ mice only showed slight differences in lymph nodes size at the age of 2 weeks when compared with littermates as a control (**Figure 12A**). This difference in size and weight progresses with age. The differences become more evident at the age of 4 weeks and even more conspicuous at the age of 10 weeks (**Figures 12A, 12B**).

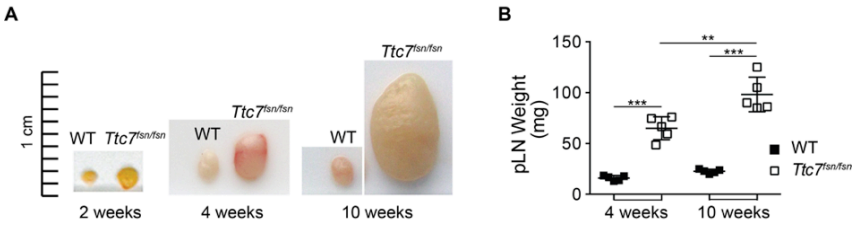

Figure 12A-B. Lymphadenopathy in *Ttc7*$^{fsn/fsn}$ mice. (**A**) Photos of axillary lymph nodes from female WT and *Ttc7*$^{fsn/fsn}$ mice at the age of 2, 4 and 10 weeks. (**B**) Skin-draining lymph node (pLN = axillary, brachial and inguinal LN) weight at the age of 2, 4, and 10 weeks. (**A**) Photos are representative of three independent experiments. (**B**) Scatter plots indicate pooled data as the mean ±SD from 3–4 independent experiments. Each symbol represents one individual mouse (n = 5).

The histopathological and immunohistochemical analysis of the skin-draining lymph nodes revealed medullary and cortical regions containing higher cell counts, thus indicating that there is a tendency of increased proliferation present in flaky skin mutant

mice when compared to age matched controls (**Figures 12C-E**). With increasing age, a reduction of the follicular and enlargement of the cortical area became apparent.

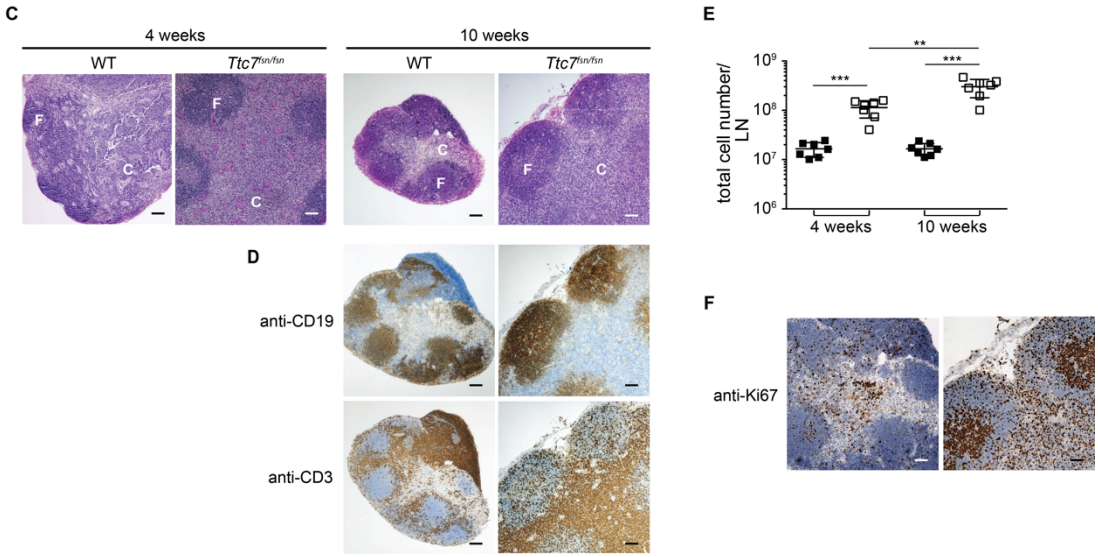

Figure 12C-F. Hyperplasia of skin-draining lymph nodes accompanied by increasing cellularity with age. (**C**) Hematoxylin-eosin staining of lymph node sections from 4- and 10-week old female WT and *Ttc7*$^{fsn/fsn}$ mice (Magnification: x5). White and black scale bars represent 100µm; "F" = follicle; "C" = Cortex. (**D**) Immunohistochemical stainings of lymph node sections with anti-CD20 and anti-CD3 antibodies of 10-week old wild-type and *Ttc7*$^{fsn/fsn}$ mice (Magnification: x5). White and black scale bars correspond to 100µm. (**E**) Total cell numbers per lymph node in 4- and 10-week old WT and *Ttc7*$^{fsn/fsn}$ mice. (**F**) Immunohistochemical staining of lymph node sections with anti-Ki-67 antibody from 10-week old WT and *Ttc7*$^{fsn/fsn}$ mice (Magnification: x20). White and black scale bars correspond to 50µm. (**C, D, F**) Representative microscopic images of >3 independent experiments. (**E**) Each symbol of the scatter plot represents one individual mouse (n = 6–7) and visualizes cumulative data with average mean ±SD from >3 independent experiments.

Based on this observation, we characterized the distribution of immune cells by flow cytometric analysis in 10-week old female *Ttc7*$^{fsn/fsn}$ mice. We observed a significant increase in total numbers of CD45-positive cells. Amongst these CD45$^+$ cells, the frequency and total number of CD19$^+$ B cells were elevated. Furthermore, when quantifying CD3$^+$ T cells, that were subdivided into CD4$^+$ and CD8$^+$ T cells, higher total numbers were present in the *Ttc7*$^{fsn/fsn}$ mice when compared to controls (**Figures 12J-M**). Also the *Ttc7*$^{fsn/fsn}$ mice had proportionally more CD8$^+$ than CD4$^+$ T cells in their lymph nodes. Consequently, the CD4$^+$/CD8$^+$ ratio was remarkably reduced in *Ttc7*$^{fsn/fsn}$ mice (0.78 ± 0.16, mean ±SD) compared to WT mice (3.02 ± 0.86, mean ±SD). This result was consistent with a previous publication [128].

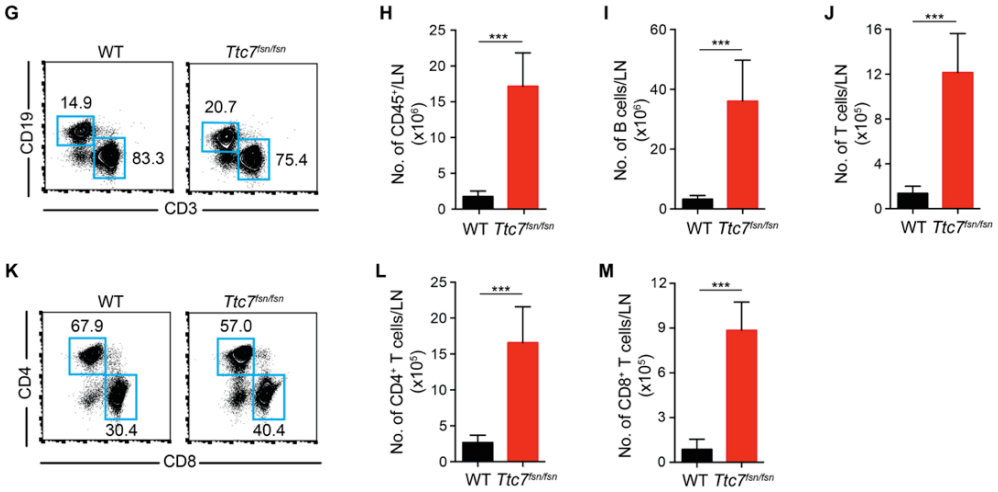

Figure 12G-M. The skin-draining lymph nodes of *Ttc7*$^{fsn/fsn}$ mice are filled predominately with CD8+ T cells. (**G**) Representative flow cytometric dot plots of CD19^{+} B cells and CD3^{+} T cells in skin-draining lymph nodes of 10-week old female WT and *Ttc7*$^{fsn/fsn}$ mice. (**H**) Total number of CD45^{+} cells (CD45^{+}/Alive), (**I**) CD19^{+} B cells (CD19^{+}/CD45^{+}), and (**J**) CD3^{+} T cells (CD3^{+}/CD45^{+}). (**K**) Representative flow cytometric dot plots of CD4^{+} and CD8^{+} T cells in lymph nodes of WT and *Ttc7*$^{fsn/fsn}$ mice. (**L**) Total number of CD4^{+} T cells (CD4^{+}/CD45^{+}CD3^{+}) and (**M**) CD8^{+} T cells (CD8^{+}/CD45^{+}CD3^{+}) per lymph node. (**H-J, L-M**) Bar plots indicate pooled data from >3 independent experiments as the mean +SD (n = 10 mice).

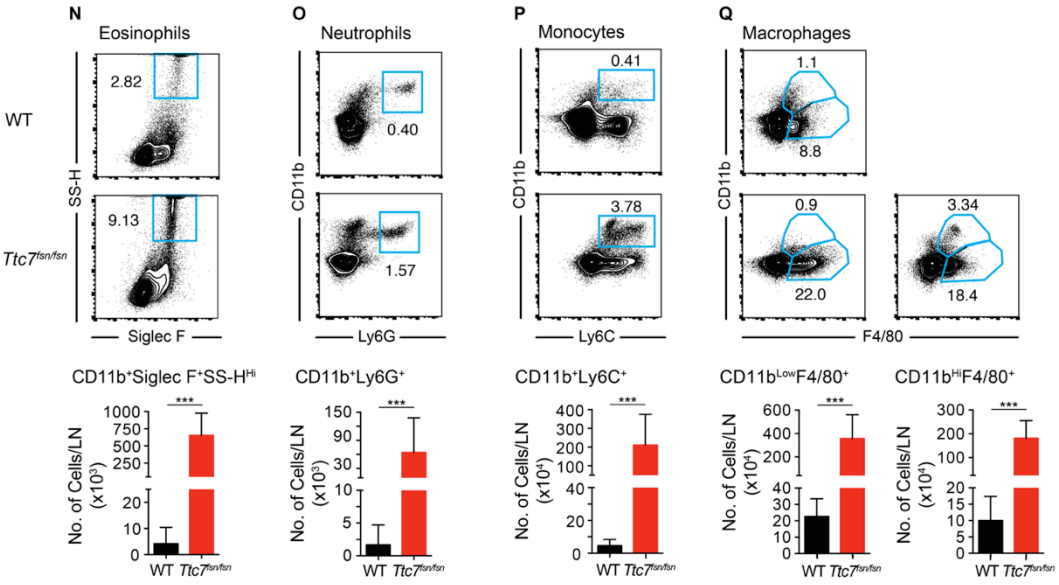

Figure 12N-Q. Lymphadenopathy is also associated with increased numbers of eosinophils, neutrophils, monocytes, and macrophages in *Ttc7*$^{fsn/fsn}$ mice. (**N-Q**) Representative flow cytometric dot plots of eosinophils, neutrophils, monocytes, and macrophages in skin-draining lymph nodes of 10-week old female WT and *Ttc7*$^{fsn/fsn}$ mice. (**N**) Eosinophils (CD11b^{+}, Siglec F^{+} and SS-H^{Hi}/CD45^{+}), (**O**) neutrophills (CD11b^{+}, Ly6G^{+}/CD45^{+} Siglec F^{+} and SS-H^{Hi}), (**P**) monocytes (CD11b^{+}, Ly6C^{+}/CD45^{+} Siglec F^{+} SS-H^{Hi} and Ly6G^{+}), (**Q**) CD11b^{Low} macrophages (CD11b^{Low}, F4/80^{+}/CD45^{+} Siglec F^{+} SS-H^{Hi} Ly6G^{+} and Ly6C^{+}), and CD11b^{Hi} macrophages (CD11b^{Hi}, F4/80^{+}/CD45^{+} Siglec F^{+} SS-H^{Hi} Ly6G^{+} and Ly6C^{+}) given as total number per lymph node of the indicated gate. (**N-Q**) Bar plots represent pooled data from >3 independent experiments as the mean +SD (n = 10 mice).

In the myeloid-derived cell compartment, both the frequencies and total numbers of eosinophils, neutrophils, monocytes, and macrophages were increased (**Figures 12N-Q**).

Overall, these results show that cells of the lymphoid and myeloid lineage both contribute to hyperplasia of the skin-draining lymph nodes, but they do not disrupt the lymph node architecture in *Ttc7*$^{fsn/fsn}$ mice.

1.4. Premature thymic atrophy

The thymus is a primary lymphoid organ that undergoes dynamic physiological changes with age and is additionally very sensitive to stress and toxic injury. The intrathymic maturation of T cells consists of several phases that require the dynamic relocation of maturing lymphocytes within multiple architectural structures. As part of this process, the thymocytes interact with specialized thymic epithelial cells. Our next aim was to clarify whether the thymic development is disturbed in *Ttc7*$^{fsn/fsn}$ mice. We assessed thymi of female *Ttc7*$^{fsn/fsn}$ mice and WT mice at the ages of 2, 4, and 10 weeks. At 2 weeks of age, there were no differences in size or total thymocyte numbers and the cortical and medullary architecture was normal (**Figures 13A, 13B**). In contrast, the thymi of 4-week old *Ttc7*$^{fsn/fsn}$ mice were macroscopically smaller in size and lower in weight, although the intrathymic architecture (**Figure 13A**) and thymocyte numbers were comparable to controls (**Figures 13B**-**13D**). A reduced number of thymocytes in *Ttc7*$^{fsn/fsn}$ mice was present at the age of 10 weeks (**Figures 13C, 13D**). At this age, histological analysis revealed a vague cortico-medullar demarcation and a seeming expansion of the medullary region in *Ttc7*$^{fsn/fsn}$ mice (**Figure 13A**).

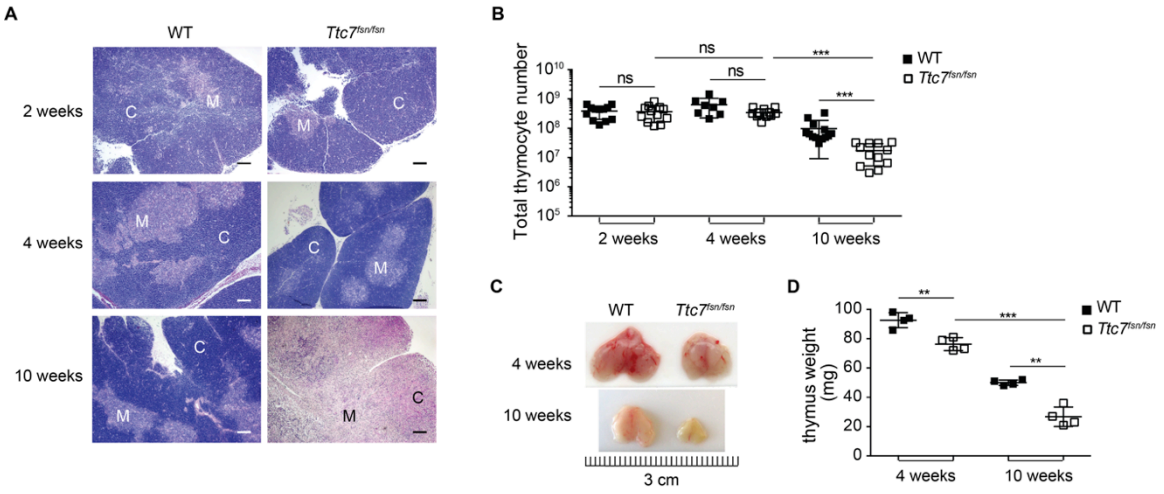

Figure 13. Thymic vague cortico-medullary demarcation accompanied by fewer thymocytes in 10-week old *Ttc7*$^{fsn/fsn}$ mice. (**A**) Hematoxylin-eosin staining of thymus sections from 2-, 4-, and 10-week old female WT and *Ttc7*$^{fsn/fsn}$ mice (Magnification: x5). White and black scale bars correspond to 100µm; "M" = Medulla; "C" = Cortex. (**B**) Total

thymocyte numbers of 2-, 4-, and 10-week old WT and *Ttc7*$^{fsn/fsn}$ mice. (**C**) Representative photos of 4- and 10-week old WT and *Ttc7*$^{fsn/fsn}$ mice. (**D**) Corresponding thymus weight of WT and *Ttc7*$^{fsn/fsn}$ mice. (**B** and **D**) Each symbol of the scatter plot represents one individual mouse (n = 4–12) and visualizes cumulative data with average mean ±SD from >3 independent experiments.

These results indicate that a premature thymic atrophy is present, which could possibly be due to an accelerated conventional aging process. One could hypothesize that this was accelerated by an intrinsic defect in thymic stromal cells, whereupon thymocyte development could have been affected.

1.5. Gastric forestomach papillomas

Previous publications have shown that forestomach papillomas can have various triggers that can include chemical compounds, dietary changes, viral, fungal or parasite infections [151]. In the *Ttc7*$^{fsn/fsn}$ mouse, forestomach papillomas occurred spontaneously [151]. We similarly observed these hyperplastic changes of forestomach epithelial cells in *Ttc7*$^{fsn/fsn}$ mice (**Figures 14A, 14B**). The formation of papillomas was already evident at the age of 2 weeks (data not shown). Based on data published by Lemoine and colleagues, describing disrupted apicobasal enterocyte polarity in human patients carrying mutations in *TTC7A*, we sought to determine whether the small and large intestine of the *Ttc7*$^{fsn/fsn}$ mouse shows similar abnormalities [108]. Thus, 3-dimensional epithelial "organoid" cultures of the small intestine and the stomach, from *Ttc7*$^{fsn/fsn}$ mice and WT littermates, were established. The forestomach papillomas grew as large clumps with a disturbed epithelial cell polarity (**Figure 14C**). While the *Ttc7*$^{fsn/fsn}$ organoids of the small intestine displayed a normal epithelial architecture with a correctly organized cell polarization pattern, the *Ttc7*$^{fsn/fsn}$ stomach corpus formed organoids with a disturbed architecture. While the lumen was present, the organoid did not display and crypt-villus domains (**Figure 14D**).

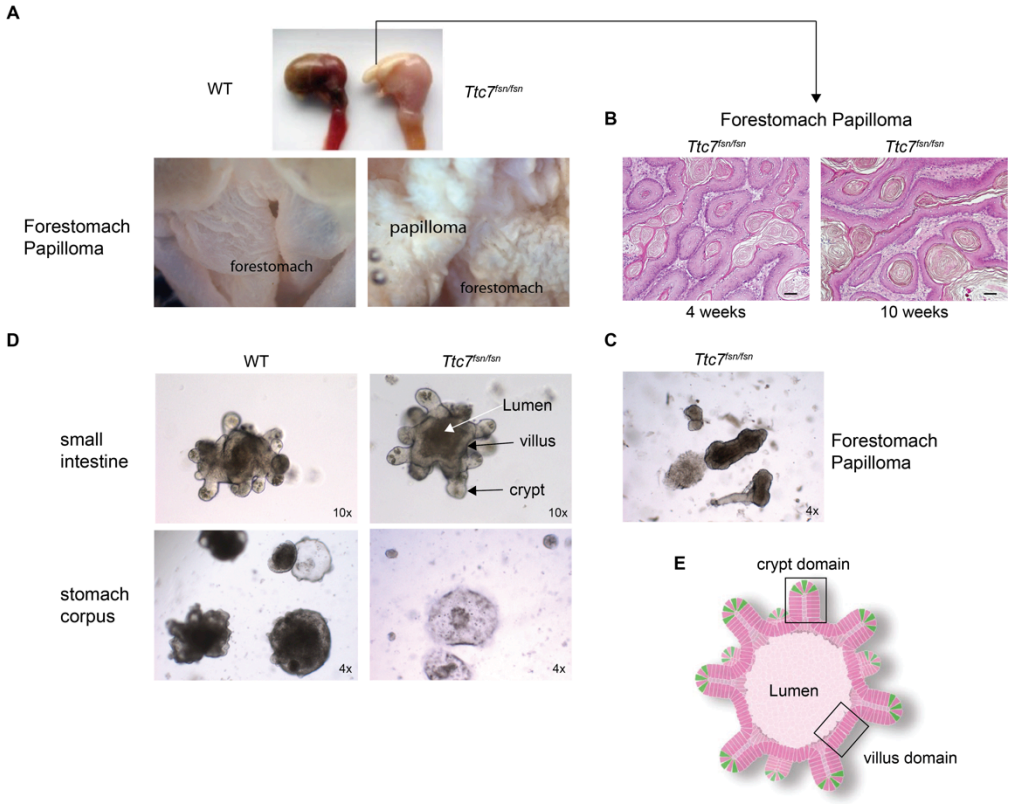

Figure 14. Organoids of gastro-intestinal (GI) tract: gastric forestomach papillomas and normal small intestine formation in *Ttc7*$^{fsn/fsn}$ mice. (**A**) Representative macro- and microscopical photos of forestomach papillomas of 10-week old female *Ttc7*$^{fsn/fsn}$ mice in comparison with WT littermates. (**B**) Hematoxylin-eosin staining of forestomach sections from WT and *Ttc7*$^{fsn/fsn}$ mice (Magnification: x10). Black scale bars correspond to 100µm. (**C**) Representative photos of forestomach papilloma organoid cultures at a magnification of 4x. (**D**) Representative photos of organoids of the small intestine and the stomach corpus from WT and *Ttc7*$^{fsn/fsn}$ mice (Magnification: x4 and x10). (**E**) Intestinal architecture scheme adapted from [152].

1.5.1. Duodenum and colon

Most patients carrying mutations in *TTC7A* suffer from multiple intestinal atresias and/or inflammatory bowel disease (OMIM #243150). Therefore, we examined the small and large intestines of *Ttc7*$^{fsn/fsn}$ mice. We were not able to find any signs of alterations in the gut. The length of small intestines and colon, which are known to be reduced in inflammatory bowel disease, did not differ between *Ttc7*$^{fsn/fsn}$ mice and WT littermates. *Ttc7*$^{fsn/fsn}$ mice displayed a normal intestinal architecture, as evidenced by histological and immunohistochemical analyses of duodenal and colonic sections (**Figures 15A-D**). We could not observe any infiltration of inflammatory immune cells or elevated numbers of apoptotic enterocytes in *Ttc7*$^{fsn/fsn}$ mice.

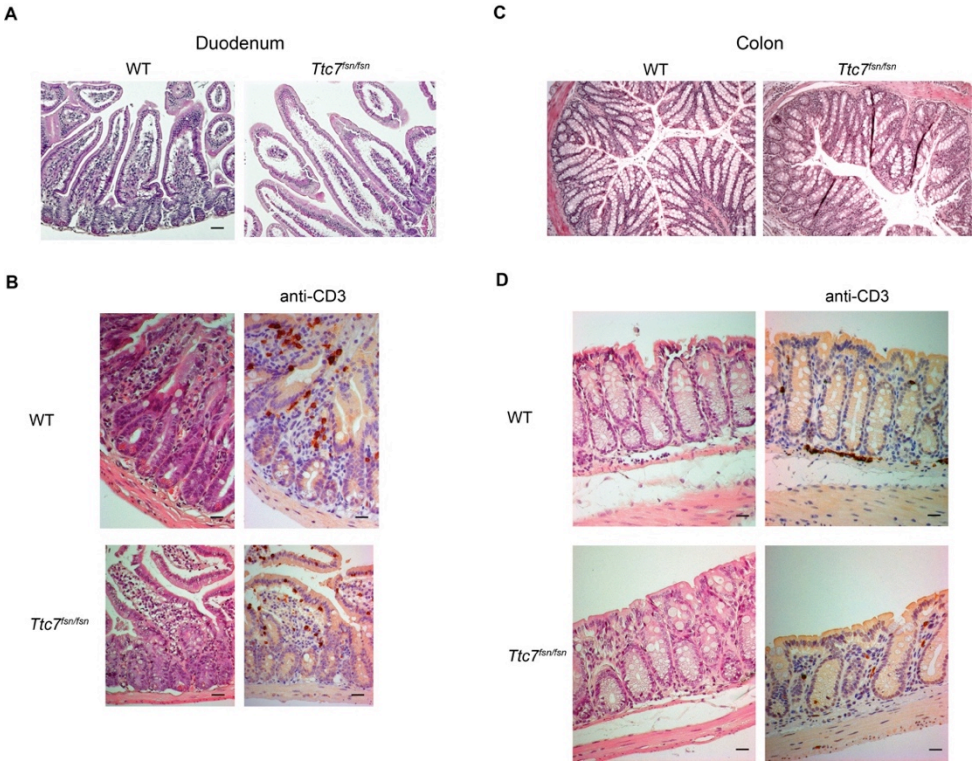

Figure 15. Duodenum and colon develop normally in *Ttc7*$^{fsn/fsn}$ mice. (**A**) Hematoxylin-eosin (H&E) staining of duodenum sections from 10-week old female WT and *Ttc7*$^{fsn/fsn}$ mice (Magnification: x10). Black scale bars correspond to 100µm. (**B**) H&E and immunohistochemical stainings with anti-CD3 antibodies of duodenum sections of 10-week old WT and *Ttc7*$^{fsn/fsn}$ mice (Magnification: x20). Black scale bars correspond to 50µm. (**C**) H&E staining of colon sections from 10-week old female WT and *Ttc7*$^{fsn/fsn}$ mice (Magnification: x10). Black scale bars correspond to 100µm. (**D**) H&E and Immunohistochemical stainings with anti-CD3 antibody of colon sections of 10-week old WT and *Ttc7*$^{fsn/fsn}$ mice (Magnification: x20). Black scale bars correspond to 50µm.

1.6. Hyperplastic dermatitis

Ttc7$^{fsn/fsn}$ mice present with a severe hyperplastic dermatitis as the main feature of their complex phenotype [126]. Ruffled fur and thick, white, patchy scales are visible from the age of 6–8 weeks onwards.

Scheme for skin classification and quantification:

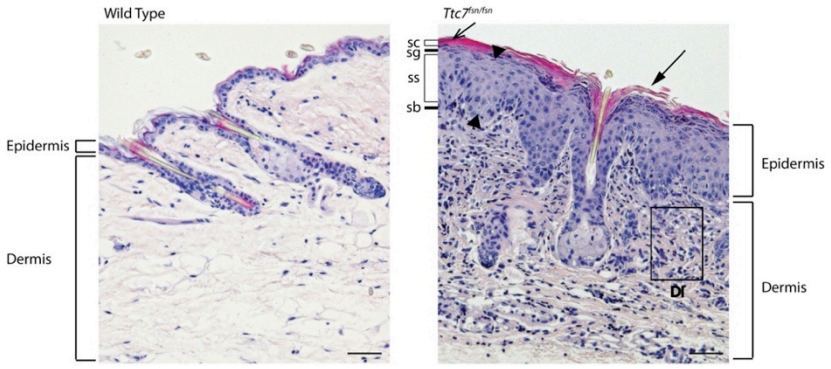

Figure 16A: Skin Scheme for classification and quantification. Back skin sections of female wild-type and *Ttc7*$^{fsn/fsn}$ mice at 10 weeks stained with hematoxylin-eosin reagent (Magnification: x20). Black scale bars correspond to 50µm.

Hyperkeratosis (thickening of the stratum corneum (sc) – dead epidermis) with ablation of keratin scales at the surface (right black arrow) in combination with parakeratosis depicting preserved nuclei (left black arrow). Acanthosis corresponds to thickening of the viable epidermis (stratum ganulosum (sg) and stratum spinosum (ss)) (indicated by black arrowheads) between stratum corneum (sc) and stratum basale (sb) with elongation of rete-like ridges. Mononuclear dermal infiltrates (black retangle – DI).

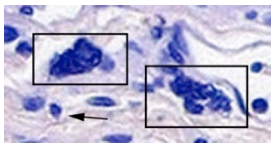

Figure 16B. Distinction between dermal infiltrates. The black rectangle depicts mast cells found in the dermis of *Ttc7*$^{fsn/fsn}$ mice. They can be distinguished from other granulocytes by their clear formation of granules stained by the hematoxylin-eosing reagent. The black arrow depicts a mononuclear cell in the dermis.

Histological analysis of skin sections revealed acanthosis (thickening of the viable epidermis), hyperkeratosis, and dermal infiltrates by leukocytes beginning at 4 weeks of age (**Figure 17A**).

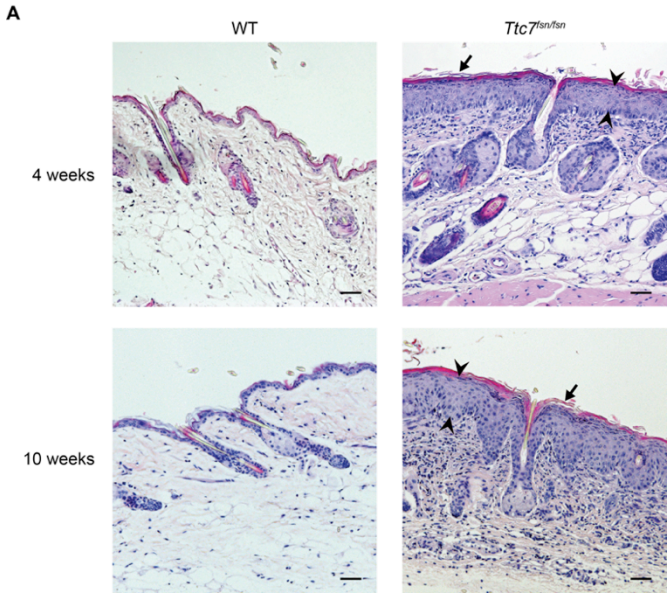

Figure 17A. Early onset of hyperplastic dermatitis in *Ttc7*$^{fsn/fsn}$ mice. (**A**) Back skin sections of female WT and *Ttc7*$^{fsn/fsn}$ mice at the age of 4 and 10 weeks stained with hematoxylin-eosin reagent (Magnification: x10). Black scale bars represent 50µm. Acanthosis corresponds to thickening of the viable epidermis (black arrowheads) and hyperkeratosis showing thickening of the dead epidermis with ablation of keratin scales at the surface of the stratum corneum (black arrows).

Based on the age-related worsening of skin lesions, we quantified the severity of the lesions in both 4- and 10-week old mice. When comparing 4-week-old mice with 10-week old mice, the difference in dermal infiltration between *Ttc7*$^{fsn/fsn}$ mice and WT littermates was more pronounced than the difference in the severity of acanthosis (**Figures 17B-E**); this implies that acanthosis had occurred before dermal inflammation.

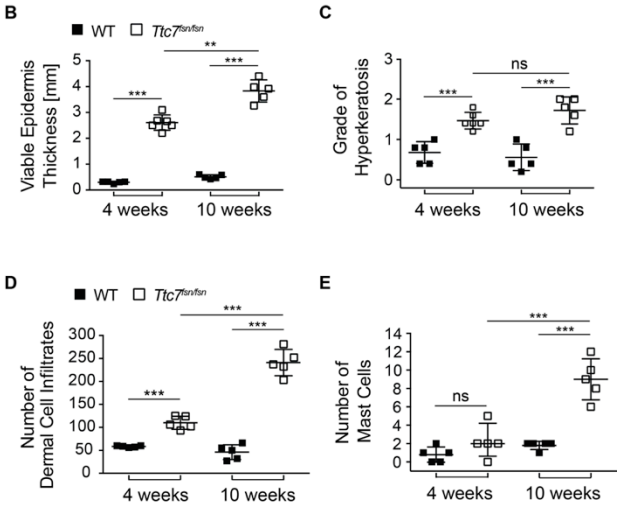

Figure 17B-E. Hyperplastic dermatitis gets more severe with age. (**B**) Quantification of acanthosis in WT and *Ttc7*$^{fsn/fsn}$ in three different visual fields (each of which was divided into five quadrants) per mouse. (Objective lens magnification: x10). Each symbol on the scatter plot represents the mean ±SD of 15 stratum spinosum thickness measurements in an individual mouse. (C) Hyperkeratosis of the stratum corneum was quantified by rating the severity per mouse. Grade 0: one or two peeled-off corneal layers at the surface; Grade 1: two or three peeled-off corneal layers; Grade 2: four or more peeled-off corneal layers. Each symbol represents the mean grade from three different pictures per mouse in each group. (**E**) Inflammation of the dermis was quantified by counting the total number of inflammatory cell infiltrates in the dermis underneath the basal layer. Three different images per mouse dermis (Magnification: x40) were captured and printed as 13x18 cm photos for evaluation. The symbols represent the mean number of cell infiltrates per mouse in each group. (**E**) Numbers of mast cells having infiltrated the dermis. The number of mast cells is included in the number of dermal cell infiltrates. Three different images per mouse dermis (Magnification: x40) were captured and printed as 13x18 cm photos for evaluation. Each symbol represents the mean mast cell count per mouse in each group. Each symbol in the scatter plots corresponds to an individual mouse (n = 5 mice), mean ±SD are indicated.

To characterize dermal leukocytes, we performed immunohistochemical staining of skin sections for lymphoid and myeloid markers. These stainings revealed high numbers of cells expressing CD4 and IL-17 (**Figures 17F-H**).

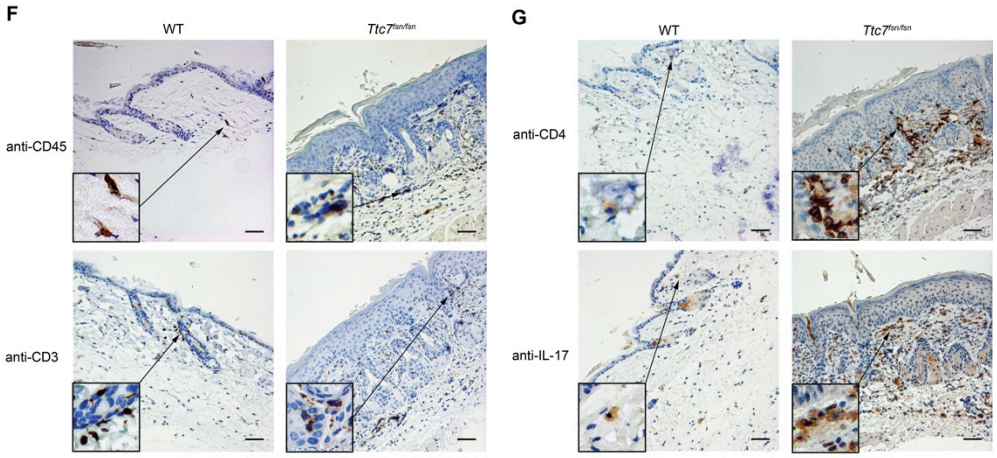

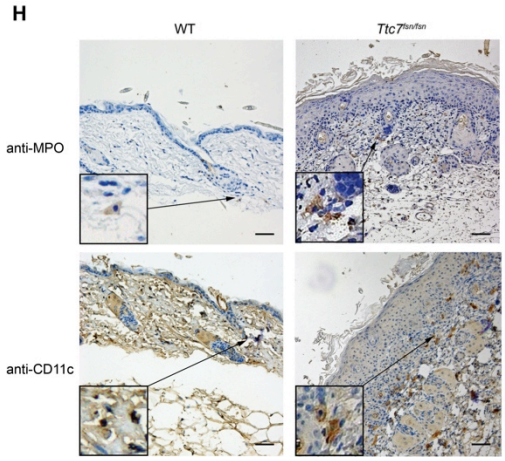

Figure 17F-H. Most dermal infiltrates belong to the lymphoid cell fraction in *Ttc7*$^{fsn/fsn}$ skin. (**F**) Skin sections stained with anti-CD45, anti-CD3, (**G**) anti-CD4 and anti-IL-17 antibodies of female WT and *Ttc7*$^{fsn/fsn}$ mice at the age of 10 weeks (Magnification: x10). Black scale bars correspond to 50µm. (**H**) Skin sections of female WT and *Ttc7*$^{fsn/fsn}$ mice at the age of 10 weeks stained with anti-MPO and anti-CD11c antibodies (Magnification: x10). Black scale bars correspond to 100µm.

1.7. Serum cytokine profile

Welner and colleagues showed that isolated splenic T cells from *Ttc7*$^{fsn/fsn}$ mice spontaneously produced high amounts of IL-4 [121]. Others correspondingly described higher serum levels of IL-5 [119]. To determine the possible effectors of hyperplasia and immune cell infiltration in the skin, we measured serum levels of cytokines known to be involved in inflammatory skin diseases, such as psoriasis or atopic dermatitis [153-155]. The serum levels of IL-4, IL-5, IL-10, IL-17 and IL-22 were significantly higher in *Ttc7*$^{fsn/fsn}$ mice than in WT littermates (**Figures 18A, 18B**). In both strains, levels of IFN-γ and TNF-α were apparently below the corresponding assay's limit of detection, while IL-15 and TGF-β levels were measurable but did not show significant differences between the two mouse strains (data not shown).

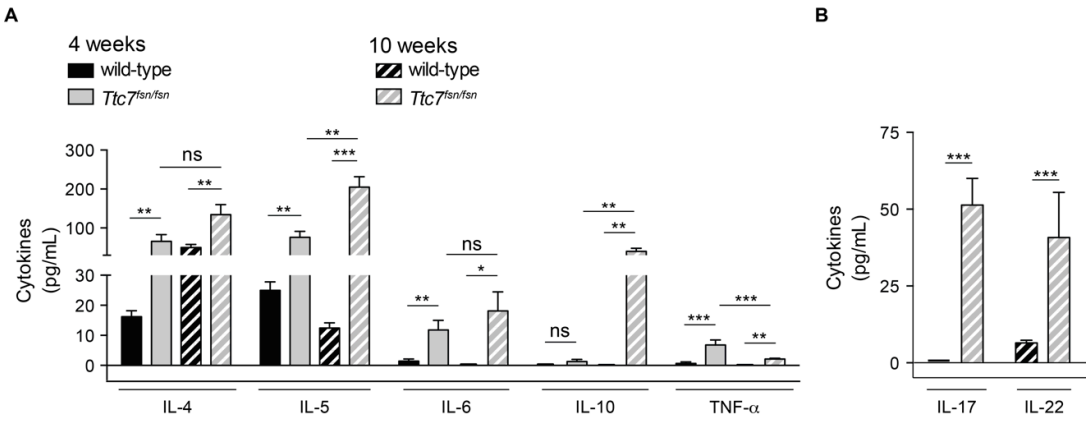

Figure 18. Serum cytokine profiles. (**A**) Serum cytokine levels of IL-4, IL-5, IL-6, IL-10 and TNF-α in 4-and 10-week old WT and *Ttc7*$^{fsn/fsn}$ mice. (**B**) Serum cytokine levels of IL-17 and IL-22 in 10-week old WT and *Ttc7*$^{fsn/fsn}$ mice. Cytokine profiles were measured in serum of gender-matched mice. Bars indicate pooled data from >3 independent experiments as the mean +SD (n = 6–11 mice).

Cytokines can modulate the proliferation of keratinocytes; this has been shown for IL4/IL-13 in atopic dermatitis and for the IL-23/IL-17 axis in psoriatic mouse models, in *in vitro* analysis and clinical studies [91, 154]. A high proportion of cells in *Ttc7*$^{fsn/fsn}$ skin sections stained positive for IL-17. Together with elevated serum IL-17 levels, this suggests that Th2 and Th17 cells promote the flaky skin phenotype.

Taking into account the ubiquitous expression of *Ttc7* and the multisystemic nature of the disease seen in both patients and *Ttc7*$^{fsn/fsn}$ mice — both developing an epithelial barrier dysfunction — we decided to further analyze the impact of hematopoietic and stromal cells on the hyperproliferative skin phenotype seen in the *Ttc7*$^{fsn/fsn}$ mouse.

2. Double and Triple Homozygous Mutant Mice

First, we generated immunodeficient double homozygous *Rag2*$^{-/-}$*Ttc7*$^{fsn/fsn}$ and triple homozygous *Rag2*$^{-/-}$*IL2rg*$^{-/-}$*Ttc7*$^{fsn/fsn}$ mutant mice and assessed their pathophysiology. The double mutant lacks lymphocytes from the adaptive immune system, whereas the triple mutant lacks lymphocytes from both the adaptive and innate immune system.

2.1. Splenomegaly associated with anemia

Double (*Rag2*$^{-/-}$*Ttc7*$^{fsn/fsn}$) and triple (*Rag2*$^{-/-}$*IL2rg*$^{-/-}$*Ttc7*$^{fsn/fsn}$) mutant strains presented with a severe anemia with low red blood cell counts and low hemoglobin levels (**Figures 19A, 19B**). The spleens were enlarged resulting in a 3–4-fold increase of the spleen/body weight ratio in mutant strains (**Figures 19C, 19D**). Histopathologic analysis of the spleen showed enlarged red pulp areas in spleens of double and triple mutant mice when compared with WT mice (**Figure 19E**).

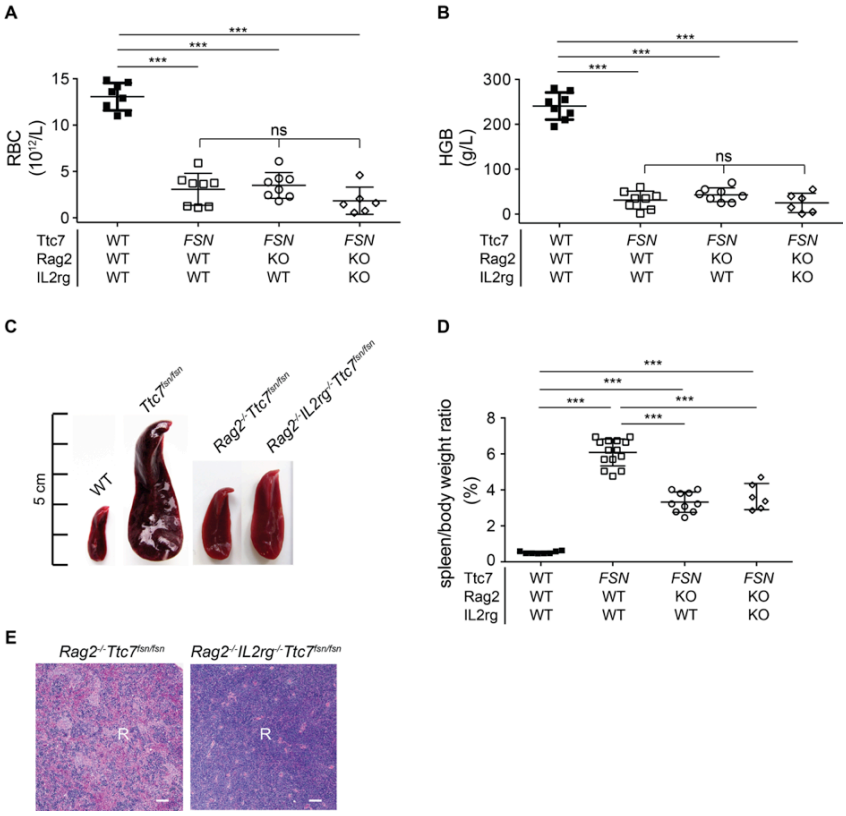

Figure 19A-E. Splenomegaly and anemia are preserved in double and triple mutant mice. (**A**) Red blood cells (RBC) and (**B**) hemoglobin (HGB) counts in peripheral blood of WT, single (*Ttc7*$^{fsn/fsn}$), double (*Rag2*$^{-/-}$*Ttc7*$^{fsn/fsn}$), and triple (*Rag2*$^{-/-}$*IL2rg*$^{-/-}$*Ttc7*$^{fsn/fsn}$) mutant mice at 10 weeks. (**C**) Photos of spleens from female WT, single, double, and triple mutant mice. (**D**) Spleen to body weight ratios. (**E**) Hematoxylin-eosin staining of splenic sections from double and triple mutant mice (Magnification: x5). White scale bars represent 100µm. "R" = red pulp. (**A**, **B**, **D**) The genotype of each mouse is shown below the chart (WT = wild-type, *FSN* = *Ttc7*$^{fsn/fsn}$, Rag2 = *Rag2*$^{-/-}$ (KO), IL2rg = *IL2rg*$^{-/-}$ (KO)). Scatter plots indicate pooled data as the mean ±SD from >3 independent experiments. Each symbol represents one individual mouse (n = 8–12 mice).

Further flow cytometric analysis of the spleens showed higher total numbers of splenocytes in double and triple mutant mice (**Figure 19F**). Despite higher CD45-positive cell counts, we did not find an increase in total numbers of any myeloid cell types in double nor in triple mutant mice when compared to the corresponding controls (**Figures 19G-K**). The increase in CD45-positive cells resulted from an increase in cells of the erythroid lineage (data not shown).

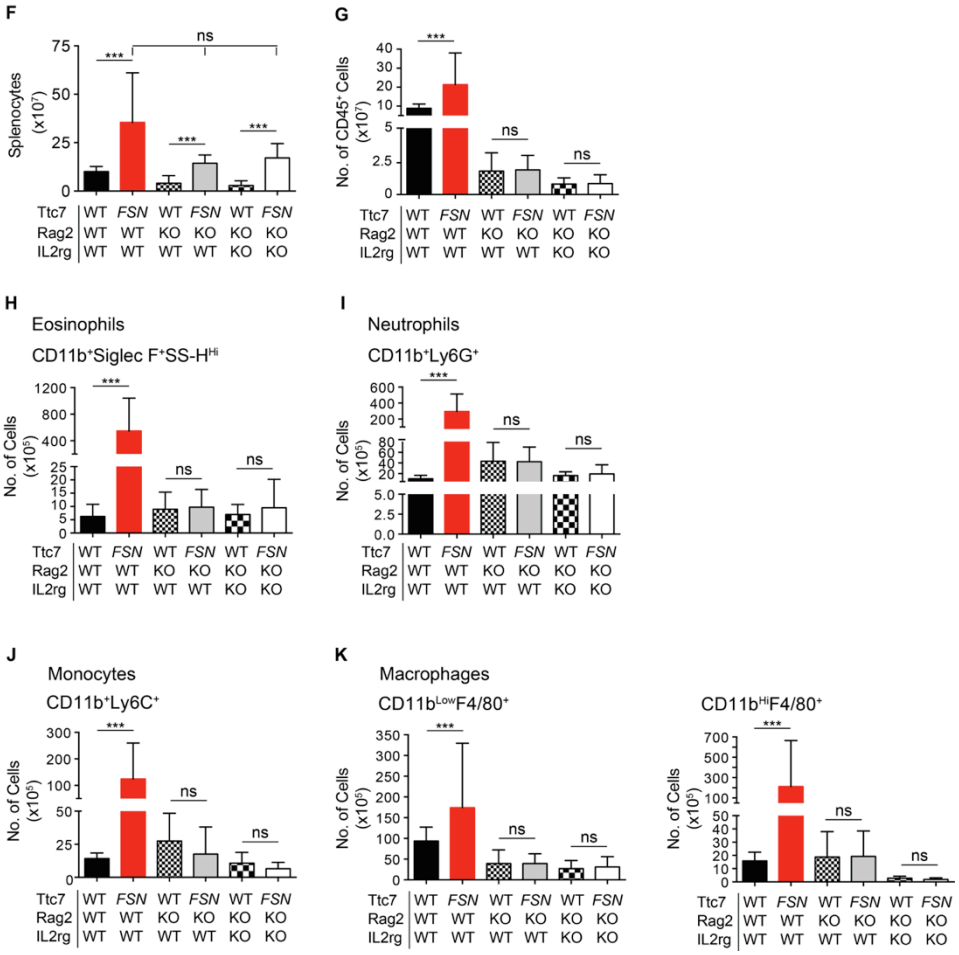

Figure 19F-K. Equal total numbers of eosinophils, neutrophils, monocytes, and macrophages in double and triple mutant mice. (**F**) Total number of splenocytes of 10-week old female WT, single, double, and triple mutant mice. (**G**) Total number of CD45$^+$ cells (CD45$^+$/Alive). (**H**) Eosinophils (CD11b$^+$, Siglec F$^+$ and SS-H^{Hi}/CD45$^+$), (**I**) neutrophils (CD11b$^+$, Ly6G$^+$/CD45$^+$ Siglec F$^+$ and SS-H^{Hi}), (**J**) monocytes (CD11b$^+$, Ly6C$^+$/CD45$^+$ Siglec F$^+$ SS-H^{Hi} and Ly6G$^+$), (**K**) CD11b^{Low} macrophages (CD11b^{Low}, F4/80$^+$/CD45$^+$ Siglec F$^+$ SS-H^{Hi} Ly6G$^+$ and Ly6C$^+$), and CD11b^{Hi} macrophages (CD11b^{Hi}, F4/80$^+$/CD45$^+$ Siglec F$^+$ SS-H^{Hi} Ly6G$^+$ and Ly6C$^+$) indicated as the total number per spleen. (**F-K**) The genotype of each mouse is shown below the chart (WT = wild-type, *FSN* = *Ttc7*$^{fsn/fsn}$, Rag2 = *Rag2*$^{-/-}$ (KO), IL2rg = *IL2rg*$^{-/-}$ (KO)). Bars indicate pooled data from >3 independent experiments as the mean +SD (n = 8–12 mice).

2.2. Hyperplastic skin-draining lymph nodes

The skin-draining lymph nodes in double and triple mutant strains were smaller than in single mutant mice but still remarkably larger than in the *Rag2*$^{-/-}$ and *Rag2*$^{-/-}$*IL2rg*$^{-/-}$ mice, in which lymph nodes cannot be seen macroscopically. (**Figure 20A**).

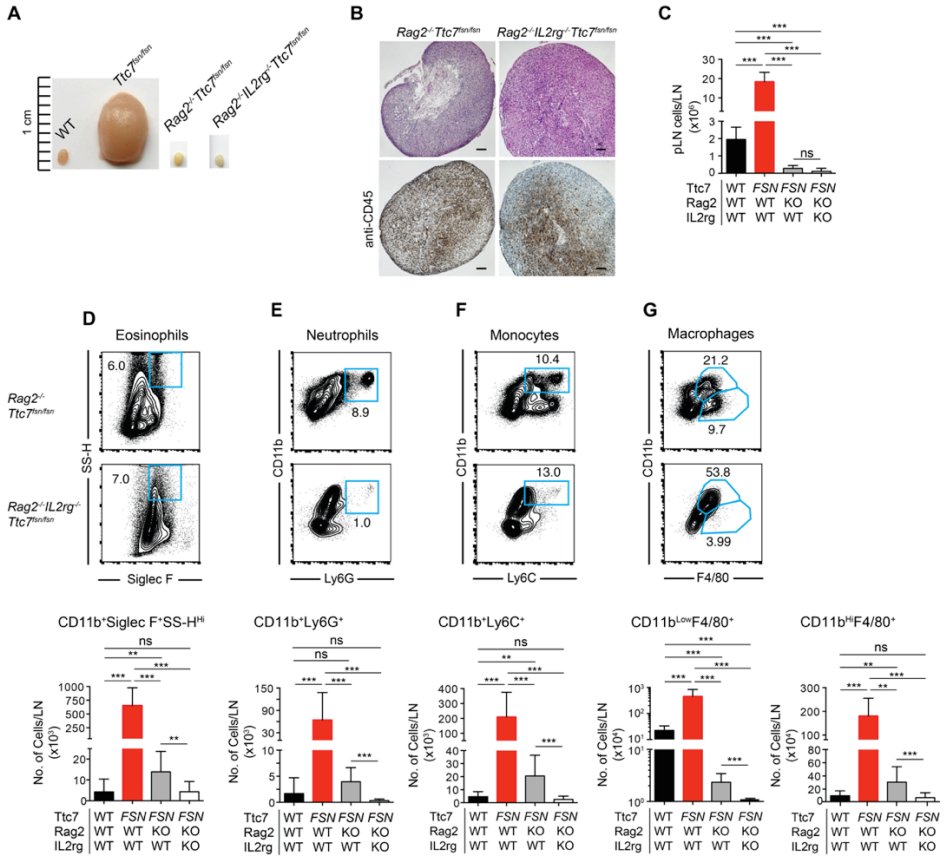

Figure 20. Non-lymphoid cells are markedly expanded in skin-draining lymph nodes. (**A**) Representative photos of axillary lymph nodes from 10-week old female mice. (**B**) Axillary lymph node sections of double and triple mutant mice stained with hematoxylin-eosin reagent and anti-CD45 antibodies (Magnification: x5). Black scale bars represent 100µm. (**C**) Total cell count per skin-draining lymph node. (**D**) Eosinophils (CD11b^{+}, Siglec F^{+} and SS-H^{Hi}/CD45^{+}), (**E**) neutrophils (CD11b^{+} and Ly6G^{+}/CD45^{+} Siglec F^{+} and SS-H^{Hi}), (**F**) monocytes (CD11b^{+} and Ly6C^{+}/CD45^{+} Siglec F^{+} SS-H^{Hi} and Ly6G^{+}), (**G**) CD11b^{Low} macrophages (CD11b^{Low} and F4/80^{+}/CD45^{+} Siglec F^{+} SS-H^{Hi} Ly6G^{+} and Ly6C^{+}), and CD11b^{Hi} macrophages (CD11b^{Hi} and F4/80^{+}/CD45^{+} Siglec F^{+} SS-H^{Hi} Ly6G^{+} and Ly6C^{+}) given as total numbers per lymph node of indicated gates. The genotype is indicated below the chart (WT = wild-type, *FSN* = *Ttc7*$^{fsn/fsn}$, Rag2 = *Rag2*$^{-/-}$ (KO), IL2rg = *IL2rg*$^{-/-}$ (KO)). Bars represent pooled data as the mean +SD (n = 7–16 mice).

In double and triple mutant mice, the skin-draining lymph nodes were filled with nucleated cells that stained positive for CD45 (**Figure 20B**). The total number of cells per lymph node was proportional to the organ size (**Figure 20C**). Absolute eosinophil, neutrophil, monocyte, and macrophage counts were elevated in double and triple mutant mice, relative to the corresponding controls (**Figures 20D-G**). In contrast to the high proportion of CD11b^{Low} macrophages seen in single (*Ttc7*$^{fsn/fsn}$) mutant mice, the lymph nodes of double and triple mutant mice showed markedly elevated levels of CD11b^{Hi} macrophages; these probably corresponded to tissue-resident anti-inflammatory M2 macrophages. Overall, eosinophils, neutrophils, monocytes, and macrophages accounted for the main cell populations in skin-draining lymph nodes of the double and triple mutant mice.

2.3. Spontaneous formation of forestomach papillomas

Double and triple mutant mice also developed forestomach papillomas (**Figures 21A, 21B**). Interestingly, this intrinsic epithelial dysregulation persisted in the epithelium of the forestomach of the mutant strains.

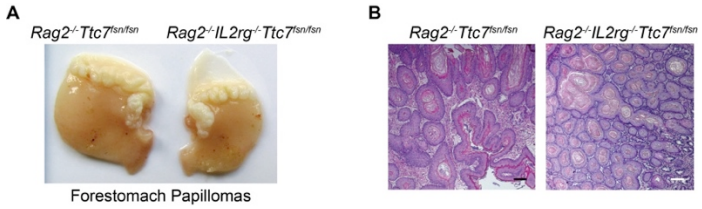

Figure 21. Spontaneous formation of forestomach papillomas is preserved in double and triple mutant strains. (**A**) Representative macro- and microscopic photos of forestomach papillomas from 10-week old female double and triple mutant mice. (**B**) Hematoxylin-eosin staining of forestomach sections (Magnification: x10). Black scale bars correspond to 100μm.

2.4. Hyperproliferative skin is linked with increased IL-22 but not IL-17 production

To attain further insights into the role of *Ttc7*$^{fsn/fsn}$ lymphocytes in the development of the flaky skin phenotype, we next compared the skin phenotypes of double and triple mutant strains. Both groups developed ruffled fur and white scaly skin. Interestingly, we found IL-22-positive cells not only in the dermis of double mutant mice but also in triple mutant mice (**Figure 22A**).

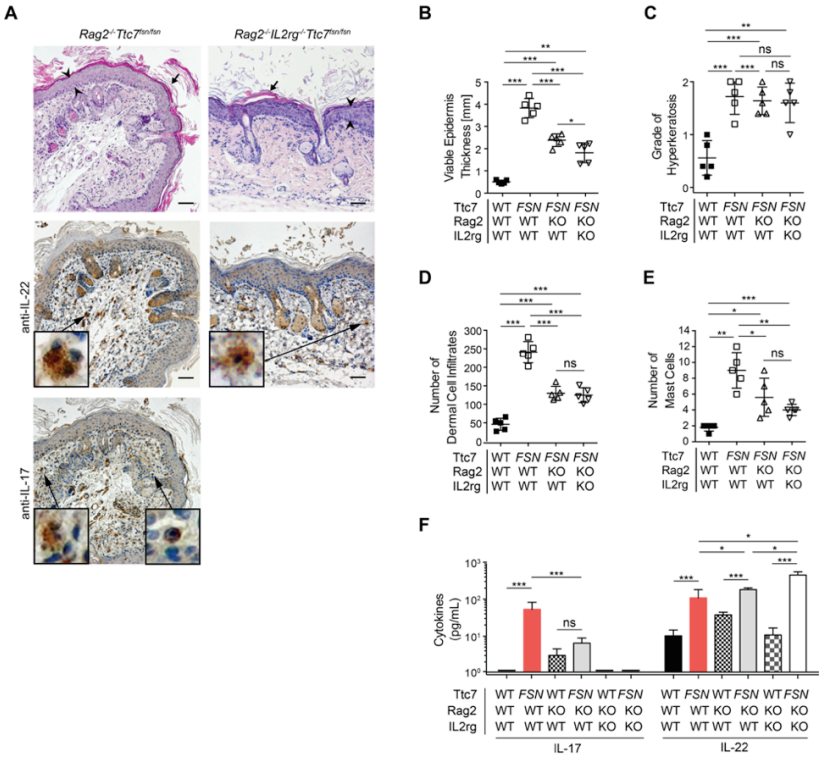

Figure 22. Diffuse epidermal hyperplasia of the skin remains even without systemic IL-17 hypercytokinemia in the triple mutant strains. (**A**) Back skin sections of gender-matched double and triple mutant mice stained with hematoxylin-eosin reagent, anti-IL22 antibodies and anti-IL-17 antibodies (Magnification: x10). Black scale bars represent to 50µm. Acanthosis (black arrowheads) and hyperkeratosis with ablation of keratin scales at the surface (black arrows). (**B-E)** Quantification of acanthosis (**B**), hyperkeratosis (**C**), inflammation of the dermis by total number of infiltrates (**D**), and the number of mast cells in the dermis (**E**), (Strategy is described under Figures 17B-E). (**F**) Serum cytokine levels of IL-17 and IL-22 in gender-matched WT, single, double and triple mutant mice serum. (**B**-**E**) The genotype is indicated below the chart (WT = wild-type, *FSN* = *Ttc7*$^{fsn/fsn}$, Rag2 = *Rag2*$^{-/-}$ (KO), IL2rg = *IL2rg*$^{-/-}$ (KO)). Bars indicate pooled data from >3 independent experiments as the mean +SD (n = 8 mice). Each symbol in the scatter plots corresponds to an individual mouse (n = 5) and expresses the mean ±SD values.

We then quantified the histological changes of the skin (**Figures 22B-E**). Severity for all parameters was significantly altered in all three mutant strains when compared to WT mice. Notably though, the double and triple mutant mice showed reduced severity grades compared to the single mutant mice in all parameters, except hyperkeratosis. To determine possible effectors causing hyperplasia and immune cell infiltration in the skin, we measured IL-17 and IL-22. Strikingly, serum IL-17 levels were similar between double mutant mice and corresponding controls, but significantly elevated serum IL-22 levels were observed in both the double and triple mutants (**Figure 22F**). Interestingly, the highest IL-22 serum levels were measured in the triple mutant mice. This indicates that neither T cells, B cells, NK cells nor other innate lymphocytes (ILCs) are the essential sources of IL-22 in this murine mutant model. Mast cells predominantly stained positive for IL-22 in immunohistochemical assessments (**Figure 22A**). IFN-γ levels were below the

detection limit, and TGF-β levels were equal between mutant strains and the corresponding controls (data not shown).

Collectively, these results suggest that the hematopoietic system is not critical in inducing the flaky skin phenotype, although lymphocytes aggravate the clinical course of the disease.

3. Bone Marrow Chimera

In order to determine the influence of mutated hematopoietic cells in causing the hyperplastic skin of the flaky skin mutant model, we generated gender-matched bone marrow chimeras. The mean level of chimerism 84 days after bone marrow transfer was 67.5% (range: 40-95%).

Unfortunately, we were not able to perform an efficient bone marrow transfer of wild-type cells into *Ttc7*$^{fsn/fsn}$ mice. These mice died within few days after the transfer, most probably due to the pre-existing anemia.

3.1. Slight anemia but no splenomegaly in bone marrow chimera

Initially, we examined whether the anemia can be transferred leading to hyperplasia of the spleen. We did indeed measure slightly reduced red blood cell counts in mice having received *Ttc7*$^{fsn/fsn}$ bone marrow (*Ttc7*$^{fsn/fsn}$ > *WT*) (**Figures 23A, 23B**). However, *Ttc7*$^{fsn/fsn}$ > *WT* chimeras had equal spleen sizes and spleen/body weight ratios when compared to control chimeras (*WT* > *WT*) (**Figures 23C, 23D**).

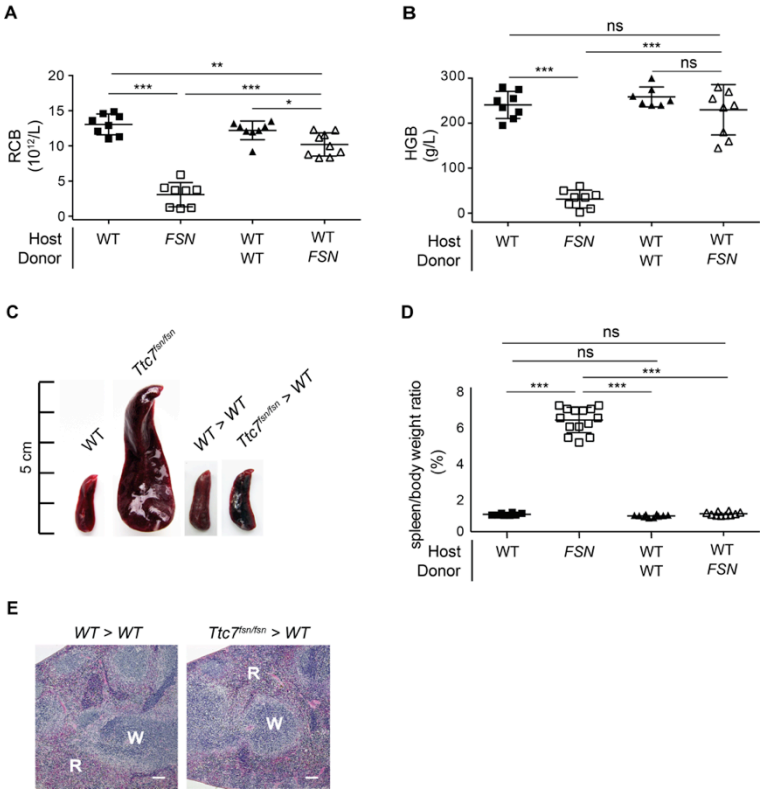

Figure 23A-E. No sign of splenomegaly in *Ttc7*$^{fsn/fsn}$ > *WT* chimera mice. (**A**) Red blood cells (RBC) and (**B**) hemoglobin (HGB) counts in peripheral blood of *WT* > *WT* and *Ttc7*$^{fsn/fsn}$ > *WT* chimera mice. (**C**) Representative photos of spleens from female WT, *Ttc7*$^{fsn/fsn}$, *WT* > *WT*, and *Ttc7*$^{fsn/fsn}$ > *WT* mice. (**D**) Spleen to body weight ratios. (**E**) Hematoxylin-eosin staining of splenic sections from *WT* > *WT* and *Ttc7*$^{fsn/fsn}$ > *WT* chimera mice (magnification: x5). White scale bars represent 100µm. "W" = white pulp; "R" = red pulp. (**A**, **B**, **D**) The genotype of each mouse is shown below the chart (WT = wild-type, *FSN* = *Ttc7*$^{fsn/fsn}$). Scatter plots indicate pooled data the mean ±SD from >3 independent experiments. Each symbol represents one individual mouse (n = 10–14).

Histopathologic analysis showed normal splenic architecture (**Figure 23E**). This data was consistent with the results from flow cytometric analysis, revealing no difference in splenocyte numbers (**Figure 23F).**

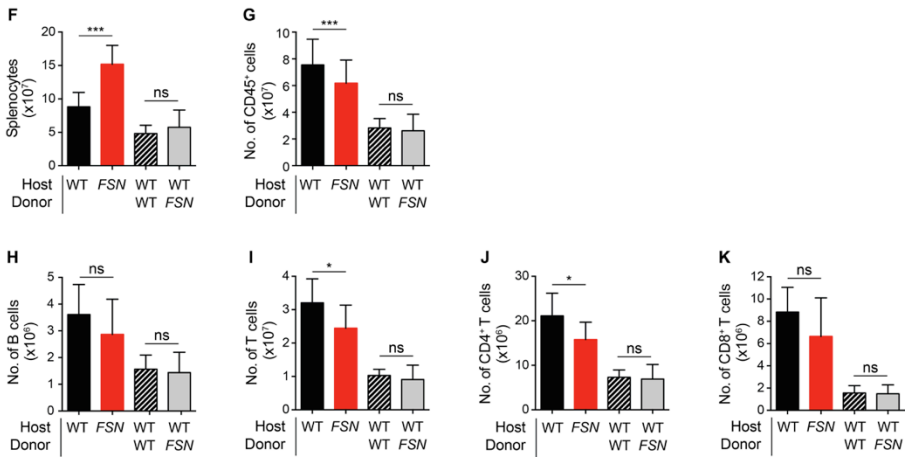

Figure 23F-K. No difference in lymphoid cells numbers. (**F**) Total number of splenocytes in WT, *Ttc7*$^{fsn/fsn}$, *WT* > *WT*, and *Ttc7*$^{fsn/fsn}$ > *WT* chimera mice. (**G**) Total number of CD45$^+$ cells (CD45$^+$/Alive). (**H**) Total number of CD19$^+$ B cells (CD19$^+$/CD45$^+$). (**I**) Total number of CD3$^+$ T cells (CD3$^+$/CD45$^+$). (**J**) Total number of CD4$^+$ T cells (CD4$^+$/CD45$^+$CD3$^+$). (**J**) Total number of CD8$^+$ T cells (CD8$^+$/CD45$^+$CD3$^+$). (**F-K**) The genotype of each mouse is shown below the chart (WT = wild-type, *FSN* = *Ttc7*$^{fsn/fsn}$). Bars indicate pooled data from >3 independent experiments as the mean +SD (n = 7–12 mice).

The lymphoid and myeloid cell counts were similar when comparing the two chimera strains (**Figures 23G-P**).

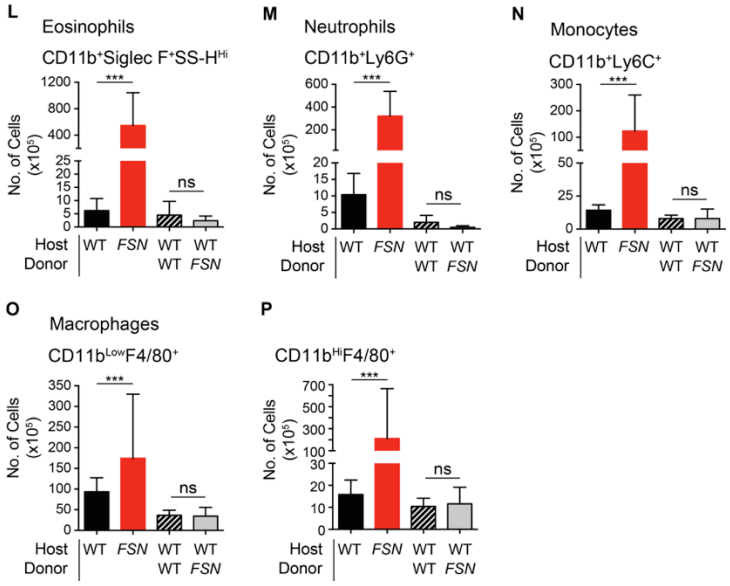

Figure 23L-P. No difference in myeloid cell numbers. (**L**) Eosinophils (CD11b$^+$, Siglec F$^+$ and SS-H^{Hi}/CD45$^+$), (**M**) neutrophils (CD11b$^+$, Ly6G$^+$/CD45$^+$ Siglec F$^+$ and SS-H^{Hi}), (**N**) monocytes (CD11b$^+$, Ly6C$^+$/CD45$^+$ Siglec F$^+$ SS-H^{Hi} and Ly6G$^+$), (**O**) CD11b^{Low} macrophages (CD11b^{Low}, F4/80$^+$/CD45$^+$ Siglec F$^+$ SS-H^{Hi} Ly6G$^+$ and Ly6C$^+$), and (**P**) CD11b^{Hi} macrophages (CD11b^{Hi}, F4/80$^+$/CD45$^+$ Siglec F$^+$ SS-H^{Hi} Ly6G$^+$ and Ly6C$^+$) indicated as the total number per spleen. (**L-P**) The genotype of each mouse is shown below the chart (WT = wild-type, *FSN* = *Ttc7*$^{fsn/fsn}$). Bars indicate pooled data from >3 independent experiments as the mean +SD (n = 8–12 mice).

In summary, although we observed a slight reduction of the red blood cell count after transplant of *Ttc7*$^{fsn/fsn}$ bone marrow, there was no transfer of the other parameters indicative of severe anemia via bone marrow transplant.

3.2. No peripheral lymphadenopathy

Skin-draining lymph nodes of *Ttc7*$^{fsn/fsn}$ > *WT* chimera mice had a normal lymph node size and correctly organized architecture (**Figures 24A, 24B**). Both chimera strains gathered an equal number of cells in their skin-draining lymph nodes (**Figure 24C**). Also, flow

cytometric analysis of the lymphoid and myeloid cell fraction did not show any significant alterations (**Figures 24D-L**).

Taking these findings together, there was no transfer of the hyperplastic *Ttc7*$^{fsn/fsn}$ phenotype to the *Ttc7*$^{fsn/fsn}$ > *WT* chimera lymph nodes.

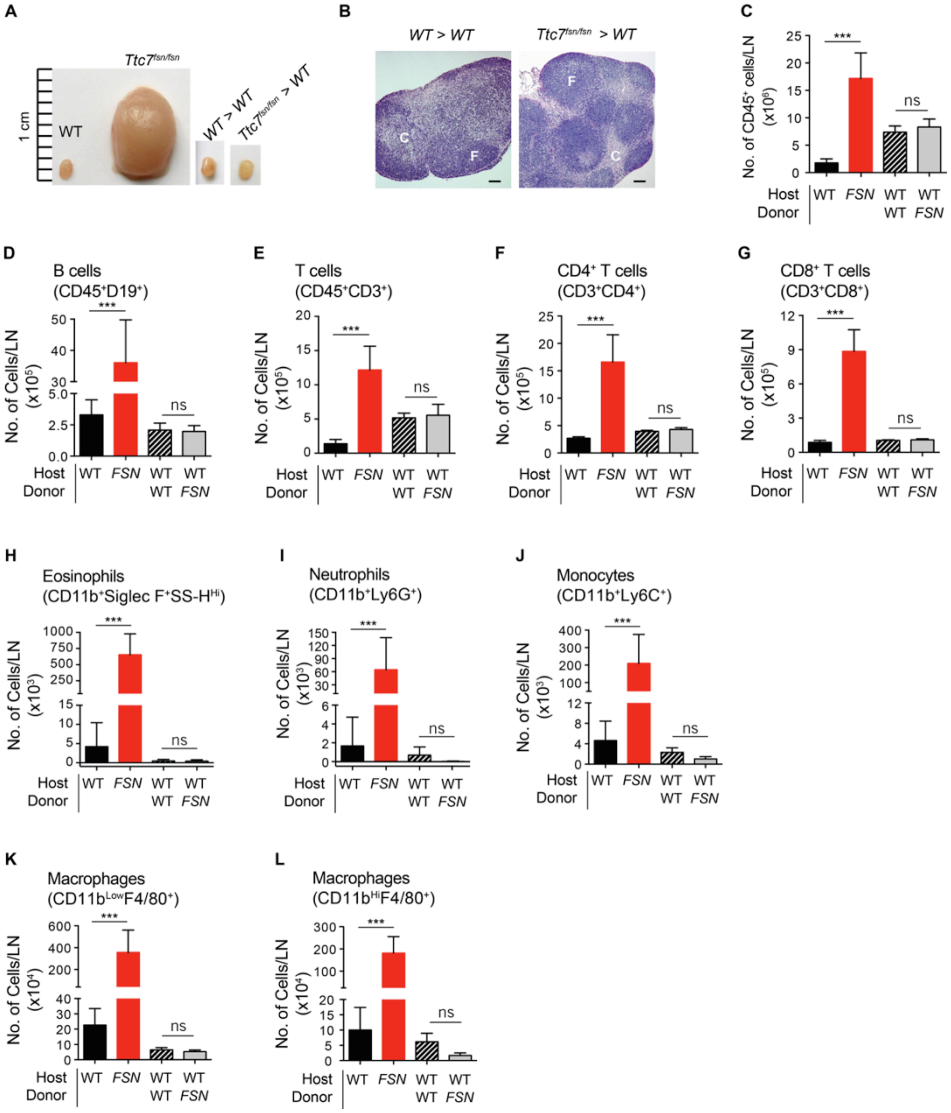

Figure 24. No lymphadenopathy in *Ttc7*$^{fsn/fsn}$ chimera mice. (**A**) Representative photos of axillary lymph nodes from WT, *Ttc7*$^{fsn/fsn}$, *WT* > *WT*, and *Ttc7*$^{fsn/fsn}$ > *WT* mice. (**B**) Axillary lymph node sections of *WT* > *WT* and *Ttc7*$^{fsn/fsn}$ > *WT* chimera mice stained with hematoxylin-eosin reagent (Magnification: x5). Black scale bars represent 100µm. F = follicle; C= cortex. (**C**) Total CD45$^+$ cell number per skin-draining lymph node. (**D**) Total numbers of CD19$^+$ B cells (CD19$^+$/CD45$^+$), (**E**) CD3$^+$ T cells, (**F**) CD4$^+$ T cells (CD4$^+$/CD45$^+$CD3$^+$), and (**G**) CD8$^+$ T cells (CD8$^+$/CD45$^+$CD3$^+$) per lymph node. (**H**) Eosinophils (CD11b$^+$, Siglec F$^+$ and SS-H^{Hi}/CD45$^+$), (**I**) neutrophils (CD11b$^+$, Ly6G$^+$/CD45$^+$ Siglec F$^+$ and SS-H^{Hi}), (**J**) monocytes (CD11b$^+$, Ly6C$^+$/CD45$^+$ Siglec F$^+$ SS-H^{Hi} and Ly6G$^+$), (**K**) CD11b^{Low} macrophages (CD11b^{Low}, F4/80$^+$/CD45$^+$ Siglec F$^+$ SS-H^{Hi} Ly6G$^+$ and Ly6C$^+$) and (**L**) CD11b^{Hi} macrophages (CD11b^{Hi}, F4/80$^+$/CD45$^+$ Siglec F$^+$ SS-H^{Hi} Ly6G$^+$ and Ly6C$^+$), indicated as the total number per lymph node. (**C-L**) The genotype of each mouse is shown below the chart (WT = wild-type, *FSN* = *Ttc7*$^{fsn/fsn}$). Bars indicate pooled data with average mean ±SD (n = 7 –10 mice).

3.3. Unaffected thymic structure

Thymi of *Ttc7*$^{fsn/fsn}$ > *WT* chimera mice were equal in size and had a normal architecture with clearly marked cortical and medullary regions as in control chimeras (**Figures 25A, 25B**). Therefore, we did not further investigate this organ.

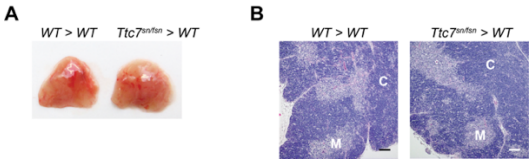

Figure 25. Normal thymic cortical and medullar architecture. (**A**) Representative photos of thymi from *WT* > *WT* and *Ttc7*$^{fsn/fsn}$ > *WT* chimera mice. (**B**) Hematoxylin-eosin staining of thymus sections from *WT* > *WT* and *Ttc7*$^{fsn/fsn}$ > *WT* chimera mice. (Magnification: x5). White and black scale bars correspond to 100µm; "M" = Medulla; "C" = Cortex.

This observation suggests that the pre-mature thymic atrophy observed in *Ttc7*$^{fsn/fsn}$ mice is not caused by hematopoietic-derived cells

3.4. Normal forestomach epithelium

The formation of the forestomach epithelium was not disturbed in *Ttc7*$^{fsn/fsn}$ > *WT* chimeras (**Figures 26A, 26B**). This indicates that forestomach papillomas in the *Ttc7*$^{fsn/fsn}$ mouse occur without the influence of the hematopoietic system. This points towards an intrinsic defect in the epithelial cells of *Ttc7*$^{fsn/fsn}$ mouse.

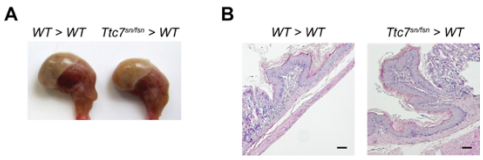

Figure 26. Forestmach papillomas do not develop after bone marrow transfer. (**A**) Representative photos of stomach from *WT* > *WT* and *Ttc7*$^{fsn/fsn}$ > *WT* chimera mice. (**B**) Hematoxylin-eosin staining of forestomach sections from *WT* > *WT* and *Ttc7*$^{fsn/fsn}$ > *WT* chimera mice. (Magnification: x10). White and black scale bars correspond to 100µm.

3.5. Healthy skin and normal serum cytokine profiles

To determine the influence of hematopoietic cells on the skin of bone marrow chimeras we analyzed the skin of *Ttc7*$^{fsn/fsn}$ > WT chimeras. No macro- or microscopic lesions could be found in the skin of these mice (**Figure 27A**). Acanthotic or hyperkeratotic signs were

absent, although the mean chimerism level was 67.5% at day 84 after bone marrow transfer (**Figures 27B, 27C**). Similarly, dermal inflammation was not present in bone marrow chimeras (**Figures 27D, 27E**).

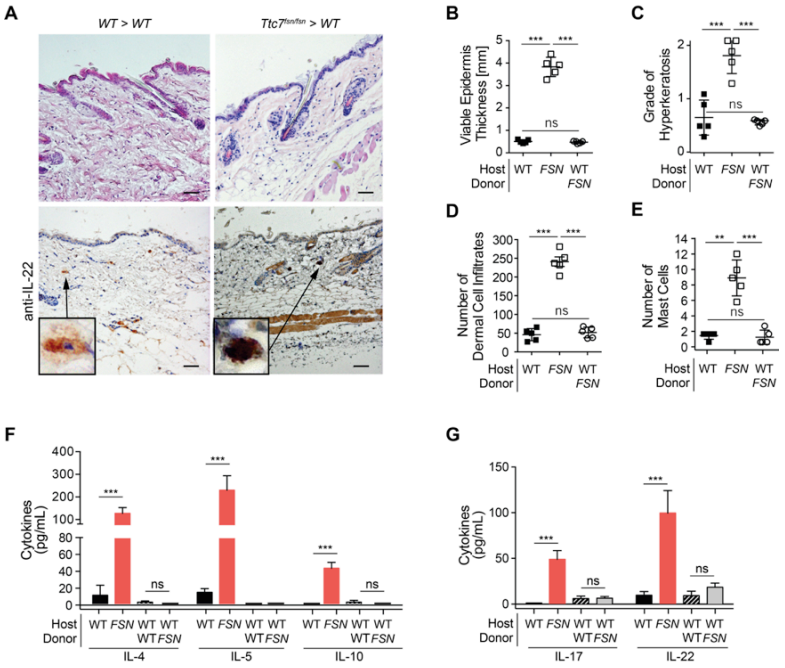

Figure 27. Hematopoietic-derived cells do not induce flaky skin. (**A**) Back skin sections of *WT* > *WT* and *Ttc7*$^{fsn/fsn}$ chimera mice stained with hematoxylin-eosin reagent and anti-IL22 antibodies (Magnification: x10). Black scale bars represent 50µm. (**B**) Quantification of acanthosis, (**C**) hyperkeratosis, (**D**) inflammation of the dermis by total number of infiltrates and (**E**) the number of mast cells in the dermis; (Strategy is described under Figures 17B-E). (**F**) Serum cytokine levels of IL-4, IL-5 and IL-10. (**G**) Serum cytokine levels of IL-17 and IL-22. (**B**-**E**) The genotype is indicated below the chart (WT = wild-type, *FSN* = *Ttc7*$^{fsn/fsn}$). Each symbol in the scatter plots corresponds to an individual mouse (n = 5) and expresses the mean ±SD values. Bars indicate pooled data from >3 independent experiments as the mean +SD (n = 8 mice).

Finally, the serum cytokine profiles of IL-4, IL-5, IL-10, IL-17, and IL-22 were measured and did not reveal any significant differences between *Ttc7*$^{fsn/fsn}$ > WT and control bone marrow chimeras.

Overall, this data indicates that the hematopoietic system does not transfer the flaky skin mutant phenotype. Accordingly, lymphoid cells do not play a central role in inducing the flaky skin disease, although they can aggravate the severity.

4. Xenograft Model – Dermal-Epidermal Skin Substitutes (DESSs)

After assessing the development of the flaky skin disorder in the presence (bone marrow chimera) or absence of *Ttc7*$^{fsn/fsn}$ lymphocytes (double and triple mutant mice), we set up an *in vitro* co-culture system of stromal and epithelial skin cells across different species. This allowed us to specifically study and interrogate the relationship between non-hematopoietic cell types in the flaky skin phenotype.

Here, tissue-engineered dermo-epidermal skin substitutes (DESSs, based on collagen type I hydrogels) were populated with either WT or *Ttc7*$^{fsn/fsn}$ fibroblasts and seeded with human keratinocytes (**Figure 28**). The DESSs were then transplanted onto full-thickness skin wounds of immunocompromised nude (athymic) rats. Three weeks after transplantation, the DESSs were analyzed.

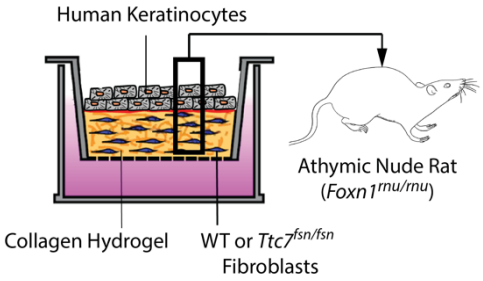

Figure 28. Xenograft Model. Schematic structure of the *in vitro* culture system of dermo-epidermal skin substitutes (DESSs).

4.1. *Ttc7*$^{fsn/fsn}$ fibroblasts drive keratinocyte hyperproliferation

The analysis of the skin architecture on the DESSs revealed a markedly thicker epidermis produced by *Ttc7*$^{fsn/fsn}$ fibroblasts than by WT fibroblasts (**Figure 29B**). We used immunofluorescence staining to detect loricrin (a major component of the cornified cell envelope) and E-cadherin (a transmembrane protein with important functions in morphogenesis, the separation of different tissue layers, and cell migration) in combination with DAPI. Cell layers co-expressing loricrin and E-cadherin were thicker, and the number of cell layers was higher in *Ttc7*$^{fsn/fsn}$ DESSs than in WT DESSs.

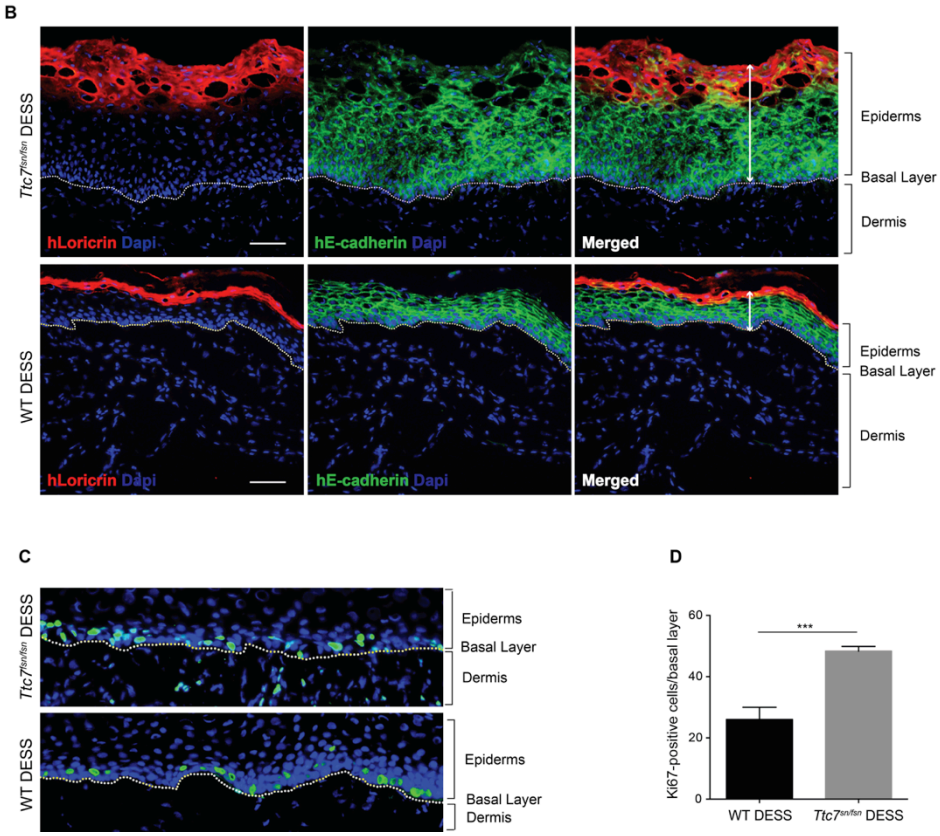

Figure 29. ***In vitro,* $Ttc7^{fsn/fsn}$ fibroblasts induce hyperkeratosis in tissue-engineered skin with human keratinocytes and athymic rat dermis.** (**B**) Immunochemical staining of loricrin (red) and E-cadherin (green) in $Ttc7^{fsn/fsn}$ and WT DESSs on day 21 after transplantation onto athymic nude rats (white arrows indicate the epidermis). (**C**) Immunofluorescence staining of Ki-67 (green) in $Ttc7^{fsn/fsn}$ and control DESSs on day 21 after transplantation onto athymic nude rats (white dotted lines indicate the dermo-epidermal junction). (**D**) Quantification of Ki-67-positive cells in the basal cell layer of $Ttc7^{fsn/fsn}$ and control DESSs. The white scale bar corresponds to 100µm.

Despite this difference, the distribution of loricrin and E-cadherin was similar in $Ttc7^{fsn/fsn}$ and WT DESSs. In both cases, loricrin was most prominently expressed in the granular layer of the epidermis in terminally differentiated keratinocytes. E-cadherin was most prominently expressed in the viable epidermis (as is observed in healthy skin *in vivo*).

Remarkably, in contrast to its restricted expression in the basal layers of WT DESSs, the proliferation marker Ki-67 was expressed in both dermal and epidermal layers in $Ttc7^{fsn/fsn}$ DESSs (**Figure 29C**). Moreover, human Ki-67 epidermal cells in the basal layer of $Ttc7^{fsn/fsn}$ DESSs were more numerous than the equivalent cells in WT DESSs (**Figure 29D**). Thus, $Ttc7^{fsn/fsn}$ fibroblasts were identified as key players in hyperproliferation of normal keratinocytes, even across species borders.

5. Next Generation Sequencing of RNA Fibroblast

To gain further insights into *Ttc7*$^{fsn/fsn}$ fibroblasts, we isolated RNA from primary WT and *Ttc7*$^{fsn/fsn}$ fibroblast cultures and performed next generation sequencing (NGS) analyses.

5.1. Transcriptomic pattern of *Ttc7*$^{fsn/fsn}$ fibroblasts shows an inflammatory pattern, cytoskeleton modeling, and plasma membrane pathways and processes

The fact that *Ttc7*$^{fsn/fsn}$ fibroblasts were able to induce keratinocyte hyperproliferation suggests that mutations in *Ttc7* alter the expression of regulatory molecules in fibroblasts. We therefore used NGS to analyze and compare the transcriptomes in *Ttc7*$^{fsn/fsn}$ and WT fibroblasts. This method revealed that the expression of more than 1,000 genes was significantly altered in *Ttc7*$^{fsn/fsn}$ fibroblasts. In the latter, there were more upregulated genes than downregulated genes (false discovery rate (FDR) = 0.5, log fold change (FC) > 1; **Figure 30A**). Cluster and MetaCore™ analyses of the top 10% of genes revealed a high degree of variance between *Ttc7*$^{fsn/fsn}$ and WT fibroblasts. Thus, the genes with significantly altered expression could be clustered and associated to key molecular pathways (**Figures 30B-E**; **Supplemental Figures 1–4**). When comparing *Ttc7*$^{fsn/fsn}$ fibroblasts with WT fibroblasts, six distinct clusters were identified. Upregulated transcripts were present in clusters 1, 2, 3, and 5; downregulated transcripts were present in cluster 6, and differentially regulated transcripts were present in cluster 4. Genes related to cell adhesion, the cytoskeleton, and ECM interactions were significantly affected, and they were present in all six clusters (**Supplemental Figures 1-5**). Significantly altered expressions of genes involved in processes related to angiogenesis, vasoconstriction, signal transduction, inflammation and immune responses were additionally present in all six clusters (**Supplemental Figures 1–4**). Transcripts related to development and multicellular organisms were mainly upregulated (i.e., in clusters 1, 2, and 3). Cluster 5 (upregulated genes) generally contained transcripts involved in immune cell activation (**Supplemental Figures 1–4**). Also, cluster 6 grouped pathways and processes related to immune responses and inflammation (downregulated transcripts, **Supplemental Figures 1** and **3**).

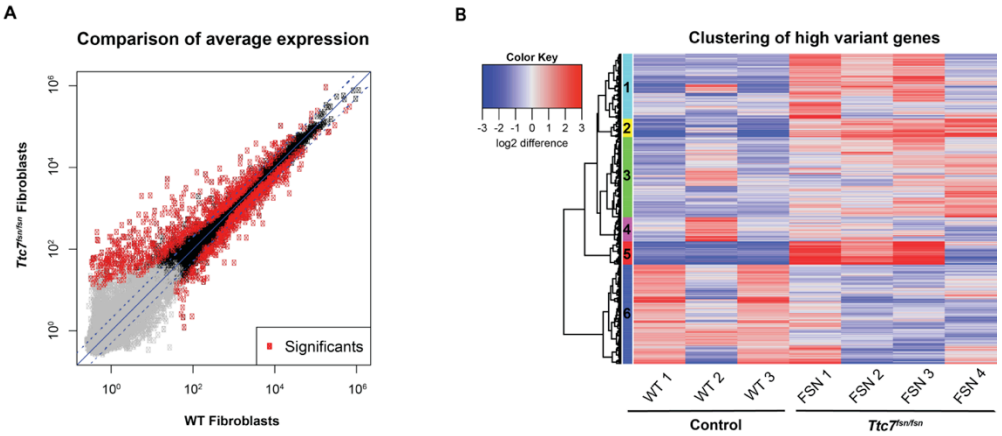

Figure 30A-B. The NGS of fibroblast RNA extracted from WT and *Ttc7*$^{fsn/fsn}$ mice.
(**A**) A scatterplot showing differentially expressed genes in *Ttc7*$^{fsn/fsn}$ fibroblasts vs. WT fibroblasts on an exponential scale. More than 1,000 genes were significantly differentially expressed ($p \leq 0.01$). (**B**) A heat map showing the expression patterns for the 2,500 top-ranked genes in six different clusters. Log2-transformed signals are shown according to the scale bar (color key). Each column represents an experimental sample, and each row represents a gene. Red corresponds to high expression, while blue corresponds to low expression.

When comparing *Ttc7*$^{fsn/fsn}$ fibroblasts with WT fibroblasts, the overexpression of genes involved in cell adhesion, G-protein-coupled-receptor activity and the plasma membrane were also revealed by a detailed cluster analysis (**Figure 30C**, **Supplemental Figures 1–5**).

By performing a gene ontology functional enrichment for endogenous metabolic networks and then a MetaCore™ analysis, we found that the phosphatidylinositol-4,5-disphosphate ($PI(4,5)P_2$) pathway was the most significantly upregulated pathway in *Ttc7*$^{fsn/fsn}$ fibroblasts when compared with WT fibroblasts (**Figure 30D**). Together with the phosphatidylinositol-3,4,5-triphosphate ($PI(3,4,5)P_3$) pathway at position 10, these two metabolic pathways play crucial roles in cytoskeletal regulation and signal transduction.

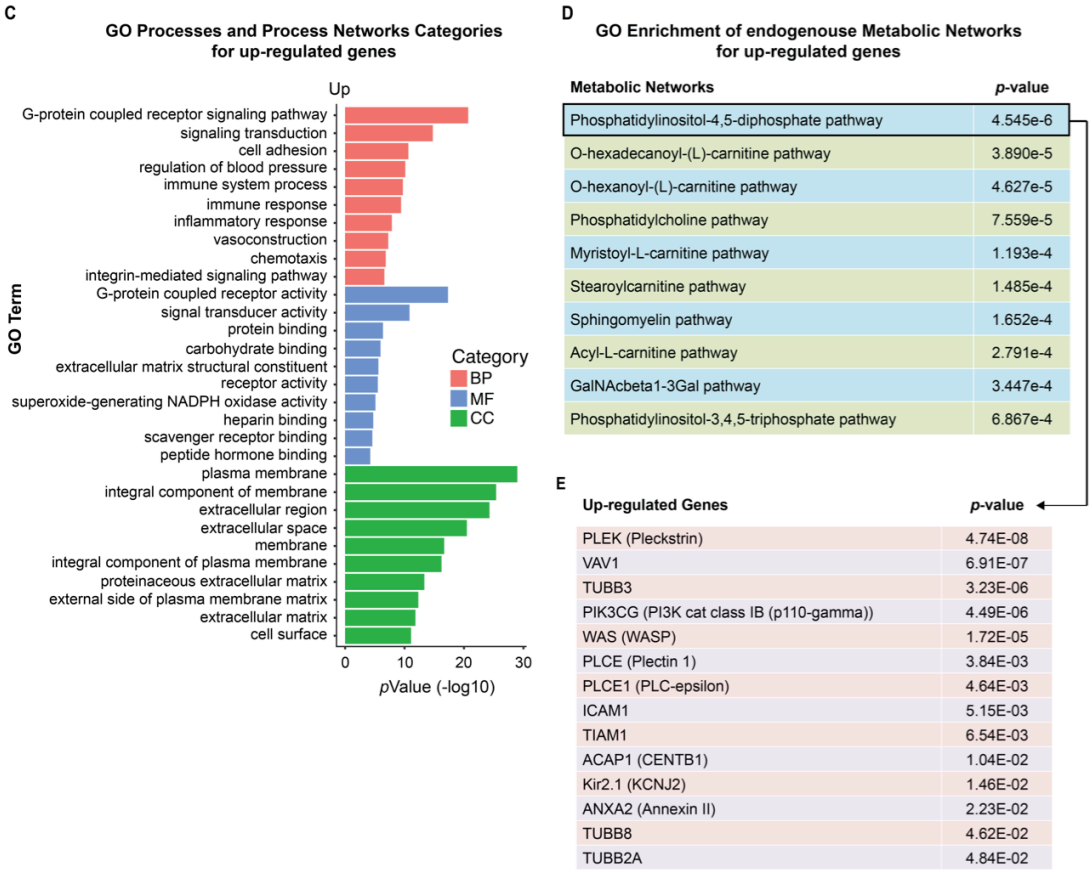

Figure 30C-E. Defined cluster 1-6 and MetaCore™ analysis of transcriptomic data. (**C**) The enriched gene ontology (GO) categories of clusters 1-6 combining upregulated gene candidates, presented on a *p*-value (-log10) scale. BP: biological process (red); MF: molecular function (blue); CC: cellular component (green). (**D**) A table showing GO enrichment for metabolic network processes of upregulated genes, followed by a MetaCore™ analysis (endogenous, $p < 0.05$). The top 10 metabolic pathways are listed. (**E**) Upregulated genes in the phosphatidylinositol-4,5-biphosphate pathway, as determined in the MetaCore™ analyses depicted in (**D**).

MetaCore™ pathway analyses of all six clusters simultaneously revealed a set of key signaling pathways. These include cytoskeletal remodeling pathways as well as signaling pathways related to immune responses and stimulation (**Table A**).

When screening for factors that might drive fibroblast and keratinocyte proliferation, we observed significantly enhanced expression (p=0.0109, **Figure 30F**) of insulin-like growth factor 1 (IGF-1, cluster 2, and **Supplemental Figure 1**); IGF-1 is known to induce keratinocyte proliferation. The expression of other growth factors, including fibroblast growth factors 3, 7, and 10, epidermal growth factors, and others were downregulated (data not shown).

Pathway Maps		
pathway term	count	*p*-value
Immune response IL-6 signaling pathway via JAK/STAT	42/72	2.012e-13
Transcription Epigenetic regulation of gene expression	35/57	2.562e-12
Development, Insulin, IGF-1 and TNF-alpha in brown adipocyte differentiation	33/52	2.888e-12
Apoptosis and survival FAS signaling cascades	29/44	1.530e-11
Cytoskeleton remodeling, TGF, WNT and cytoskeletal remodeling	52/111	2.917e-11
Signal transduction mTORC1 downstream signaling	35/61	3.975e-11
Immune response IL-3 signaling via ERK and PI3K	48/102	1.382e-10
Transcription Sirtuin6 regulation and function	35/64	2.469e-10
Signal transduction of mTORC2 downstream signaling	36/68	4.624e-10
Immune response IFN-alpha/beta signaling via MAPKs	39/77	4.918e-10
Development, cytokine-mediated regulation of megakaryopoiesis	32/57	5.909e-10
Apoptosis and survival, Caspase activity	23/34	9.259e-10
Transcription, p53 signaling pathway	25/39	9.586e-10
Cytoskeleton remodeling	45/102	6.703e-9
Apoptosis and survival NGF/TrkA PI3K-mediated signaling	37/77	8.794e-9
Immune response IL-6 signaling pathway via MEK/ERK and PI3K/AKT cascade	36/74	9.210e-9
Putative pathway for stimulation of fat cell differentiation by Bisphenol A	21/32	1.164e-8
Immune response, IL-4 signaling pathway	42/94	1.349e-8
Aopoptosis and survival, Granzyme B signaling	21/33	2.621e-8
Development FLT3 signaling	25/44	3.282e-8

Table A. The NGS of mouse fibroblasts from WT and *Ttc7*$^{fsn/fsn}$. Enriched pathway maps for differentially expressed and upregulated genes of all six clusters. The first 20 results out of 50 are listed with the number of counted positive hits (count) and their *p*-values.

Furthermore, all clusters displayed significantly enhanced expression of genes related to ECM remodeling. The ECM is involved in most basic cell behaviors, such as cell proliferation, adhesion, migration, differentiation, and death [156]. We identified alterations in ECM components, such as collagen types III, V, and VI, fibronectin, elastin, laminin, and others (**Supplemental Figure 6**).

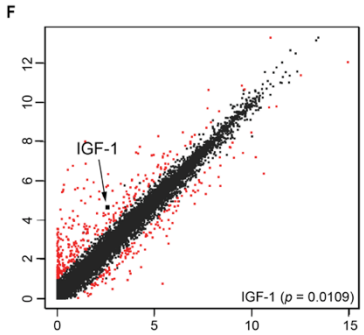

Figure 30F. (**F**) Position of upregulated IGF-1 (black arrow) in the scatter dot plot with corresponding *p*-values (p = 0.0109) on a log2 scale.

Altogether, this data shows that the *Ttc7* mutation in fibroblasts is associated with alterations in the expression of many genes. The fibroblasts play a critical role in regulating epithelial proliferation and might also influence surrounding cells in the dermis. An array of processes at the plasma membrane appears to be particularly affected. This includes the $PI(4,5)P_2$ pathway and important components of cell adhesion and receptor signaling processes. These changes might influence cell–cell interaction, cell development, cell differentiation, and inflammation. The disturbance of processes in the plasma membrane might explain why a *Ttc7* mutation with minor cell-intrinsic consequences has effects on neighboring cells — even when the latter express WT *Ttc7*. Taken as a whole, this is line with a hyper-responsiveness of stromal cells, which has been observed in isolated $Ttc7^{fsn/fsn}$ lymphocytes in previous publications [121, 128, 150].

5.1.1. Supplemental Figures 1 — 6

Supplemental Figure 1

Cluster Term	Pathway Maps	count	*p*-value
1	Cytoskeleton remodeling, keratin filaments	10	2.340e-10
	Cell adhesion, ECM remodeling	7	2.648e-5
	Development, Notch Signaling Pathway	5	7.182e-4
	Cell adhesion, Integrin inside-out signaling in neutrophils	6	1.804e-3
	Development, Transcription regulation of granulocyte development	4	1.902e-3
	Development, Trancriptional regulation of megakaryopoiesis	4	2.664e-3
	Complement pahtway disruption in thrombotic microangiopathy	4	3.973e-3
	Development, BMP7 in brown adiopcyte differentiation	4	3.973e-3
	Blood coagulation	4	3.973e-3
	Chemotaxis, CCL16-, CCL20-, CXCL16- and CCL25-mediated cell migration	4	4.897e-3
2	Protein folding and maturation angiotensin system maturation	9	8.945e-11
	Development, Insulin, IGF-1 and TNF-alpha in cell differentiation	9	5.540e-9
	Development, Differentiation of white adipocyte	8	3.234e-6
	Development, Beta adrenergic receptors in adiopocyte differentiation	6	1.883e-4
	Regulation of lipid metabolism, Insulin regulation of fatty acid metabolism	4	6.406e-4
	Role of Diethylhexyl Phthalate and Tributyltin in fat cell differentiation	5	1.455e-3
	Putative pathways for stimulation of fat cell differentiation by Bisphenol A	3	1.942e-3
	Signal transduction mTORC1 upstream signaling	3	2.637e-3
	Immune response IL-6-induced acute-phase response in hepatocytes	4	2.734e-3
3	Muscle contraction GPCRs in the regulation of smooth muscle tone	10	9.507e-6
	Airway smooth muscle contraction in asthma	8	2.146e-5
	Glucocorticoid-induced elevation of intracellular pressure as glaucoma risk factor	8	4.581e-5
	Cytoskeleton remodeling, Regulation of actin cytoskeleton by Rho GTPases	5	1.016e-4
	Role of Diethylhexyl Phthalate and Tributyltin in fat cell differentiation	5	3.232e-4
	Cell adhesion, integrin-mediated cell adhesion and migration	6	4.988e-4
	Chemotaxis, inhibitory action of lipoxins in IL-8 and Leukotrien B4-induced migration	6	8.545e-4
	Cytoskeleton remodeling, Role of PKA in cytoskeleton reorganisation	5	1.482e-3
	Immune response IL-4-responsive genes in type 2 immunity	6	3.623e-3
	Immune response IL-6 signaling pathway via JAK/STAT	6	4.168e-3
4	Develpment, Regulationof epithelial-to-mesenchymal transition (EMT)	5	3.627e-5
	Cytoskeleton remodeling, TGF, WNT and cytoskeletal remodeling	6	4.728e-5
	Cell adhesion, Plasmin signaling	4	5.125e-5
	Development, Regulation of lung epithelail progenitor cell differentiation	4	9.652e-5
	Development, S1P2,and S1P3 receptors in cell proliferation and differentiation	3	4.699e-4
	Development, TGF-beta-dependent induction of EMT via SMADs	3	1.139e-3
	Muscle contraction, GPCR in the regulation of smooth muscle tone	4	1.455e-3
	Development, TGF-beta-dependent induction of EMT via RhoA, PI3K and ILK	3	2.522e-3
	Transcription, Androgen Receptor nuclear signaling	3	2.522e-3
	Development, TGF-beta-dependent induction of EMT via MAPK	3	2.683e-3
5	Oxidatve stress, activation of NADPH oxidase	11	5.020e-12
	Oxidative stress, Role of IL-8 signaling pathway in respiratory burst	9	4.565e-10
	Immune response, Antigen presentation by MHC class I: cross presentation	11	1.383e-9
	Blood coagulation, GPVI-dependent platelet activation	9	1.668e-9
	Immune response, PIP3 signaling in B lymphocytes	8	3.482e-9
	Immune response, Immunological synapse formation	8	5.758e-8
	Inhibition of neutrophil migration by proresolving lipid mediators in COPD	8	2.525e-7
	Cell adhesion, Integrin inside-out signaling in T cells	8	3.497e-7
	Cell adhesion, Integrin inside-out signaling in neutrophils	8	4.774e-7
	Development, Gastrin in differentiation of the gastric mucosa	6	1.132e-6
6	Immune response, IL-17 signaling pathway	12	8.940e-8
	Alternative complement cascade disruption in age-related macular degeneration	9	1.223e-7
	Immune response, Alternative complement pathway	11	2.086e-6
	Th17 cells in CF	10	2.2883-6
	Th17 cell in CF (mouse model)	9	7.961e-6
	Glomerular injury in Lupus Nephritis	12	1.032e-5
	Apoptosis and survivial, NGF activation of NF-kB	8	1.329e-5
	Immune response, MIF-mediated glucocorticoid regulation	6	3.326e-5
	NALP3 inflammosome activation in age-related macular degeneration (AMD)	7	4.675e-5
	Rheumatoid arthritis (general schema)	8	7.253e-5

Supplemental Figure 1. Next generation sequencing of mouse fibroblasts from WT and *Ttc7*$^{fsn/fsn}$ mice. The enriched pathway maps for differentially expressed genes for clusters 1 to 6. The first 10 results of each cluster are listed.

Supplemental Figure 2

Cluster Term	GO Processes	count	*p*-value
1	Single organismal cell-cell adhesion	59	5.366e-21
	Single-multicellular organism process	241	6.497e-21
	Regulation of immune system process	108	1.625e-20
	Single organism cell adhesion	59	4.792e-20
	Cell activation	67	9.075e-20
	Inflammatory response	59	1.900e-19
	Regulation of multicellular organismal process	151	2.152e-19
	Regulation of response to stimulus	181	6.810e-19
	Biological adhesion	91	1.336e-18
	Cell adhesion	90	2.861e-18
2	Positive regulation of phosphorus metabolic process	42	3.215e-18
	Positive regulation of phosphate metabolic process	42	3.215e-18
	Response to organic substances	68	8.182e-17
	Regulation of phosphate metabolic process	49	1.403e-16
	Regulation of phosphorus metabolic process	49	1.428e-16
	Chemical homeostasis	40	1.430e-16
	Response to chemicals	82	2.781e-16
	Regulation of locomotion	35	6.353e-16
	Response to endogenous stimulus	50	6.865e-16
	Single-organism metabolic process	68	1.092e-15
3	Single-multicellular organism process	294	6.565e-28
	System development	245	2.802e-26
	Multicellular organism development	263	8.443e-25
	Regulation of multicellular organismal process	180	3.245e-23
	Anatomical structure development	270	5.361e-23
	Single-organism developmental process	277	1.705e-22
	Developmental process	279	5.361e-23
	Multicellular organismal process	320	1.705e-22
	Animal organ development	193	3.057e-22
	Cell differentiation	199	1.590e-21
4	Anatomical structure development	108	2.930e-20
	Multicellular organism development	103	2.110e-19
	System development	96	2.414e-19
	Single-multicellular organism process	110	3.510e-19
	Developmental process	109	9.938e-19
	Single-organism developmental process	108	1.263e-18
	Cellular developmental process	84	1.391e-17
	Cell differentiation	82	6.560e-17
	Multicellular organismal process	116	4.030e-15
	Anatomical structure morphogenesis	57	8.284e-14
5	Immune system process	91	7.424e-34
	Cell activation	53	8.871e-31
	Regulation of immune system process	73	1.796e-29
	Myeloid leukocyte activation	28	9.646e-29
	Leukocyte activation	45	5.862e-28
	Immune response	63	2.613e-27
	Regulation of immune response	57	9.235e-27
	Positive regulation of immune response	57	1.483e-26
	Myeloid cell activation involved in immune response	20	2.386e-25
	Mast cell activation	15	9.270e-24
6	Single-multicellular organism process	393	1.911e-45
	Multicellular organism development	361	2.404e-44
	System development	332	1.241e-43
	Anatomical structure development	374	1.626e-43
	Single-organism development process	380	2.328e-41
	Developmental process	382	1.023e-40
	Nervous system process	220	8.811e-38
	Cell differentiation	280	1.740e-37
	Neurogenesis	178	2.120e-37
	Cellular developmental process	281	2.222e-36

Supplemental Figure 2. Next generation sequencing of mouse fibroblasts from WT and *Ttc7*$^{fsn/fsn}$ mice. The enriched GO processes for differentially expressed genes for clusters 1 to 6. The first 10 results of each cluster are listed.

Supplemental Figure 3

Cluster Term	Process Networks	count	*p*-value
1	Cytoskeleton, Intermediate filaments	11	9.875e-6
	Development, blood vessel morphogenesis	15	1.248e-3
	Cell adhesion, cell junction	12	1.408e-3
	Blood cuagulation	8	3.775e-3
	Inflammation, Jak-STAT pathway	12	4.443e-3
	Proteolysis, connective tissue degradation	9	4.791e-3
	Cell adhesion, platelet-endothelium-leukocyte interactions	11	7.382e-3
	Proteolysis, ECM remodeling	7	7.905e-3
	Inflammation, Kallikrein-kinin system	11	1.144e-2
	Chemotaxis	9	1.173e-2
2	Development, ossification and bone remodeling	10	7.793e-6
	Inflammation, complement system	5	1.379e-3
	Cell adhesion, attractive and repulsive receptors	7	3.102e-3
	Development, neurogenesis, axonal guidance	8	3.744e-3
	Transport, Iron transport	5	6.711e-3
	Cell ahesion, glycoconjugates	6	8.852e-3
	Development, regulation of angiogenesis	7	1.113e-2
	Inflammation, Jak-STAT pathway	6	1.667e-2
	Reproduction, progesterone signaling	6	3.070e-2
	Cell adhesion, integrin-mediated cell-matrix adhesion	6	3.070e-2
3	Muscle contraction	22	4.216e-8
	Cell adhesion, cell-matrix interactions	24	8.823e-8
	Development, skeletal muscle development	19	2.045e-7
	Development, cartilage development	9	2.809e-4
	Development, neurogenesis, axonal guidance	16	3.696e-3
	Transport, potassium transport	13	1.151e-2
	Cell ahesion, platelet-endothelium-leucocyte interactions	12	1.208e-2
	Development, regulation of angiogenesis	14	1.463e-2
	Proteolysis, connective tissue degradation	9	1.633e-2
	Development, blood vessel morphogenesis	14	1.807e-2
4	Development, skeletal muscle development	9	3.274e-5
	Development, neurogenesis, synaptogenesis	9	1.847e-4
	Development, neurogenesis, axonal guidance	10	2.507e-4
	Cell adhesion, amyloid proteins	9	3.362e-4
	Reprodcution, feeding and neurohormone signaling	9	5.787e-4
	Muscle contraction	8	7.225e-4
	Reproduction, gonadotropin regulation	8	1.785e-3
	Development, ossification and bone remodeling	7	1.939e-3
	Reproduction, GnRH signaling pathway	7	2.660e-3
	Reproduction, progesterone signaling	8	2.813e-3
5	Immune response, phagocytosis	21	8.404e-14
	Cell adhesion, leukocyte chemotaxis	19	2.038e-12
	Cell adhesion, platelet aggregation	12	3.391e-7
	Inflammaion, IgE signaling	11	6.248e-7
	Chemotaxis	11	6.248e-7
	Immune response, phagosome in antigen presentation	14	9.864e-7
	Inflammation, neutrophil adhesion	13	1.460e-6
	Immune response, BCR pathway	9	3.575e-5
	Proliferation, lymphocyte proliferation	11	4.090e-5
	Cell adhesion, platelet-endothelium-leukocyte interactions	10	6.634e-5
6	Development, neurogenesis in general	25	2.012e-6
	Proteolysis, ECM remodeling	14	2.784e-5
	Chemotaxis	17	1.649e-4
	Cell adhesion, cell-matrix interactions	22	2.550e-4
	Muscle contraction	19	3.473e-4
	Immune response, Th17-derived cytokines	13	5.034e-4
	Inflammation, innate inflammatory response	19	5.734e-4
	Development, neurogenesis, axonal guidance	22	8.415e-4
	Inlammation, TREM1 signaling	15	2.609e-3
	Cell adhesion, attractive and repulsive receptors	17	2.729e-3

Supplemental Figure 3. Next generation sequencing of mouse fibroblasts from WT and *Ttc7*$^{fsn/fsn}$ mice. The enriched process networks for differentially expressed genes for clusters 1 to 6. The first 10 results of each cluster are listed.

Supplemental Figure 4

Cluster Term	GO Molecular Function	count	*p*-value
1	Protein binding	303	2.315e-9
	Receptor binding	72	4.007e-8
	G-protein coupled purinergic nucleotide receptor activity	6	1.550e-6
	G-protein coupled nucleotide receptor activity	6	1.550e-6
	Purinergic receptor activity	7	2.653e-6
	Purinergic nucleotide receptor activity	6	1.322e-5
	Nucleotide receptor activity	6	8.351e-5
	Growth factor activity	13	1.374e-4
	Cell adhesive protein binding invol. in His cell-Purkinje myocyte communication	3	1.981e-4
	Molecular function regulator	54	2.511e-4
2	Type 2 angiotensin receptor binding	8	1.459e-18
	Type 1 angiotensin receptor binding	9	1.935e-16
	Angiotensin receptor binding	9	7.279e-16
	Acetyltransferase activator activity	7	9.074e-15
	Alpha1-adrenergic receptor activity	7	3.009e-14
	Alpha-adrenergic receptor activity	7	4.239e-13
	Adrenergic receptor activity	7	8.090e-11
	Endopeptidase inhibitor activity	14	1.106e-9
	Endopeptidase regulator activity	14	1.611e-9
	Peptidase inhibitor activity	14	2.320e-9
3	Extracellular matrix structural constituent	15	6.250e-10
	Binding	416	4.199e-8
	Cargo receptor activity	11	2.729e-6
	Protein dimerization activity	57	1.449e-5
	Steroid delta-isomerase activity	4	1.550e-5
	Protein heterodimerization activity	31	2.103e-5
	Inerleukin-2 receptor activity	3	4.248e-5
	Interleukin-2 binding	3	4.248e-5
	Growth factor binding	13	5.978e-5
	Cytokine receptor activity	10	8.201e-5
4	Cell adhesion molecule binding	13	3.248e-5
	Natriuretic peptide receptor activity	2	1.324e-4
	Adenylate cyclase activity	3	4.099e-4
	Receptor activity	30	4.538e-4
	Molecular transducer activity	30	4.538e-4
	Cyclase activity	3	6.032e-4
	Beta-catenin binding	5	6.427e-3
	Phosphorus-oxygen lyase activity	3	6.786e-4
	Cadherin binding	8	1.161e-3
	Ligand-gated sodium channel activity	2	1.548e-3
5	Immunological binding	6	4.683e-8
	Singnal transducer activity	42	1.089e-7
	Receptor activity	42	1.442e-7
	Molecular transducer activity	42	1.442e-7
	Immunoglobulin receptor activity	4	2.240e-7
	IgE receptor activity	3	4.373e-7
	Protein binding	125	2.844e-6
	IgE binding	3	4.324e-6
	Signal receptor activity	34	4.848e-6
	Transmembrane signaling receptor activity	32	8.695e-7
6	Receptor binding	125	2.819e-18
	Calcium ion binding	64	4.233e-12
	Growht factor activity	26	4.289e-11
	C5L2 anaphylatoxin chemotactic receptor binding	6	5.663e-10
	Protein binding	436	5.027e-9
	Molecular function regulator	91	5.801e-9
	Ras guanyl-nucleotide exchange factor activity	26	9.547e-9
	Cytokine receptor binding	31	1.635e-8
	C5a anaphylatoxin chemotactic receptor binding	6	4.416e-8
	Cytokine activity	25	1.039e-7

Supplemental Figure 4. Next generation sequencing of mouse fibroblasts from WT and *Ttc7*$^{fsn/fsn}$ mice. The enriched GO of molecular function for differentially expressed genes for clusters 1 to 6. The first 10 results of each cluster are listed.

Supplemental Figure 5

Cluster Term	GO Cellular Localization	count	*p*-value
1	Cell periphery	214	4.353e-24
	Plasma membrane	209	3.472e-23
	Membrane	279	1.705e-13
	Extracellular space	76	2.179e-12
	Plasma membrane part	111	3.603e-12
	Extracellular region part	137	9.924e-12
	Extracellular region	157	1.279e-10
	Membrane part	211	3.878e-10
	Integral component of plasma membrane	75	4.995e-10
	Intrinsic component of plasma membrane	184	6.584e-10
2	Extracellular region	66	3.804e-11
	Extracellular space	30	5.604e-8
	Cytoplasmic vesicle lumen	8	2.249e-7
	Extracellular region part	50	2.218e-7
	Vesicle lumen	8	3.151e-7
	Blood microparticle	9	5.004e-7
	Lipid particle	7	5.403e-7
	Integral component of plasma membrane	29	5.936e-7
	Intrinsic component of plasma membrane	29	1.427e-6
	Membrane region	13	1.457e-6
3	Intrinsic component of plasma membrane	88	2.467e-11
	Plasma membrane part	123	2.793e-11
	Extracellular matrix	40	7.533e-11
	Integral component of plasma membrane	84	9.005e-11
	Cell periphery	203	9.801e-11
	Proteinaceous extracellular matrix	33	1.532e-10
	Extracellular region	179	2.061e-10
	Extracellular region part	150	5.736e-10
	Plasma membrane	195	1.575e-9
	Cell surface	54	3.138e-9
4	Integral component of plasma membrane	38	1.445e-9
	Extracellular region	72	2.811e-9
	Intrinsic component of plasma membrane	38	4.750e-9
	Plasma membrane part	50	1.107e-8
	Extracellular region part	60	3.138e-8
	Cell periphery	77	7.178e-8
	Collagen network	4	7.178e-8
	Network-forming collagen trimer	4	7.825e-8
	Plasma membrane	75	1.746e-7
	Extracellular space	33	2.560e-7
5	Cell periphery	117	3.120e-30
	Plasma membrane	114	7.470e-29
	Plasma membrane part	72	7.409e-21
	Integral component of plasma membrane	52	3.366e-18
	Intrinsic component of plasma membrane	52	2.116e-17
	Membrane	131	1.147e-15
	Side of membrane	27	2.690e-13
	Mast cell granule	9	5.631e-13
	External side of plasma membrane	20	4.946e-12
	Membrane part	102	6.201e-12
6	Extracellular space	127	3.247e-24
	Extracellular region	256	4.361e-22
	Cell periphery	284	1.780e-21
	Plasma membrane	277	1.466e-20
	Neuronal cell body	64	1.148e-18
	Cell body	67	7.755e-18
	Extracellular region part	207	1.414e-17
	Plasma membrane part	164	7.981e-17
	Neuron projection	88	5.978e-16
	Neuron part	106	8.703e-16

Supplemental Figure 5. Next generation sequencing of mouse fibroblasts from WT and *Ttc7*$^{fsn/fsn}$ mice. The enriched GO of cellular localization for differentially expressed genes for clusters 1 to 6. The first 10 results of each cluster are listed.

Supplemental Figure 6

cell adhesion, cell-matrix interaction components

Extracellular Matrix Components
up-regulated

Collagen	*p*-value
COL1A1	8.43E-05
COL3A1	1.24E-09
COL4A1	0.01828
COL5A1	7.52E-06
COL5A2	2.87E-03
COL6A1	1.27E-04
COL6A2	2.88E-05
COL6A3	1.59E-12
COL14A1	2.45E-07
COL15A1	1.41E-06
COL17A1	8.00E-04
Laminin	
LAMB1	2.06E-02
LAMB3	2.60E-02
Fibrillin	
FBN1	1.18E-05
FBN2	8.87E-07
FLRT2	1.43E-02
ELFN1	2.45E-02
EFEMP1	1.27E-03
EFEMP2	8.14E-03
Other ECM proteins	
CCN3/NOV	8.31E-04
ECM2	1.72E-03
EFEMP1	1.27E-03
ELN (elastin)	5.47E-05
Fibronectin 1	4.49E-02
LUM	4.24E-03
MFAP4	1.73E-04
NID1	2.64E-04
SPON1	1.03E-08
TNN	1.75E-03
TNR	4.06E-02
TNXB	1.26E-02
VCAN (versican)	1.05E-08
WISP-1	4.29E-04
Proteoclycans	
ASPN	9.58E-08
EPYC	2.30E-02
FMOD	1.22E-02
LUM	4.24E-03
PODN	2.41E-03
PRELP	1.13E-02
PRG4	9.03E-05
SRGN	1.06E-36
Metalloprotease	
ADAM-TS1	1.45E-04
ADAM-TS15	4.56E-04
ADAM-TS5	4.47E-04
ADAM-TS9	2.93E-03
ADAM-TS10	3.98E-02
ADAM8	2.42E-08
ADAM12	1.34E-08
ADAM33	2.55E-02

Cell Adhesion Components
up-regulated

Integrin	*p*-value
ITGAX	3.41E-15
ITGAM	1.66E-08
ITGA11	8.43E-05
ITGB2	1.31E-04
ITGA6	2.51E-02
ITGA1	4.94E-02

down-regulated

Matrix Metallopeptidase	*p*-value
MMP-3	3.33E-05
MMP-8	1.71E-03
MMP-10	6.60E-05
MMP-12	2.62E-27
MMP-16	6.58E-03

Supplemental Figure 6. Next generation sequencing of mouse fibroblasts from WT and *Ttc7*$^{fsn/fsn}$ mice. Lists of statistically significant up- and down-regulated genes of the extracellular matrix and list of up-regulated integrins in cell adhesion, cell-matrix interaction processes.

VI. DISCUSSION

In the case of TTC7A deficiency, there is an ongoing debate about whether *TTC7A* mutations dysregulate epithelial cell functions alone or in combination with T cells' intrinsic functions. In the flaky skin mutant mouse (*Ttc7*$^{fsn/fsn}$), a murine model of TTC7A deficiency, we analyzed whether the epithelial phenotype is influenced by other cell types. We found that the hyperproliferative skin disease developed in the absence of lymphocytes. We furthermore observed that *Ttc7*$^{fsn/fsn}$ hematopoietic cells do not per se induce pathological changes when transferred to wild-type (WT) animals. Remarkably, *Ttc7*$^{fsn/fsn}$ fibroblasts disordered the proliferation of normal human epithelial cells in dermo–epidermal skin cultures and displayed an array of transcriptomic alterations in molecular networks required for cell–cell interactions. Our results show that defective Ttc7 in the flaky skin mutant mouse model is associated with fibroblast-driven keratinocyte hyperproliferation and lymphocyte-propagated skin inflammation in the presence of the proliferation-inducing factors IL-22 and IGF-1. Thus, our results indicate that Ttc7 plays a critical role in the crosstalk between cells from different tissues.

It is worthwhile to mention that other researchers have also encountered the involvement of fibroblasts in keratinocyte hyperproliferation. In co-cultures with dermal fibroblasts from psoriatic patients, keratinocytes from healthy donors showed hyperproliferation on *in vitro* skin equivalents [157]. This observation points toward a diffusible factor from fibroblasts which may also be involved in our system, irrespective of the question whether the flaky skin mouse should be regarded as a model for psoriasiform dermatitis or a disease in the group of syndromic ichthyosis, as proposed by some researchers [125, 126, 130]. The importance of growth-factor mediated cross-talk between keratinocytes and fibroblasts also becomes evident during cutaneous tissue repair aiming to restore and maintain the barrier function of the skin [79]. With a view to identifying such factors in *Ttc7*$^{fsn/fsn}$ fibroblasts, we compared the latter's transcriptome with the one of their WT counterparts. Overall, our transcriptomic analyses revealed that various endogenous cellular functions in the fibroblasts were altered. With regard to factors that might influence the growth of keratinocytes, we found that transcription of the IGF1 gene was markedly upregulated in *Ttc7*$^{fsn/fsn}$

fibroblasts, but this was not the case for other growth factors such as FGF3, FGF7, FGF10, or EGF.

We observed elevated serum levels of IL-22 in all mouse strains with *Ttc7*$^{fsn/fsn}$ germline mutation. IL-22 is mainly produced by different leukocyte subtypes but can also be produced by stromal cells under harmful condition [158, 159]. Therefore, IL-22 is another candidate that could play an important role in the pathogenesis of the hyperproliferative skin disease. We observed elevated serum levels of IL-22 even in *Ttc7*$^{fsn/fsn}$ mice crossed with *Rag2*$^{-/-}$ and *Rag2*$^{-/-}$*IL2rg*$^{-/-}$ mice. Remarkably, IL-22 serum levels were particularly elevated in the mice lacking all lymphoid cells. Using anti-IL-22 antibodies in immunohistochemical staining, we identified mast cells as being strongly positive. In contrast, based on transcriptome data and immunohistochemistry, fibroblasts did not seem to be a major source for IL-22 in *Ttc7*$^{fsn/fsn}$ mice. Thus, our data suggest that mast cells were the predominant non-lymphoid source for IL-22 in the *Ttc7*$^{fsn/fsn}$ strains [160-163]. Mast cells and Neutrophils are known to play a prominent role in different skin diseases [164, 165]. In the *Ttc7*$^{fsn/fsn}$ mouse, the phenotype could not be transferred by hematopoietic stem cell transplants. We therefore think that, if IL-22 is predominately produced by mast cells, it is not needed to trigger the skin disease. Lastly, serum levels of IL-17 were only elevated in *Ttc7*$^{fsn/fsn}$ mice and were not increased or null in *Ttc7*$^{fsn/fsn}$ mice crossed with *Rag2*$^{-/-}$ or *Rag2*$^{-/-}$*IL2rg*$^{-/-}$ mice, reflecting a lymphoid-restricted source of IL-17. Hence, IL-22 and IL-17 are both probably not the key factor in inducing hyperproliferative skin disease in the flaky skin model. Nevertheless, both cytokines may exacerbate the phenotype.

It is noteworthy that within the heterodimeric IL-22 receptor, specifically IL-22R1 has a tightly regulated expression and is predominantly found on cells of epithelial origin, including intestinal and lung epithelial cells and keratinocytes [71]. Based on the known function of IL-22 in upregulating anti-bacterial peptides such as defensins and lipocalin [166, 167], skin inflammation in *Ttc7*$^{fsn/fsn}$ mice might be a consequence of abnormal epidermal barrier dysfunction due to hyperproliferation and subsequent IL-22-mediated inflammation perpetuating keratinocyte proliferation.

A previous study using immunofluorescence analysis showed elevated numbers of Langerhans cells and Thy-1^{+} dendritic epidermal cells in skin sections of *Ttc7*$^{fsn/fsn}$ mice,

suggesting an immune-system-related abnormality [168]. We cannot rule out an effect of Langerhans cells on the skin phenotype in our mouse models. However, the results of our *Rag2*$^{-/-}$ crossing experiment confirmed that γδTCR-expressing Thy-1^{+} dendritic epithelial cells (DETCs) are not the main elicitors of the skin disease.

As exemplified by our findings in the flaky skin mutant mouse, the pathogenesis underlying an immunodeficiency disease can also originate from major defects in non-hematopoietic-derived cells. Our work thus calls the prevailing therapeutic strategy of hematopoietic stem cell transplantation for TTC7A deficiency into question. Systemic therapeutic agents therefore represent promising tools directed at the specific disease-causing abnormality. The target of such therapeutic agents has to be able to regulate cellular functions that are activated or suppressed to compensate for altered functionality of the affected gene. The analyses of transcriptomic data from Ttc7-mutated fibroblasts displayed an mRNA expression pattern that suggested alterations in phosphoinositide-dependent key signaling pathways. The list of these key-signaling pathways indicates the ERK and PI3K pathways to be important players in cellular functions. The extracellular signal-regulated kinase (ERK) and phosphatidylinositol 3-kinase (PI3K) pathway are evolutionarily conserved and present in various cells. Both pathways are involved in controlling many fundamental cellular processes that include cell proliferation, survival, differentiation, apoptosis, motility, and metabolism, and they may have a cross-regulating function [169, 170]. It has been noted that the phosphorylation of ERK is elevated in transitional B cells in the *Ttc7*$^{fsn/fsn}$ mouse [171].

Our effort at finding a potential target has led us to the observation that *Ttc7*$^{fsn/fsn}$ fibroblasts synthetize increased RNA expression of IGF-1. This is in accordance with previous publications, showing that the major sources of IGF-1 in the skin are dermal fibroblasts [172]. The insulin-like growth factor 1 receptor (IGF-1R) is expressed by epithelial and immune cell [173-175]. Activated IGF-1R triggers several signaling cascades, including PI3K and MAPK pathways [176]. Early *in vivo* studies have demonstrated that the Igf-1 receptor on the cell surface of keratinocytes is confined to the basal layer of the epidermis [177]. In the skin, the IGF-1 system is used by keratinocytes for epidermal development and maintenance [178, 179]. Keratinocyte proliferation is restricted to the basal layer. Upon division, keratinocytes do either

replace progenitor cells or undergo terminal differentiation to become fully mature corneocytes at the outer surface of the epidermis [180]. Overexpression of IGF-1 in the skin results in epidermal "hyperthickening" and spontaneous tumor formation, whereas IGF-1R-deficient mice present an underdeveloped epidermis [181]. Nevertheless, several endogenous substances regulate proliferation and growth of keratinocytes. Our study of the cytokine signatures between different mouse strains has also highlighted that IL-4, IL-17, and IL-22 are main factors characterizing the hyper-proliferative immune response in *Ttc7*$^{fsn/fsn}$ mice. This raises the question as to whether targeting these cytokines individually, simultaneously or together with IGF-1 or targets in the ERK/PI3K pathway could reverse the phenotype.

We do report a multiple-organ defect in *Ttc7*$^{fsn/fsn}$ mice but with different organs being affected to varying degrees. There might be the possibility of yet unknown compensatory mechanisms that could be more active in some cell types than others. In humans, TTC7A defects show developmental disorders in form of atresia, whereas in the *Ttc7*$^{fsn/fsn}$ mouse model, the onset of the skin defect develops later supporting the possibility of species-specific difference in the function of TTC7A, respectively Ttc7. This also strengthens the possibility of compensatory mechanisms that could be more active during developmental stages in mice [182]. It is also important to note that there might be differences in the reaction of soluble factors such as IL-22 dependent on the organ-specific environment. For instance, the intestinal epithelium comprises several intestinal epithelial cell (IEL) lineages with distinct functions [183]. The IL-22 receptor is expressed on IECs [184], and IL-22 plays an important role in the maintenance of intestinal epithelial polarity when gut tissue is damaged by various disorders, such as IBD and GvHD [185, 186]. This protective function of IL-22 in IBD could further explain why the *Ttc7*$^{fsn/fsn}$ mouse does not present with intestinal symptoms, in contrast to humans. However, in humans, inverted apicobasal polarity of patients' enterocytes has been shown in pathological assessments of gut biopsies and was recapitulated in patient-derived organoid cultures [107, 108]. In the presence of RhoA kinase inhibitors, the abnormal polarity of epithelial cells was reversed. RhoA kinase might therefore be another interesting therapeutic target also in mice.

It has been suggested, that Ttc7 controls the spatial synthesis of phosphatidylinositol 4-phosphates at the plasma membrane (PI4P), the metabolic precursor of $PI(4,5)P_2$. $PI(4,5)P_2$ is important for cell regulation and membrane dynamics, including endocytosis, cell motility, cell adhesion, or signaling transduction. All these cellular processes could be affected by mutated Ttc7. Our transcriptomic analysis revealed that several cellular functions in the Ttc7-mutated fibroblasts themselves are disrupted. Bearing in mind that Ttc7 is a ubiquitously expressed protein, all cell–cell interactions could therefore induce an aberrant cellular behavior.

In conclusion, our data opt for a multi-facetted interaction network consisting of fibroblasts, epithelial cells, and hematopoietic cells as driving force in the pathomechanism leading to the flaky skin phenotype. Our findings highlight a function of fibroblasts in controlling cellular behavior and epithelial cell proliferation, while the soluble factors (i) IGF-1 and (ii) IL-22 play a role together with lymphocytes in aggravating skin inflammation in the *Ttc7*$^{fsn/fsn}$ mouse model.

Indeed, Ttc7 appears to play a central role in different cellular dynamics and behaviors. The dysfunctional crosstalk between stromal cells adds an unsuspected new dimension to the pathogenesis of the multisystemic disease associated with TTC7A-deficiency. This suggested mechanism reveals why previous HSCT treatments together with intestinal surgery may only partially relieve the multisystemic disease seen in patients with *TTC7A* deficiency, and also provides potential new molecular targets for achieving systemic therapeutic effects that intervene in the disturbed interaction between stromal cells.

VII. LITERATURE

1. Johns, J.L. and M.M. Christopher, *Extramedullary hematopoiesis: a new look at the underlying stem cell niche, theories of development, and occurrence in animals.* Vet Pathol, 2012. **49**(3): p. 508-23.
2. Wang, L.D. and A.J. Wagers, *Dynamic niches in the origination and differentiation of haematopoietic stem cells.* Nat Rev Mol Cell Biol, 2011. **12**(10): p. 643-55.
3. Sharpless, N.E. and R.A. DePinho, *How stem cells age and why this makes us grow old.* Nat Rev Mol Cell Biol, 2007. **8**(9): p. 703-13.
4. Trinchieri, G. and A. Sher, *Cooperation of Toll-like receptor signals in innate immune defence.* Nat Rev Immunol, 2007. **7**(3): p. 179-90.
5. Carroll, M.C., *The complement system in regulation of adaptive immunity.* Nat Immunol, 2004. **5**(10): p. 981-6.
6. Boehm, T., *Design principles of adaptive immune systems.* Nat Rev Immunol, 2011. **11**(5): p. 307-17.
7. Chaplin, D.D., *Overview of the immune response.* J Allergy Clin Immunol, 2010. **125**(2 Suppl 2): p. S3-23.
8. Gordon, S. and P.R. Taylor, *Monocyte and macrophage heterogeneity.* Nat Rev Immunol, 2005. **5**(12): p. 953-64.
9. Shi, C. and E.G. Pamer, *Monocyte recruitment during infection and inflammation.* Nat Rev Immunol, 2011. **11**(11): p. 762-74.
10. Gordon, S., A. Pluddemann, and F. Martinez Estrada, *Macrophage heterogeneity in tissues: phenotypic diversity and functions.* Immunol Rev, 2014. **262**(1): p. 36-55.
11. Lavin, Y., et al., *Regulation of macrophage development and function in peripheral tissues.* Nat Rev Immunol, 2015. **15**(12): p. 731-44.
12. Davies, L.C., et al., *Tissue-resident macrophages.* Nat Immunol, 2013. **14**(10): p. 986-95.
13. Murray, P.J. and T.A. Wynn, *Protective and pathogenic functions of macrophage subsets.* Nat Rev Immunol, 2011. **11**(11): p. 723-37.
14. Ginhoux, F., et al., *New insights into the multidimensional concept of macrophage ontogeny, activation and function.* Nat Immunol, 2016. **17**(1): p. 34-40.
15. Minutti, C.M., et al., *Tissue-specific contribution of macrophages to wound healing.* Semin Cell Dev Biol, 2017. **61**: p. 3-11.
16. Rosenberg, H.F., K.D. Dyer, and P.S. Foster, *Eosinophils: changing perspectives in health and disease.* Nat Rev Immunol, 2013. **13**(1): p. 9-22.
17. Kita, H., *Eosinophils: multifaceted biological properties and roles in health and disease.* Immunol Rev, 2011. **242**(1): p. 161-77.
18. Kouro, T. and K. Takatsu, *IL-5- and eosinophil-mediated inflammation: from discovery to therapy.* Int Immunol, 2009. **21**(12): p. 1303-9.
19. Schroeder, J.T., *Basophils: emerging roles in the pathogenesis of allergic disease.* Immunol Rev, 2011. **242**(1): p. 144-60.
20. Karasuyama, H., et al., *Emerging roles of basophils in protective immunity against parasites.* Trends Immunol, 2011. **32**(3): p. 125-30.
21. Karasuyama, H., et al., *Nonredundant roles of basophils in immunity.* Annu Rev Immunol, 2011. **29**: p. 45-69.
22. Ito, T., et al., *Stem cell factor programs the mast cell activation phenotype.* J Immunol, 2012. **188**(11): p. 5428-37.
23. Bulfone-Paus, S., et al., *Positive and Negative Signals in Mast Cell Activation.* Trends Immunol, 2017.
24. Krystel-Whittemore, M., K.N. Dileepan, and J.G. Wood, *Mast Cell: A Multi-Functional Master Cell.* Front Immunol, 2015. **6**: p. 620.
25. Wernersson, S. and G. Pejler, *Mast cell secretory granules: armed for battle.* Nat Rev Immunol, 2014. **14**(7): p. 478-94.
26. Soehnlein, O., et al., *Neutrophils as protagonists and targets in chronic inflammation.* Nat Rev Immunol, 2017. **17**(4): p. 248-261.
27. Manz, M.G. and S. Boettcher, *Emergency granulopoiesis.* Nat Rev Immunol, 2014. **14**(5): p. 302-14.
28. Kruger, P., et al., *Neutrophils: Between host defence, immune modulation, and tissue injury.* PLoS Pathog, 2015. **11**(3): p. e1004651.
29. Kolaczkowska, E. and P. Kubes, *Neutrophil recruitment and function in health and inflammation.* Nat Rev Immunol, 2013. **13**(3): p. 159-75.

30. Rose, S., A. Misharin, and H. Perlman, *A novel Ly6C/Ly6G-based strategy to analyze the mouse splenic myeloid compartment.* Cytometry A, 2012. **81**(4): p. 343-50.
31. Shortman, K. and S.H. Naik, *Steady-state and inflammatory dendritic-cell development.* Nat Rev Immunol, 2007. **7**(1): p. 19-30.
32. Villadangos, J.A. and P. Schnorrer, *Intrinsic and cooperative antigen-presenting functions of dendritic-cell subsets in vivo.* Nat Rev Immunol, 2007. **7**(7): p. 543-55.
33. Guilliams, M., et al., *Dendritic cells, monocytes and macrophages: a unified nomenclature based on ontogeny.* Nat Rev Immunol, 2014. **14**(8): p. 571-8.
34. Klose, C.S. and D. Artis, *Innate lymphoid cells as regulators of immunity, inflammation and tissue homeostasis.* Nat Immunol, 2016. **17**(7): p. 765-74.
35. Spits, H., J.H. Bernink, and L. Lanier, *NK cells and type 1 innate lymphoid cells: partners in host defense.* Nat Immunol, 2016. **17**(7): p. 758-64.
36. Spits, H., et al., *Innate lymphoid cells--a proposal for uniform nomenclature.* Nat Rev Immunol, 2013. **13**(2): p. 145-9.
37. Cording, S., et al., *Innate lymphoid cells in defense, immunopathology and immunotherapy.* Nat Immunol, 2016. **17**(7): p. 755-7.
38. Zook, E.C. and B.L. Kee, *Development of innate lymphoid cells.* Nat Immunol, 2016. **17**(7): p. 775-82.
39. Brennan, P.J., M. Brigl, and M.B. Brenner, *Invariant natural killer T cells: an innate activation scheme linked to diverse effector functions.* Nat Rev Immunol, 2013. **13**(2): p. 101-17.
40. Godfrey, D.I., S. Stankovic, and A.G. Baxter, *Raising the NKT cell family.* Nat Immunol, 2010. **11**(3): p. 197-206.
41. Rothenberg, E.V., J.E. Moore, and M.A. Yui, *Launching the T-cell-lineage developmental programme.* Nat Rev Immunol, 2008. **8**(1): p. 9-21.
42. Blackburn, C.C. and N.R. Manley, *Developing a new paradigm for thymus organogenesis.* Nat Rev Immunol, 2004. **4**(4): p. 278-89.
43. Takahama, Y., *Journey through the thymus: stromal guides for T-cell development and selection.* Nat Rev Immunol, 2006. **6**(2): p. 127-35.
44. Vantourout, P. and A. Hayday, *Six-of-the-best: unique contributions of gammadelta T cells to immunology.* Nat Rev Immunol, 2013. **13**(2): p. 88-100.
45. Germain, R.N., *T-cell development and the CD4-CD8 lineage decision.* Nat Rev Immunol, 2002. **2**(5): p. 309-22.
46. Smith-Garvin, J.E., G.A. Koretzky, and M.S. Jordan, *T cell activation.* Annu Rev Immunol, 2009. **27**: p. 591-619.
47. Wan, Y.Y., *Multi-tasking of helper T cells.* Immunology, 2010. **130**(2): p. 166-71.
48. Andersen, M.H., et al., *Cytotoxic T cells.* J Invest Dermatol, 2006. **126**(1): p. 32-41.
49. Barry, M. and R.C. Bleackley, *Cytotoxic T lymphocytes: all roads lead to death.* Nat Rev Immunol, 2002. **2**(6): p. 401-9.
50. Melchers, F., *Checkpoints that control B cell development.* J Clin Invest, 2015. **125**(6): p. 2203-10.
51. Klein, U. and R. Dalla-Favera, *Germinal centres: role in B-cell physiology and malignancy.* Nat Rev Immunol, 2008. **8**(1): p. 22-33.
52. Nutt, S.L., et al., *The generation of antibody-secreting plasma cells.* Nat Rev Immunol, 2015. **15**(3): p. 160-71.
53. Kurosaki, T., K. Kometani, and W. Ise, *Memory B cells.* Nat Rev Immunol, 2015. **15**(3): p. 149-59.
54. Shapiro-Shelef, M. and K. Calame, *Regulation of plasma-cell development.* Nat Rev Immunol, 2005. **5**(3): p. 230-42.
55. Sato, S., et al., *Regulation of B lymphocyte development and activation by the CD19/CD21/CD81/Leu 13 complex requires the cytoplasmic domain of CD19.* J Immunol, 1997. **159**(7): p. 3278-87.
56. Bousfiha, A., et al., *The 2015 IUIS Phenotypic Classification for Primary Immunodeficiencies.* J Clin Immunol, 2015. **35**(8): p. 727-38.
57. Picard, C., et al., *Primary Immunodeficiency Diseases: an Update on the Classification from the International Union of Immunological Societies Expert Committee for Primary Immunodeficiency 2015.* J Clin Immunol, 2015. **35**(8): p. 696-726.
58. Pannicke, U., et al., *Reticular dysgenesis (aleukocytosis) is caused by mutations in the gene encoding mitochondrial adenylate kinase 2.* Nat Genet, 2009. **41**(1): p. 101-5.
59. Mueller, S.N. and R.N. Germain, *Stromal cell contributions to the homeostasis and functionality of the immune system.* Nat Rev Immunol, 2009. **9**(9): p. 618-29.
60. Wreede, S.W.R.d., *Embryology at a Glance*. 2nd Edition ed. 2015: Wiley-Blackwell.

61. Fuchs, E. and S. Raghavan, *Getting under the skin of epidermal morphogenesis.* Nat Rev Genet, 2002. **3**(3): p. 199-209.
62. Pasparakis, M., I. Haase, and F.O. Nestle, *Mechanisms regulating skin immunity and inflammation.* Nat Rev Immunol, 2014. **14**(5): p. 289-301.
63. Gilliet, M. and R. Lande, *Antimicrobial peptides and self-DNA in autoimmune skin inflammation.* Curr Opin Immunol, 2008. **20**(4): p. 401-7.
64. Lowes, M.A., M. Suarez-Farinas, and J.G. Krueger, *Immunology of psoriasis.* Annu Rev Immunol, 2014. **32**: p. 227-55.
65. Barrandon, Y. and H. Green, *Three clonal types of keratinocyte with different capacities for multiplication.* Proc Natl Acad Sci U S A, 1987. **84**(8): p. 2302-6.
66. Nestle, F.O., et al., *Skin immune sentinels in health and disease.* Nat Rev Immunol, 2009. **9**(10): p. 679-91.
67. Schauber, J. and R.L. Gallo, *Antimicrobial peptides and the skin immune defense system.* J Allergy Clin Immunol, 2009. **124**(3 Suppl 2): p. R13-8.
68. Gallo, R.L. and L.V. Hooper, *Epithelial antimicrobial defence of the skin and intestine.* Nat Rev Immunol, 2012. **12**(7): p. 503-16.
69. Meephansan, J., et al., *Regulation of IL-33 expression by IFN-gamma and tumor necrosis factor-alpha in normal human epidermal keratinocytes.* J Invest Dermatol, 2012. **132**(11): p. 2593-600.
70. Heath, W.R. and F.R. Carbone, *The skin-resident and migratory immune system in steady state and memory: innate lymphocytes, dendritic cells and T cells.* Nat Immunol, 2013. **14**(10): p. 978-85.
71. Sonnenberg, G.F., L.A. Fouser, and D. Artis, *Border patrol: regulation of immunity, inflammation and tissue homeostasis at barrier surfaces by IL-22.* Nat Immunol, 2011. **12**(5): p. 383-90.
72. Hynes, R.O. and K.M.e. Yamada, *Extracellular Matrix Biology*. Cold Spring Harbor Lab Press. 2012.
73. Mecham, R.P.e., *The Extracellular Matrix: an Overview*. Springer. 2011.
74. Kalluri, R. and M. Zeisberg, *Fibroblasts in cancer.* Nat Rev Cancer, 2006. **6**(5): p. 392-401.
75. Tomasek, J.J., et al., *Myofibroblasts and mechano-regulation of connective tissue remodelling.* Nat Rev Mol Cell Biol, 2002. **3**(5): p. 349-63.
76. Barrientos, S., et al., *Growth factors and cytokines in wound healing.* Wound Repair Regen, 2008. **16**(5): p. 585-601.
77. Ornitz, D.M. and N. Itoh, *The fibroblast growth factor signaling pathway.* WIREs Dev Biol, 2015. **4**: p. 215-266.
78. Sorrell, J.M. and A.I. Caplan, *Fibroblast heterogeneity: more than skin deep.* J Cell Sci, 2004. **117**(Pt 5): p. 667-75.
79. Werner, S., T. Krieg, and H. Smola, *Keratinocyte-fibroblast interactions in wound healing.* J Invest Dermatol, 2007. **127**(5): p. 998-1008.
80. Mouw, J.K., G. Ou, and V.M. Weaver, *Extracellular matrix assembly: a multiscale deconstruction.* Nat Rev Mol Cell Biol, 2014. **15**(12): p. 771-85.
81. Humphrey, J.D., E.R. Dufresne, and M.A. Schwartz, *Mechanotransduction and extracellular matrix homeostasis.* Nat Rev Mol Cell Biol, 2014. **15**(12): p. 802-12.
82. Charras, G. and E. Sahai, *Physical influences of the extracellular environment on cell migration.* Nat Rev Mol Cell Biol, 2014. **15**(12): p. 813-24.
83. Bonnans, C., J. Chou, and Z. Werb, *Remodelling the extracellular matrix in development and disease.* Nat Rev Mol Cell Biol, 2014. **15**(12): p. 786-801.
84. Hood, J.D. and D.A. Cheresh, *Role of integrins in cell invasion and migration.* Nat Rev Cancer, 2002. **2**(2): p. 91-100.
85. Bosman, F.T. and I. Stamenkovic, *Functional structure and composition of the extracellular matrix.* J Pathol, 2003. **200**(4): p. 423-8.
86. Frantz, C., K.M. Stewart, and V.M. Weaver, *The extracellular matrix at a glance.* J Cell Sci, 2010. **123**(Pt 24): p. 4195-200.
87. Austin, L.M., et al., *The majority of epidermal T cells in Psoriasis vulgaris lesions can produce type 1 cytokines, interferon-gamma, interleukin-2, and tumor necrosis factor-alpha, defining TC1 (cytotoxic T lymphocyte) and TH1 effector populations: a type 1 differentiation bias is also measured in circulating blood T cells in psoriatic patients.* J Invest Dermatol, 1999. **113**(5): p. 752-9.
88. Yawalkar, N., et al., *Increased expression of IL-12p70 and IL-23 by multiple dendritic cell and macrophage subsets in plaque psoriasis.* J Dermatol Sci, 2009. **54**(2): p. 99-105.
89. Zaba, L.C., et al., *Psoriasis is characterized by accumulation of immunostimulatory and Th1/Th17 cell-polarizing myeloid dendritic cells.* J Invest Dermatol, 2009. **129**(1): p. 79-88.

90. Kagami, S., et al., *Circulating Th17, Th22, and Th1 cells are increased in psoriasis.* J Invest Dermatol, 2010. **130**(5): p. 1373-83.
91. Di Cesare, A., P. Di Meglio, and F.O. Nestle, *The IL-23/Th17 axis in the immunopathogenesis of psoriasis.* J Invest Dermatol, 2009. **129**(6): p. 1339-50.
92. van der Fits, L., et al., *Imiquimod-induced psoriasis-like skin inflammation in mice is mediated via the IL-23/IL-17 axis.* J Immunol, 2009. **182**(9): p. 5836-45.
93. Wohn, C., et al., *Langerin(neg) conventional dendritic cells produce IL-23 to drive psoriatic plaque formation in mice.* Proc Natl Acad Sci U S A, 2013. **110**(26): p. 10723-8.
94. Wagner, E.F., et al., *Psoriasis: what we have learned from mouse models.* Nat Rev Rheumatol, 2010. **6**(12): p. 704-14.
95. Pantelyushin, S., et al., *Rorgammat+ innate lymphocytes and gammadelta T cells initiate psoriasiform plaque formation in mice.* J Clin Invest, 2012. **122**(6): p. 2252-6.
96. Keijsers, R.R., et al., *Cellular sources of IL-17 in psoriasis: a paradigm shift?* Exp Dermatol, 2014. **23**(11): p. 799-803.
97. Patel, U., et al., *Imiquimod 5% cream induced psoriasis: a case report, summary of the literature and mechanism.* Br J Dermatol, 2011. **164**(3): p. 670-2.
98. Papp, K.A., et al., *Brodalumab, an anti-interleukin-17-receptor antibody for psoriasis.* N Engl J Med, 2012. **366**(13): p. 1181-9.
99. Tausend, W., C. Downing, and S. Tyring, *Systematic review of interleukin-12, interleukin-17, and interleukin-23 pathway inhibitors for the treatment of moderate-to-severe chronic plaque psoriasis: ustekinumab, briakinumab, tildrakizumab, guselkumab, secukinumab, ixekizumab, and brodalumab.* J Cutan Med Surg, 2014. **18**(3): p. 156-69.
100. Mansouri, Y. and E. Guttman-Yassky, *Immune Pathways in Atopic Dermatitis, and Definition of Biomarkers through Broad and Targeted Therapeutics.* J Clin Med, 2015. **4**(5): p. 858-73.
101. Brandt, E.B. and U. Sivaprasad, *Th2 Cytokines and Atopic Dermatitis.* J Clin Cell Immunol, 2011. **2**(3).
102. Leung, D.Y., *New insights into atopic dermatitis: role of skin barrier and immune dysregulation.* Allergol Int, 2013. **62**(2): p. 151-61.
103. Kubo, A., K. Nagao, and M. Amagai, *Epidermal barrier dysfunction and cutaneous sensitization in atopic diseases.* J Clin Invest, 2012. **122**(2): p. 440-7.
104. Yoon, J., et al., *IL-23 induced in keratinocytes by endogenous TLR4 ligands polarizes dendritic cells to drive IL-22 responses to skin immunization.* J Exp Med, 2016.
105. Samuels, M.E., et al., *Exome sequencing identifies mutations in the gene TTC7A in French-Canadian cases with hereditary multiple intestinal atresia.* J Med Genet, 2013. **50**(5): p. 324-9.
106. Chen, R., et al., *Whole-exome sequencing identifies tetratricopeptide repeat domain 7A (TTC7A) mutations for combined immunodeficiency with intestinal atresias.* J Allergy Clin Immunol, 2013. **132**(3): p. 656-664 e17.
107. Bigorgne, A.E., et al., *TTC7A mutations disrupt intestinal epithelial apicobasal polarity.* J Clin Invest, 2013.
108. Lemoine, R., et al., *Immune deficiency-related enteropathy-lymphocytopenia-alopecia syndrome results from tetratricopeptide repeat domain 7A deficiency.* J Allergy Clin Immunol, 2014. **134**(6): p. 1354-1364 e6.
109. Fernandez, I., et al., *Multiple intestinal atresia with combined immune deficiency related to TTC7A defect is a multiorgan pathology: study of a French-Canadian-based cohort.* Medicine (Baltimore), 2014. **93**(29): p. e327.
110. Agarwal, N.S., et al., *Tetratricopeptide repeat domain 7A (TTC7A) mutation in a newborn with multiple intestinal atresia and combined immunodeficiency.* J Clin Immunol, 2014. **34**(6): p. 607-10.
111. Avitzur, Y., et al., *Mutations in Tetratricopeptide Repeat Domain 7A Result in a Severe Form of Very Early Onset Inflammatory Bowel Disease.* Gastroenterology, 2014. **146**(4): p. 1028-39.
112. Guana, R., et al., *The complex surgical management of the first case of severe combined immunodeficiency and multiple intestinal atresias surviving after the fourth year of life.* Pediatr Gastroenterol Hepatol Nutr, 2014. **17**(4): p. 257-62.
113. Woutsas, S., et al., *Hypomorphic mutation in TTC7A causes combined immunodeficiency with mild structural intestinal defects.* Blood, 2015. **125**(10): p. 1674-6.
114. Moshous, D., et al., *Whole-exome sequencing identifies Coronin-1A deficiency in 3 siblings with immunodeficiency and EBV-associated B-cell lymphoproliferation.* J Allergy Clin Immunol, 2013. **131**(6): p. 1594-603.

115. Shimizu, K., et al., *Hereditary erythroblastic anaemia in the laboratory mouse.* Lab Anim, 1983. **17**(3): p. 198-202.
116. Kasahara, Y., K. Shimizu, and K. Kuribayashi, *Developmental abnormalities of the thymus in hea/hea mutant mice.* Exp Anim, 2008. **57**(2): p. 85-94.
117. Takabayashi, S., et al., *The novel tetratricopeptide repeat domain 7 mutation, Ttc7fsn-Jic, with deletion of the TPR-2B repeat causes severe flaky skin phenotype.* Exp Biol Med (Maywood), 2007. **232**(5): p. 695-9.
118. White, R.A., et al., *Positional cloning of the Ttc7 gene required for normal iron homeostasis and mutated in hea and fsn anemia mice.* Genomics, 2005. **85**(3): p. 330-7.
119. Pelsue, S.C., et al., *Lymphadenopathy, elevated serum IgE levels, autoimmunity, and mast cell accumulation in flaky skin mutant mice.* Eur J Immunol, 1998. **28**(4): p. 1379-88.
120. Withington, S., et al., *Antinuclear autoantibodies in flaky skin (fsn) mutant mice.* Autoimmunity, 2002. **35**(3): p. 175-81.
121. Welner, R., et al., *Hyperactivation and proliferation of lymphocytes from the spleens of flaky skin (fsn) mutant mice.* Autoimmunity, 2004. **37**(3): p. 227-35.
122. Welner, R., D.J. Swett, and S.C. Pelsue, *Age-related loss of bone marrow pre-B- and immature B-lymphocytes in the autoimmune-prone flaky skin mutant mice.* Autoimmunity, 2005. **38**(6): p. 399-408.
123. Beamer, W.G., et al., *The flaky skin (fsn) mutation in mice: map location and description of the anemia.* Blood, 1995. **86**(8): p. 3220-6.
124. Pelsue, S.C., et al., *Mapping of the flaky skin (fsn) mutation on distal mouse chromosome 17.* Mamm Genome, 1995. **6**(10): p. 758.
125. Morita, K., et al., *Cutaneous ultrastructural features of the flaky skin (fsn) mouse mutation.* J Dermatol, 1995. **22**(6): p. 385-95.
126. Sundberg, J.P., et al., *Development and progression of psoriasiform dermatitis and systemic lesions in the flaky skin (fsn) mouse mutant.* Pathobiology, 1997. **65**(5): p. 271-86.
127. Helms, C., et al., *The Tetratricopeptide repeat domain 7 gene is mutated in flaky skin mice: a model for psoriasis, autoimmunity, and anemia.* Exp Biol Med (Maywood), 2005. **230**(9): p. 659-67.
128. Abernethy, N.J., et al., *The peripheral lymphoid compartment is disrupted in flaky skin mice.* Immunol Cell Biol, 2000. **78**(1): p. 5-12.
129. Mattsson, N., E.G. Duzevik, and S.C. Pelsue, *Expansion of CD22lo B cells in the spleen of autoimmune-prone flaky skin mice.* Cell Immunol, 2005. **234**(2): p. 124-32.
130. Leclerc-Mercier, S., et al., *Ichthyosis as the dermatological phenotype associated with TTC7A mutations.* Br J Dermatol, 2016. **175**(5): p. 1061-1064.
131. Zeytuni, N. and R. Zarivach, *Structural and functional discussion of the tetra-trico-peptide repeat, a protein interaction module.* Structure, 2012. **20**(3): p. 397-405.
132. Nakatsu, F., et al., *PtdIns4P synthesis by PI4KIIIalpha at the plasma membrane and its impact on plasma membrane identity.* J Cell Biol, 2012. **199**(6): p. 1003-16.
133. Baskin, J.M., et al., *The leukodystrophy protein FAM126A (hyccin) regulates PtdIns(4)P synthesis at the plasma membrane.* Nat Cell Biol, 2016. **18**(1): p. 132-8.
134. Janmey, P.A. and U. Lindberg, *Cytoskeletal regulation: rich in lipids.* Nat Rev Mol Cell Biol, 2004. **5**(8): p. 658-66.
135. Fooksman, D.R., et al., *Cutting edge: phosphatidylinositol 4,5-bisphosphate concentration at the APC side of the immunological synapse is required for effector T cell function.* J Immunol, 2009. **182**(9): p. 5179-82.
136. Friedl, P., A.T. den Boer, and M. Gunzer, *Tuning immune responses: diversity and adaptation of the immunological synapse.* Nat Rev Immunol, 2005. **5**(7): p. 532-45.
137. Tan, X., et al., *Emerging roles of PtdIns(4,5)P2--beyond the plasma membrane.* J Cell Sci, 2015. **128**(22): p. 4047-56.
138. Thapa, N. and R.A. Anderson, *PIP2 signaling, an integrator of cell polarity and vesicle trafficking in directionally migrating cells.* Cell Adh Migr, 2012. **6**(5): p. 409-12.
139. Di Paolo, G. and P. De Camilli, *Phosphoinositides in cell regulation and membrane dynamics.* Nature, 2006. **443**(7112): p. 651-7.
140. Sato, T., et al., *Long-term expansion of epithelial organoids from human colon, adenoma, adenocarcinoma, and Barrett's epithelium.* Gastroenterology, 2011. **141**(5): p. 1762-72.
141. Bolger, A.M., M. Lohse, and B. Usadel, *Trimmomatic: a flexible trimmer for Illumina sequence data.* Bioinformatics, 2014. **30**(15): p. 2114-20.
142. Dobin, A., et al., *STAR: ultrafast universal RNA-seq aligner.* Bioinformatics, 2013. **29**(1): p. 15-21.

143. Li, B. and C.N. Dewey, *RSEM: accurate transcript quantification from RNA-Seq data with or without a reference genome.* BMC Bioinformatics, 2011. **12**: p. 323.
144. Robinson, M.D., D.J. McCarthy, and G.K. Smyth, *edgeR: a Bioconductor package for differential expression analysis of digital gene expression data.* Bioinformatics, 2010. **26**(1): p. 139-40.
145. Robinson, M.D. and A. Oshlack, *A scaling normalization method for differential expression analysis of RNA-seq data.* Genome Biol, 2010. **11**(3): p. R25.
146. Marino, D., et al., *Bioengineering dermo-epidermal skin grafts with blood and lymphatic capillaries.* Sci Transl Med, 2014. **6**(221): p. 221ra14.
147. Jelkmann, W., *Regulation of erythropoietin production.* J Physiol, 2011. **589**(Pt 6): p. 1251-8.
148. Kress, R.L., *Characterization of urinary iron loss in the fsn (flaky skin) anemia mouse mutant*. 2014, University of Kansas.
149. Klei, T.R., et al., *From the Cradle to the Grave: The Role of Macrophages in Erythropoiesis and Erythrophagocytosis.* Front Immunol, 2017. **8**: p. 73.
150. Abernethy, N.J., et al., *Dysregulated expression of CD69 and IL-2 receptor alpha and beta chains on CD8+ T lymphocytes in flaky skin mice.* Immunol Cell Biol, 2000. **78**(6): p. 596-602.
151. Sundberg, J.P., et al., *Forestomach papillomas in flaky skin and steel-Dickie mutant mice.* J Vet Diagn Invest, 1992. **4**(3): p. 312-7.
152. Sato, T., et al., *Single Lgr5 stem cells build crypt-villus structures in vitro without a mesenchymal niche.* Nature, 2009. **459**(7244): p. 262-5.
153. Ward, N.L. and D.T. Umetsu, *A new player on the psoriasis block: IL-17A- and IL-22-producing innate lymphoid cells.* J Invest Dermatol, 2014. **134**(9): p. 2305-7.
154. Nograles, K.E., et al., *IL-22-producing "T22" T cells account for upregulated IL-22 in atopic dermatitis despite reduced IL-17-producing TH17 T cells.* J Allergy Clin Immunol, 2009. **123**(6): p. 1244-52 e2.
155. Dhingra, N. and E. Guttman-Yassky, *A possible role for IL-17A in establishing Th2 inflammation in murine models of atopic dermatitis.* J Invest Dermatol, 2014. **134**(8): p. 2071-4.
156. Hynes, R.O., *The extracellular matrix: not just pretty fibrils.* Science, 2009. **326**(5957): p. 1216-9.
157. Saiag, P., et al., *Psoriatic fibroblasts induce hyperproliferation of normal keratinocytes in a skin equivalent model in vitro.* Science, 1985. **230**(4726): p. 669-72.
158. Ma, H.L., et al., *IL-22 is required for Th17 cell-mediated pathology in a mouse model of psoriasis-like skin inflammation.* J Clin Invest, 2008. **118**(2): p. 597-607.
159. Fukui, H., et al., *IL-22 produced by cancer-associated fibroblasts promotes gastric cancer cell invasion via STAT3 and ERK signaling.* Br J Cancer, 2014. **111**(4): p. 763-71.
160. Mashiko, S., et al., *Human mast cells are major IL-22 producers in patients with psoriasis and atopic dermatitis.* J Allergy Clin Immunol, 2015. **136**(2): p. 351-9 e1.
161. Chapdelaine, H., 2) , et al., *Functional common gamma chain is not required for mast cell proliferation and survival*, in *Allergy, Asthma and Clinical Immunology (AACI)*. 2012.
162. Schon, M., et al., *Critical role of neutrophils for the generation of psoriasiform skin lesions in flaky skin mice.* J Invest Dermatol, 2000. **114**(5): p. 976-83.
163. Zindl, C.L., et al., *IL-22-producing neutrophils contribute to antimicrobial defense and restitution of colonic epithelial integrity during colitis.* Proceedings of the National Academy of Sciences of the United States of America, 2013. **110**(31): p. 12768-12773.
164. Lin, A.M., et al., *Mast cells and neutrophils release IL-17 through extracellular trap formation in psoriasis.* J Immunol, 2011. **187**(1): p. 490-500.
165. Kawakami, T., et al., *Mast cells in atopic dermatitis.* Curr Opin Immunol, 2009. **21**(6): p. 666-78.
166. Wolk, K., et al., *IL-22 increases the innate immunity of tissues.* Immunity, 2004. **21**(2): p. 241-54.
167. Zhang, W., et al., *The pro-inflammatory cytokine IL-22 up-regulates keratin 17 expression in keratinocytes via STAT3 and ERK1/2.* PLoS One, 2012. **7**(7): p. e40797.
168. Sundberg, J.P., et al., *Epidermal dendritic cell populations in the flaky skin mutant mouse.* Immunol Invest, 1993. **22**(5): p. 389-401.
169. Kolch, W., *Coordinating ERK/MAPK signalling through scaffolds and inhibitors.* Nat Rev Mol Cell Biol, 2005. **6**(11): p. 827-37.
170. Mendoza, M.C., E.E. Er, and J. Blenis, *The Ras-ERK and PI3K-mTOR pathways: cross-talk and compensation.* Trends Biochem Sci, 2011. **36**(6): p. 320-8.

171. Jennifer Walker, B.H., 2), Kimberly Harris (1), Lauren Hakker (3), Paul Agris (3), Stephen Pelsue (1), *Investigating the novel protein, Ttc7, and its role in transitinal B cells.* The Journal of Immunology, 2012. **188**(60.2): p. 1.
172. Tavakkol, A., et al., *Maintenance of human skin in organ culture: role for insulin-like growth factor-1 receptor and epidermal growth factor receptor.* Arch Dermatol Res, 1999. **291**(12): p. 643-51.
173. Hodak, E., et al., *The insulin-like growth factor 1 receptor is expressed by epithelial cells with proliferative potential in human epidermis and skin appendages: correlation of increased expression with epidermal hyperplasia.* J Invest Dermatol, 1996. **106**(3): p. 564-70.
174. Knuever, J., et al., *Myeloid Cell-Restricted Insulin/IGF-1 Receptor Deficiency Protects against Skin Inflammation.* J Immunol, 2015. **195**(11): p. 5296-308.
175. Corbacho, A.M., G. Martinez De La Escalera, and C. Clapp, *Roles of prolactin and related members of the prolactin/growth hormone/placental lactogen family in angiogenesis.* J Endocrinol, 2002. **173**(2): p. 219-38.
176. Vincent, A.M. and E.L. Feldman, *Control of cell survival by IGF signaling pathways.* Growth Horm IGF Res, 2002. **12**(4): p. 193-7.
177. Krane, J.F., et al., *Synergistic effects of epidermal growth factor (EGF) and insulin-like growth factor I/somatomedin C (IGF-I) on keratinocyte proliferation may be mediated by IGF-I transmodulation of the EGF receptor.* J Invest Dermatol, 1991. **96**(4): p. 419-24.
178. Sadagurski, M., et al., *Insulin-like growth factor 1 receptor signaling regulates skin development and inhibits skin keratinocyte differentiation.* Mol Cell Biol, 2006. **26**(7): p. 2675-87.
179. Edmondson, S.R., et al., *Epidermal homeostasis: the role of the growth hormone and insulin-like growth factor systems.* Endocr Rev, 2003. **24**(6): p. 737-64.
180. Fuchs, E., *Epidermal differentiation: the bare essentials.* J Cell Biol, 1990. **111**(6 Pt 2): p. 2807-14.
181. DiGiovanni, J., et al., *Constitutive expression of insulin-like growth factor-1 in epidermal basal cells of transgenic mice leads to spontaneous tumor promotion.* Cancer Res, 2000. **60**(6): p. 1561-70.
182. Mestas, J. and C.C. Hughes, *Of mice and not men: differences between mouse and human immunology.* J Immunol, 2004. **172**(5): p. 2731-8.
183. Peterson, L.W. and D. Artis, *Intestinal epithelial cells: regulators of barrier function and immune homeostasis.* Nat Rev Immunol, 2014. **14**(3): p. 141-53.
184. Rubino, S.J., K. Geddes, and S.E. Girardin, *Innate IL-17 and IL-22 responses to enteric bacterial pathogens.* Trends Immunol, 2012. **33**(3): p. 112-8.
185. Hanash, A.M., et al., *Interleukin-22 protects intestinal stem cells from immune-mediated tissue damage and regulates sensitivity to graft versus host disease.* Immunity, 2012. **37**(2): p. 339-50.
186. Pickert, G., et al., *STAT3 links IL-22 signaling in intestinal epithelial cells to mucosal wound healing.* J Exp Med, 2009. **206**(7): p. 1465-72.

VIII. ACKNOWLEDGMENTS

I would like to express my special appreciation and thanks to my advisor Professor Dr. Jana Pachlopnik Schmid, you have been an extraordinary supervisor for me and my research but as well exceptionally encouraging and motivating in all the ups and downs during the past years. Your warm-hearted, outstanding personality became invaluable to me.

Further I would like to thank my committee members Professor Dr. Christian Münz and Professor Dr. Burkhard Becher for their excellent comments thereby helping to advance my project, and the friendly and productive atmosphere we had during our meetings. I really appreciate your help und advice during my PhD study.

A special thanks goes as well to all the members of our laboratory. You helped me out with scientific questions and problems, and supported me when I needed assistance or just encouraging words that kept me going and cheering me up. I will never forget all the funny moments we shared.

Last but not least I would like to thank my family and friends. Words cannot express how grateful I am for all the support and understanding I got from my mother, my father, my sisters and my friends. You were always there for me in good and in bad times.

IX. CURRICULUM VITAE

Name:	**Nüesch**	Seebahnstrasse 127
First Name:	**Ursina**	8003 Zürich
		Switzerland

Date of birth: 12.07.1979

Nationality: CH

Citizenship: Balgach SG

ursina.nueesch@uzh.ch

EDUCATION

10.2011 – present	PhD student, Division of Immunology, Klinik für Immunologie, University Children's Hospital Zurich, Zurich **Main Project:** Ttc7 is a *trans*-acting regulator of cell proliferation
03.2007	Swiss federal diploma in Biochemistry – Master of Science UZH, Zurich
10.2001 – 2007	Master's degree in biochemistry at the University of Zurich, Zurich **Master Thesis in the laboratory of Prof. Beat Thöny:** Substitution of Potential Phosphoserines with Asp or Glu Residues in the Human BH_4-biosynthetic Enzymes GTPCH and PTPs Identifies Phosphorylation Sites that Stimulate Activity
08. 1996 – 2000	Kantonsschule Heerbrugg, St.Gallen Matura Type E: Economy

GRANTS

EMDO STIFTUNG, University of Zurich
Forschungskredit Candoc, University of Zurich
Olga Mayenfisch Stiftung, University of Zurich
Theodor und Ida Herzog-Egli Stiftung, University of Zurich

PUBLICATIONS

Lymphadenopathy driven by TCR-Vγ8Vδ1 T-cell expansion in FAS-related autoimmune lymphoproliferative syndrome, Vavassori S, Galson J. D, Trück J, van den Berg A, Tamminga R. Y. J, Magerus-Chatinet A, Pellé O, Camenisch Gross U, Marques Maggio E, Prader S, Opitz L, Nüesch U, Mauracher A, Volkmer B, Speer O, Suda L, Rothlisberger B, Zimmermann D. R, Müller R, Diepstra A, Visser L, Haralambieva E, Neven B, Rieux-Laucat F, Pachlopnik Schmid J; Blood Advances; April 2017, 1(15):1101-1106.

Hemophagocytic lymphohistiocytosis-like disease caused by CD48 haploinsufficiency, Volkmer B, Lünemann A, Opitz L, Mauracher A, Nüesch U, Lecca R, Gayden T, Jabado N, Kaiser D, Drexel B, Pollak J, Trehkopf I, Kouzmenko E, , Vavassori S, Pachlopnik Schmid J; Blood Advances; June 2017; — in revision

Epithelial proliferation in inflammatory skin disease is regulated by Ttc7 in fibroblast and lymphocytes, Nüesch U, Opitz L, Mauracher A. A, Volkmer B, Michalak K, Kamarachev J, Hartwig T, Reichmann E, Becher B, Vavassori S, Pachlopnik Schmid J; Sciene Translational Medicine; August 2017; — in revision

POSTER AND ORAL PRESENTATION

The Role of Ttc7 in the pathogenesis of combined immunodeficiency in hereditary multiple intestinal atresia. Nüesch U, Volkmer B, Urwyler A, Vavassori S, Pachlopnik Schmid J. Poster, Clinical Research Day, ZKF, USZ, Zurich, Switzerland, 9.4.2015

Ttc7 is a *trans*-acting regulator of cell proliferation. Nüesch U, Opitz L, Mauracher A, Volkmer B, Michalak K, Kamarachev J, Reichmann E, Becher B, Vavassori S, Pachlopnik Schmid J. Poster, 4th Lymphocyte tissue meeting, St. Gallen, Switzerland, 2.-3.6.2017

Role of the hematopoietic versus non-hematopoietic system in the flaky skin mutant mouse with an altered Ttc7. Nüesch U, Mauracher A, Volkmer B, Urwyler A, Vavassori S, Pachlopnik Schmid J. Oral presentation, 5th FZK Retreat, Halbinsel Au, Switzerland, 29.10.2015

Ttc7 mutation is associated with epithelial stress, which drives immunological dysregulation. Nüesch U, Pachlopnik Schmid J. Oral presentation. 6th FZK Retreat, Halbinsel Au, Switzerland, 10/2016